#### REPUBLIC OF TURKEY

## YILDIZ TECHNICAL UNIVERSITY GRADUATE SCHOOL OF NATURAL AND APPLIED SCIENCES

# PREPARATION OF HYBRID THERMOELECTRIC MATERIALS COMPOSED OF POLY(3,4-ETHYLENE DIOXY THIOPHENE)INORGANIC NANOPARTICLES

#### Naseer Subhi A. AHMED

DOCTOR OF PHILOSOPHY THESIS

Department of Chemistry
Chemistry Program

Advisor

Prof. Dr. Ferdane KARAMAN

#### REPUBLIC OF TURKEY

#### YILDIZ TECHNICAL UNIVERSITY

#### GRADUATE SCHOOL OF NATURAL AND APPLIED SCIENCES

## PREPARATION OF HYBRID THERMOELECTRIC MATERIALS COMPOSED OF POLY(3,4-ETHYLENE DIOXY THIOPHENE)-INORGANIC NANOPARTICLES

A thesis submitted by Naseer Subhi A. AHMED in partial fulfillment of the requirements for the degree of DOCTOR OF PHILOSOPHY is approved by the committee on (11.02.2020) in Department of Chemistry / Chemistry Program.

Prof. Dr Ferdane KARAMAN

Yıldız Technical University

Advisor

#### **Approved By the Examining Committee**

Prof. Dr. Ferdane KARAMAN, Advisor

Yıldız Technical University

PROF. DR. Tarık EREN, Member

Yıldız Technical University

Prof. Dr. Bahire Filiz ŞENKAL, Member

Istanbul Technical University

Doç. Dr. Dolunay ŞAKAR DAŞDAN, Member

Yıldız Technical University

Prof. Dr. Mehmet MAHRAMANLIOĞLU, Member

Istanbul University-Cerrahpaşa

I hereby declare that I have obtained the required legal permissions during data collection and exploitation procedures, that I have made the in-text citations and cited the references properly, that I haven't falsified and/or fabricated research data and results of the study and that I have abided by the principles of the scientific research and ethics during my Preparation of thermoelectric hybrid material composed of some condactive polymer-inorganic nanoparticales supervised by my supervisor, Prof. Dr. Ferdane KARAMAN. In the case of a discovery of false statement, I am to acknowledge any legal consequence.

Naseer Subhi A. AHMED
Signature



Dedicated to my family and my friends

#### **ACKNOWLEDGEMENTS**

I would like to thank my supervisor Prof. Dr. Ferdane KARAMAN for his pure- hearted support and guidance throughout my study, also for giving me the opportunity to work on this project. I also would like to thank Yıldız Technical University for giving me the opportunity to work in their labs and for supporting this project with the necessary equipment, especially the Chemistry Department and Scientific Research Project Coordination Center of Yildiz Technical University (Project No: FDK-2017-3151)

I would like also to thank the Iraqi Cultural Attaches and the Iraqi Ministry of Education for all the facilities they have provided.

I would like to thank my friends and specially Dr. Suhaib Ghanim Hammodat, Assist Prof. Dr.Shukur Muhammad Mahoos, Assist. Prof Dr.Masher Ali, Prof Dr. Taghreed Uloom mohammad, Mohanad Abed Hameed, and also my Laboratory Friends Doç. Dr. Özlem YAZICI, Dr. Volkan Uğraşkan, Dr. Keziban HÜNER, for supporting and lifting my spirit whenever needed, thank you for being my true friends.

Ultimately I would like to thanks my mother, father, and my family beloved wife (Miami) brother (My dear brother Caesar), my sisters (especially Manahel), my children for always believing me and supporting me with my love. I would also like to extend a special thanks to my mother (Farha Khader Muhammad), who devoted her entire life to helping us reach this degree.

Naseer Subhi A. AHMED

## **TABLE of CONTENTS**

LIST OF SYMBOLS	X
LIST OF ABBREVIATIONS	XI
LIST OF FIGURES	XI
LIST OF TABLES	XV
ABSTRACT	XVI
ÖZET	XVIII
1 INTRODUCTION	1
1.1 Literature Review	1
1.2 Organic-inorganic hybrid thermoelectrics	7
1.2.1 P type hybrid TE materials	8
1.2.2 N type hybrid TE materials	11
1.3 Objective of the Thesis	13
1.4 Hypothesis	13
2 GENERAL INFORMATION	14
2.1 Historical	14
2.2 Some concept in the thermoelectric materials	17
2.2.1 Seebeck coefficient	17
2.2.2 Electrical conductivity	18
2.2.3. Figure of merit (ZT)	22
2.3 Applications of thermoelectric materials	24
2.4 The kinds of thermoelectric materials	24
2.4.1 Inorganic thermoelectric materials	24
2.4.2 Organic thermoelectric materials	24
2.5 Strategies for Improvement of the Thermoelectric Performar	ice33

	2.5.1 Doping	34
	2.5.2 Addition of Carbon Nanotubes (CNTs)	36
	2.5.3 Polymer Composite	36
	2.5.4 Addition of Semiconducting Stabilizer	37
	2.5.5 Nanostructured Thermoelectric Materials	37
3 N	MATERIALS and METHODS	39
	3.1 Instruments	39
	3.1.1 Conductivity Meter (Four Point Probe)	39
	3.1.2. Seebeck Coefficient Meter	40
	3.1.3 X-Ray Photoelectron Spectroscopy (XPS)	40
	3.1.4 Scanning electron microscope (SEM)	40
	3.1.5 X-Ray Diffractometer (XRD)	41
	3.1.6 Infrared-Reduced Total Reflection Spectroscopy with Fourier	
	Transform	41
	3.1.7 Ultraviolet-Visible Region Spectroscopy	42
	3.1.8 Sonicated homogenizer	42
	3.2 Materials	43
;	3.3 Synthesis of the samples PEDOT:PSSA	43
	3.3.1 Synthesis of the samples PP 1 (PEDOT:PSSA 1)	44
	3.3.2 Synthesis of the samples PP2 (PEDOT:PSSA 2)	44
	3.3.3 Synthesis of the samples PP3 (PEDOT:PSSA 3)	44
	3.3.4 Synthesis of the samples PP4 (PEDOT:PSSA 4)	44
	3.3.5 Synthesis of the samples PP5 (PEDOT:PSSA 5)	44
	3.3.6 Synthesis of the samples PP6 (PEDOT:PSSA 6)	44
	3.3.7 Synthesis of the samples PP7 (PEDOT:PSSA 7)	45
	3.3.8 Synthesis of the samples PP8 (PEDOT:PSSA 8	45

3.3.9 Synthesis of the samples PP9 (PEDOT:PSSA 9)	45
3.3.10 Synthesis of the samples PP10 (PEDOT:PSSA 10)	46
3.3.11 Synthesis of the samples PP11(PEDOT:PSSA 11)	46
3.3.12 Synthesis of the samples PP12 (PEDOT:PSSA 12)	46
3.4 Synthesis of ZnS	46
3.4.1 Synthesis of ZnS-PVOH	46
3.4.2 Synthesis of ZnS-G	47
3.4.3 Synthesis of ZnS-TBAB	47
3.4.4 Synthesis of ZnS –EG	47
3.5 Synthesis of the Cu <sub>1.8</sub> S	48
3.6 Preparation of the films for composites	49
3.6.1 Preparation of the films or composite 1	49
3.6.2 Preparation of the films for composite 2	49
3.6.3 Preparation of composite 3	50
3.6.4 Preparation of composite 4	51
4 RESULTS and DISCUSSION	52
4.1 Pristine PEDOT:PSSA	58
4.2 PEDOT:PSSA/ZnS-PVOH Composites	56
4.3 PEDOT:PSSA/Cu <sub>1.8</sub> S Composites	60
4.4 PEDOT:PSSA/TiS2 composites	66
4.5 PEDOT:PSSA/TiS <sub>2</sub> /CS <sub>2</sub> CO <sub>3</sub> composites	76
4.6 Conclusion	88
References	89
Publications from the thesis	101

## **LIST of SYMBOLS**

Т	Absolute temperature
σ	Electrical conductivity
ZT	Figure of merit
S	Seebeck coefficient
K	Thermal conductivity

#### LIST of ABBREVIATIONS

BE Bonding energy

CNT Carbon nanotube

CP Conductive Polymer

DMSO Dimethyl sulfoxide

EG Ethylene glycol

FTIR-ATR Fourier-pass infrared-reduced total reflection spectroscopy

HCl Hydrochloric acid

NWs Nanowires

PANI Polyaniline

PEDOT Poly (3,4-ethylenedioxy thiophene)

PF Power factor

P3HT Poly (3-hexylthiophene-2,5-diyl)

PTh Polythiophene

PSSA Poly (styrene sulfonic acid)

SEM Scanning electron microscope

TE Thermoelectric

TEG Thermoelectric generator

UV-vis Ultraviolet-visible region

XPS X-ray photoelectron spectroscopy

XRD X-ray diffractometer

## **LIST of FIGURES**

<b>Figure 2.1</b> Schematic illustration of the electrical conductivity of different	
compounds in	20
Figure 2.2 displays (a) the creation of polaron, bipolaron and bipolaron	
bands as the doping level increases for CPs	21
<b>Figure 2.3</b> Schematic illustration of a TE couple generating electricity in the presence of thermal gradient	23
<b>Figure 2.4</b> Illustrates the figure of merit for various classes of matters and their dependence on T	<b>2</b> 3
Figure 2.5 The chemical structures of typical conducting polymers	25
Figure 2.6 Chemical Structures of TTF-TCNQ (a), PETT (b), Fullerene (c), Graphene (d),and CNT (e)	26
<b>Figure 2.7</b> The graphical representation shows Progress in the ZT of various conducting polymers over the years (RT is room temperature)	27
Figure 2.8 Illustrates the both doping methods (left) and the common dopants	
used in those methods (right)	29
Figure 2.9 Chemical structure of PANI	30
Figure 2.10 Chemical structure of poly (2,7-carbazole)	32
Figure 2.11 Schematic illustration of P3HT	33
Figure 2.12 Chemical structure of PEDOT: PSSA	35
Figure 3.1 Four point probe measuring device	40
Figure 3.2 Seebeck coefficient measuring system	40
Figure 3.3 Scanning electron microscope (SEM)	41
Figure 3.4 Ultraviolet-Visible Region Spectroscopy	42
Figure 3.5 Ultrasonic homogenize	43
<b>Figure 3.6</b> Method for preparing Zinc sulfide	48

Figure 3.7 Method for preparing copper sulfide	49
Figure 3.8 PEDOT:PSSA/ZnS-POVH films	49
Figure 3.9 PEDOT:PSSA/Cu <sub>1.8</sub> S films	50
Figure 3.10 PEDOT:PSSA/TiS2 films	50
Figure 3.11 PEDOT:PSSA/TiS <sub>2</sub> -Cs <sub>2</sub> CO <sub>3</sub> films	51
Figure 4.1 XPS survey spectra of PEDOT:PSSA	54
Figure 4.2. FTIR of pristine PEDOT:PSSA (PP2)	55
Figure 4.3 SEM image of PP2	55
Figure 4.4 XPS survey spectra of-ZnS-PVOH synthesized	58
<b>Figure 4.5</b> FTIR absorption spectra. The ZnS-PVOH nanoparticle (diamond), and bottom line (circle) belongs to pristine PEDOT:PSSA and their composites in the ratio of PEDOT:PSSA/ZnS-PVOH are 1/1 (square), 1/1.5 (pentagram), 1/2 (star)	59
Figure 4.6 XRD pattern of the Cu <sub>1.8</sub> S nanoparticles powders	
Figure 4.7 UV absorption spectra of the PEDOT:PSSA and its nanocomposites.  The curves are shifted artificially. The bottom line (square) belongs to pristine PEDOT:PSSA and upward lines belong to the PEDOT:PSSA/Cu <sub>1.8</sub> S nanocomposites in the following ratios: 1/0.11 (circle), 1/0.25 (triangle), 1/0.33 (diamond), 1/0.67 (star), respectively	,
<b>Figure 4.8</b> SEM image of synthesized Cu <sub>1.8</sub> S nanoparticles dispersed in ethylene glycol	64
Figure 4.9 SEM images of composite of PEDOT:PSSA / Cu <sub>1.8</sub> S (1:0.25)	64
Figure 4.10 SEM images of composite of PEDOT:PSSA / Cu <sub>1.8</sub> S (1:0.33)	65
Figure 4.11 SEM images of composite of PEDOT:PSSA / Cu <sub>1.8</sub> S (1:0.66)	65
Figure 4.12 X- ray powder diffraction patterns of TiS2 as-received (the red line	)
and its composite with PEDOT:PSSA (blue line)	69
<b>Figure 4.13</b> FTIR spectra of TiS <sub>2</sub> as-received (the blue line), PEDOT:PSSA	
(red line) and the composite(orange line)	70
Figure 4.14 XPS survey scan of titanium sulfide as received	71
Figure 4.15 XPS survey spectra of the composite of TiS2 and PEDOT:PSSA	72
Figure 4.16 SEM image of the TiS2 as received	74

Figure 4.17	SEM image of the TiS <sub>2</sub> as received	.74
Figure 4.18	SEM image of the TiS <sub>2</sub> as received	75
Figure 4.19	SEM image of the PEDOT:PSS/TiS <sub>2</sub> composite	.75
Figure. 4.20	XPS survey scan of cesium carbonate	.77
Figure.4.21	XPS survey scan of PEDOT:PSSA/TiS <sub>2</sub> -Cs <sub>2</sub> CO <sub>3</sub> composite	.78
Figure 4.22	XPS survey scan of PEDOT:PSSA/TiS2-CsCO3	.79
Figure 4.23	SEM image of PEDOT:PSSA	80
Figure 4.24	The percentage of carbon in the PEDOT:PSSA	80
Figure 4.25	The percentage of oxygen in the PEDOT:PSSA	81
Figure 4.26	The percentage of sulfur in the PEDOT:PSSA	81
Figure 4.27	EDAX analysis of the PEDOT:PSSA	82
Figure 4.28	SEM image of the composite PEDOT:PSSA/ Cs <sub>2</sub> CO <sub>3</sub> /TiS <sub>2</sub> = 1/0.14/0.3	.82
Figure 4.29	EDAX image of respective distributions of the elements of the composite PEDOT:PSSA/ $Cs_2CO_3$ / $TiS_2$ = 1/0.14/0.3	83
Figure 4.30	Percentage of carbon in the composite PEDOT:PSSA/ Cs <sub>2</sub> CO <sub>3</sub> /TiS <sub>2</sub> =1/0.14/0.3	84
Figure 4.31	Percentage of oxygen in the composite PEDOT:PSSA/ Cs <sub>2</sub> CO <sub>3</sub> /TiS <sub>2</sub> = 1/0.14/0.3	84
Figure 4.32	Percentage of sulfur in the composite PEDOT:PSSA/Cs <sub>2</sub> CO <sub>3</sub> /TiS <sub>2</sub> = 1/0.14/0.3	85
Figure 4.33	Percentage of cesium in the composite PEDOT:PSSA/Cs <sub>2</sub> CO <sub>3</sub> /TiS <sub>2</sub> = $1/0.14/0.3$	.85
Figure 4.34	Percentage of titanium in the composite PEDOT:PSSA/Cs <sub>2</sub> CO <sub>3</sub> / $TiS_2$ = 1/0.14/0.3	.86
Figure 4.35	EDAX analysis of the composite PEDOT:PSSA/ Cs <sub>2</sub> CO <sub>3</sub> / TiS <sub>2</sub> = 1/0.14/0.3	.86

<b>Table 4.1</b> Thermoelectric parameters measured at room temperature of the PEDOT:PSSA samples synthesized using different amount of EDOT and PS	.52
<b>Table 4.2</b> Thermoelectric parameters of the various PEDOT samples, reported in the related references	.53
Table 4.3 Thermoelectric parameters measured at room temperature, of the	
composites of ZnS at different weight ratio withPP2	.56
Table 4.4 Thermoelectric parameters measured at room temperature,	
of the composites of ZnS at different weight ratio withPP7	.56
Table 4.5 Thermoelectric parameters measured at room temperature,	
of the composites of ZnS at different weight ratio withPP8	.56
Table 4.6 Thermoelectric parameters measured at room temperature,	
of the composites of ZnS at different weight ratio withPP9	.57
<b>Table 4.7</b> Thermoelectric parameters of the various PEDOT/inorganic	
hybrid composites, reported in the literature	.57
<b>Table 4.8</b> Seebeck coefficient (S,) electrical conductivity ( $\sigma$ ) measured	
at room temperature, and power factor (P) calculated by means	
of $P=\sigma$ $S^2$ , and figure-of merit (ZT) estimated at 300 K by assuming	
as $\kappa$ =0.4 of PEDOT:PSSA (PP10) and its nanocomposites with	
Cu <sub>1.8</sub> S synthesized in this study	.62
<b>Table 4.9</b> Thermoelectric parameters of thin film samples prepared from non-	
sonicated TiS <sub>2</sub> /PEDOT: PSSA (PP11) composites and tablet sample	
prepared from TiS <sub>2</sub> as received	.66
<b>Table 4.10</b> Thermoelectric parameters of thin film samples prepared from	
TiS <sub>2</sub> /PEDOT:PSSA composites homogenized ultrasonically	.68
<b>Table 4.11</b> Thermoelectric parameters measured at room temperature, of the	
composites of Cs2CO3-TiS2 at different weight ratio with PP12	76

Preparation Of Hybrid Thermoelectric Materials
Composed Of Poly(3,4-Ethylene Dioxy Thiophene)
Inorganic Nanoparticles

Naseer Subhi A. AHMED

Department of Chemistry

Doctor of Philosophy Thesis

Advisor: Prof. Dr. Ferdane KARAMAN

Thermoelectric (TE) materials can generate electricity if there is a temperature difference between their two sides. The state-of-the-art, TE materials are toxic, nonflexible, and extremely expensive inorganic semi-conductive metal alloys. In recent years, polymer TE composites have been subjected to intense research. The poly (3,4-ethylene dioxythiophene) (PEDOT) is the most studied polymer among the conductive polymers related to thermoelectricity because of its high conductivity, stability, and flexibility. It would appear that one of the most preferable ways to improve the TE properties of PEDOT is to prepare its inorganic hybrid nanocomposites.

In this study, it was aimed to prepare organic-inorganic hybrid nanocomposites which have high TE properties. The research can be summarized in three main pivots. The first axis focused on preparing the PEDOT in poly (styrene sulfonic acid) (PEDOT:PSSA) in different concentrations to obtain a conducting polymer that has large Seebeck coefficient because it is necessary to obtain high TE properties. In this context, twelve different PEDOT:PSSA have been synthesized. Those of the PEDOT:PSSA samples that have the relatively high conductivity and large Seebeck

coefficient were used to prepare the hybrid composites. As for the second axis, it was focused on preparing inorganic nanoparticles. Within this scope, zinc sulfide was prepared in several ways by using several auxiliary agents, the best of which was the preparation of zinc sulfide using the solvent ethylene glycol. Copper sulfide was prepared also in several ways and among the methods, the best one was in which the ethylene glycol was used as a solvent. It was also used the sonicated titanium sulfide of purchased from the market. On the other hand, cesium carbonate was added to the titanium sulfide and this step was done using the ultrasonic device. The third axis is preparing organic-inorganic hybrid nanocomposites such as PEDOT:PSSA/ZnS-PVOH, PEDOT:PSSA/Cu<sub>1.8</sub>S, PEDOT:PSSA/TiS2, PEDOT:PSSA/TiS<sub>2</sub>-Cs<sub>2</sub>CO<sub>3</sub>, by compounding the components. PEDOT: PSSA / Cu<sub>1.8</sub>S and PEDOT:PSSA/TiS2 can be used as p-type and n-type TE materials, respectively, due to the high power factors found by measuring their electrical conductivity and Seebeck coefficients. The composites were characterized by FTIR, UV-vis., XRD, XPS and SEM-EDAX techniques.

**Keywords:** Thermoelectric, poly (3,4-ethylene dioxythiophene) (PEDOT), nanocomposites, Seebeck coefficient, copper sulfide, titanium sulfide.

YILDIZ TECHNICAL UNIVERSITY
GRADUATE SCHOOL OF NATURAL AND APPLIED SCIENCES

# Poli(3,4-Etilen Dioksitiyofen)-Inorganik Nanopartiküllerinden Oluşmuş Hibrit Termoelektrik Materyallerin Hazırlanması

Naseer Subhi A. AHMED

Kimya Anabilim Dalı

Doktora Tezi

Danışman: Prof. Dr. Ferdane KARAMAN

İki tarafı arasında sıcaklık farkı varsa, termoelektrik (TE) malzemeler elektrik üretebilir. En son teknolojiye sahip TE malzemeleri toksik, esnek olmayan ve aşırı pahalı inorganik yarı iletken metal alaşımlarıdır. Son yıllarda, polimer TE kompozitler yoğun bir araştırmaya tabi tutulmuştur. Poli (3,4-etilen dioksitiofen) (PEDOT), yüksek iletkenliği, stabilitesi ve esnekliği nedeniyle termoelektriklik açısından, iletken polimerler arasında en çok çalışılan polimerdir. PEDOT' un TE özelliklerini geliştirmenin en tercih edilen yollarından birinin, inorganik hibrit nanokompozitlerini hazırlamak olduğu görülmektedir.

Bu çalışmada, yüksek TE özelliklere sahip organik-inorganik hibrid nanokompozitlerin hazırlanması amaçlanmıştır. Araştırma üç ana pivotta özetlenebilir. Birinci eksen, yüksek TE özellikler elde etmek gerektiğinden büyük Seebeck katsayısına sahip bir iletken polimer elde etmek için farklı konsantrasyonlarda poli (stiren sülfonik asit) içinde PEDOT (PEDOT:PSSA) hazırlanmasına odaklanılmıştır. Bu bağlamda, on iki farklı PEDOT:PSSA

sentezlenmiştir. Nispeten yüksek iletkenliğe ve büyük Seebeck katsayısına sahip olan PEDOT:PSSA numuneleri hibrid kompozitleri hazırlamak için kullanıldı. İkinci eksene gelince, inorganik nanopartiküllerin hazırlanmasına odaklanıldı. Bu kapsamda çinko sülfür, çeşitli yardımcı maddeler kullanılarak çeşitli şekillerde hazırlandı; bunların en iyisi, çözücü etilen glikol kullanılarak çinko sülfürün hazırlanması idi. Bakır sülfür de çeşitli yollarla hazırlandı ve yöntemler arasında en iyisi, etilen glikolün bir çözücü olarak kullanıldığı idi. Ayrıca piyasadan satın alınan titanyum sülfür sonike edilerek kullanıldı. Öte yandan titanyum sülfüre sezyum karbonat ilave edildi ve bu aşama ultrasonik cihaz kullanılarak yapıldı. Üçüncü getirerek PEDOT: PSSA / eksen, bilesenleri bir araya ZnS-PVOH, PEDOT:PSSA/Cu<sub>1.8</sub>S, PEDOT:PSSA/TiS<sub>2</sub>, PEDOT:PSSA/TiS<sub>2</sub>Cs<sub>2</sub>CO<sub>3</sub> gibi organikinorganik hibrid nanokompozitlerin hazırlanmasıdır. Elektriksel iletkenliklerini ve Seebeck katsayılarını ölçerek bulunan güç faktörlerinin yüksek olması nedeniyle, PEDOT:PSSA/Cu<sub>1.8</sub>S ve PEDOT:PSSA/TiS<sub>2</sub>'nin, sırasıyla p-tipi ve n-tipi TE malzeme olarak kullanılabileceği bulundu. Kompozitler FTIR, UV-vis., XRD, XPS ve SEM-EDAX teknikleri ile karakterize edildi.

**Anahtar Kelimeler:** Termoelektrik, Poli (3,4-etilen dioksitiofen) (PEDOT), Seebeck katsayısı, nanokompozitler, bakır sulfur, titanyum sülfüre.

YILDIZ TEKNİK ÜNİVERSİTESİ FEN BİLİMLERİ ENSTİTÜSÜ

# 1 INTRODUCTION

#### 1.1 Literature Review

The energy crisis is introduced as one of the most serious problems of mankind in recent years. Various renewable energy sources have been proposed since then. One of the most promising methods here is the utilization of thermoelectric (TE) material. Since they can generate electrical energy from nearly any kind of heat source and produce no waste, they have been vastly studied. Some of the sources which have attracted attention are solar thermal radiation, radioactive decay, bulk heat radiation, and industrial waste heat, etc. Also, the thermoelectric method for generating electricity is inexpensive, takes not much room, needs no high technology, and it's practical [1-3]. The figure of merit (ZT) is a dimensionless parameter defined for determining the efficacy of thermoelectric matter. It depends on the Seebeck coefficient (S), the electrical conductivity ( $\sigma$ ), the thermal conductivity ( $\kappa$ ), and absolute temperature (T) as follows;

$$ZT = S^2 \sigma T / K \tag{1.1}$$

The combination of a high Seebeck coefficient, high electrical conductivity, and low thermal conductivity guarantees the efficiency of a thermoelectric material to be high. So to improve thermoelectric performance, we need to prepare such a combination. However, since these three factors are somehow entangled, which means one cannot vary one of them without affecting the other two, improving thermoelectric response is not that easy. This is not the only obstacle to be conquered. Most of the thermoelectric materials known today are inorganic materials such as metals and inorganic semiconductors, which are toxic, brittle, expensive and their sources are limited. Nevertheless, even though the Seebeck coefficient and the electrical conductivity for them are high enough, but their thermal conductivity is also high, and this prevents ZT from getting too high for these materials. On the other hand, the figure of merit must exceed 1 for a thermoelectric material to be commercially utilized. Owing to all of these, it's so

important to find an eco-friendly and inexpensive material with high ZT to manufacture thermoelectric devices.

To overcome the shortcomings of inorganic materials, a novel class of thermoelectric materials has been proposed. Due to their ubiquity, high plasticity, low processing costs, and more importantly their poor thermal conductivity, Conductive Polymers (CPs) are considered as interesting alternatives [4]. Unfortunately, known conductive polymers do not exhibit high thermoelectric performances. However, since thermal conductivity is low for most of the CPs, and it does not vary remarkably by the addition of inorganics, there is a great potential in studying conductive polymers and try some reasonable modifications to achieve higher performance. Also, a parameter called power factor (PF) is defined for determining the thermoelectric performance of conductive polymers, since thermal conductivity doesn't play a significant role in this case, it only depends on the Seebeck coefficient (S) and the electrical conductivity ( $\sigma$ ) as follows:

$$PF = S^2 \sigma \tag{1.2}$$

It may worth to be mentioned that CPs can be used only in low temperatures up to 150 C. According to the study by Kim et al. [5] the highest figure of merit measured for CPs at 300K is something about 0.42 and they believed this number was high enough for them to be considered as an alternative for the inorganic thermoelectric materials. This number is fairly close to the figure of merit of Bismuth Telluride ( $Bi_2Te_3$ ) which is the best inorganic thermoelectric material and its ZT is about 1 at room temperature.

Poly (3,4-ethylene dioxythiophene) (PEDOT) is the best candidate for thermoelectric utilization amongst CPs so far [4]. Currently, a suspension comprised of PEDOT and the poly (styrene sulfonate) (PSS) as a solvent is commercially accessible and it can be applied on both solid and flexible substrates. The PEDOT: PSS is transparent for visible range of electromagnetic waves, stable in direct contact with the airstream, restorable, and it can be readily used as an aqueous coating. Besides, the electrical conductivity of PEDOT:PSS can be improved tremendously (up to 3 orders of magnitude) by the employment of solution processing techniques such as the addition of secondary solvents like sorbitol

 $(C_6H_{14}O_6)$ , ethylene glycol  $(C_2H_6O_2)$ , sulfuric acid  $(H_2SO_4)$  or nitric acid  $(HNO_3)$  [6-9]. PEDOT: PSS suspensions due to their commercial availability, high conductivity, easy processing, and the possibility of doping with dopants that can increase the number of charge carriers and hence the electrical conductivity without altering thermal conductivity significantly, is a promising material to be used in TE devices [6].

Kim et al. [10] reported an improvement in the electrical conductivity of PEDOT due to the formation of the ultra-thin layer of crystalline conjoined monomers. They prepared two samples, one with the addition of iron(III) chloride as an oxidizing agent and in the 2nd sample, iron(III) tosylate has been used for the same purpose. Both of the samples exhibited a great enhancement in electrical conductivity, but the one doped with iron(III) tosylate (PEDOT:Tos) was better. The best electrical conductivities were 2000 S/cm and 4500 S/cm for the first sample and PEDOT: Tos, respectively. Later, another experiment reported electrical conductivity of 3065 S/cm for thin layers of PEDOT: PSS treated with sulfuric acid while this number for pure PEDOT films is only 0.3 S/cm [11]. Kim et al. [12] announced  $\sigma$  = 4380 S/cm with the same treatment using sulfuric acid as an oxidant. They concluded this high value is due to the formation of crystalline structure. Cho and his colleagues [13] prepared nanostructured single-crystal PEDOT which was a deviation of selfassembled 3,4ethylenedioxythiophene (EDOT) monomers. They have achieved shockingly high electrical conductivity as 7619 S/cm on average, and their best was about 8797 S/cm. Culebras and Gomez [14] doped PEDOT thin layers with various counterions like ClO4-, PF6- and bis(trifluoromethyl sulfonyl)imide (BTFMSI) and achieved fairly high electrical conductivities. They believed counterions have enhanced electrical conductivity by stretching of the polymer chains.

Scholdt et al. [9] added dimethyl sulfoxide (DMSO) to the PEDOT: PSS suspension as a secondary solvent and reported an increment in the thermoelectric performance of the thin layer of the coatings made of this suspension as ZT was  $9.2\times10^{-3}$  at 300K. They also reported no change in the values of the Seebeck coefficient and thermal conductivity. Bubnova and his team [15] studied the impact of the oxidation level of PEDOT: Tos on the PF. They measured  $\sigma$  to be 300 S/cm and power factor to be 38  $\mu$ W/m K² for pristine doped PEDOT-Tos thin layers. Next, they

doped PEDOT: Tos with tetrakis (dimethylamino) ethylene (TDAE) which reduced the level of oxidation to 22 % and enhanced the PF up to 324  $\mu$ W/m K². The figure of merit, in this case, is measured to be about 0.25 at 300K.

Pipe et al. [16] used a hydrophilic solution like ethylene glycol (EG) to eliminate non-ionized doping particles from DMSO-mixed PEDOT: PSS. EG de-doping process has been done for 100 minutes and during this process, the electrical conductivity and the Seebeck coefficient have been increased while thermal conductivity has been decreased. The improvement of thermoelectric performance from 0.25 for EG [15] to 0.42 for DMSO [16] can be associated with the alignment of the layers in the polymers' molecular arrangement. This phenomenon has been confirmed in the case of PEDOT chains as any alignment there improved the thermoelectric properties and electrical conductivity by increasing the mobility of electrons. Besides, such a structure simplifies the oxidation of PEDOT, and this process in turn increases the charge carrier concentration. Now increased density and mobility can enhance electrical conductivity tremendously [17].

The impact of the doping PEDOT:PSS with sorbitol is just like the DMSO. The modified structure is the reason for the enormous jump in electrical conductivity which is 722.06 S/cm, and much greater than the one for non-doped PEDOT:PSS. Even though the addition of sorbitol diminished the Seebeck coefficient, but the PF has been increased up to 7.26  $\mu$ W/m K<sup>2</sup>, while this number for pristine layers was only 0.016 μW/m K<sup>2</sup>. The addition of TDAE to the sorbitol doped PEDOT:PSS has increased the power factor even more to the value as high as 22.28 µW/m K<sup>2</sup> [18]. Still, the figure of merit for the layer which exhibits the greatest PF is only something between 0.013 and 0.039. Due to the toxicity of organic solutions, which have been commonly utilized for increasing ZT, there are some limits for using them. Some studies have proposed deep eutectic solvents (DES) as an alternative for common organic solvents. A notable enhancement has been reported in both electrical conductivity and the Seebeck coefficient. The maximum Seebeck coefficient and, the best electrical conductivity reported while choline chloride doped PEDOT:PSS was treated with EG was 29.1 µV/K and 620.6 S/cm, respectively. PF, in this case, was  $24.08 \,\mu\text{W}/\text{mK}^2$  which was tremendously greater than the one for pristine films [19]. Mengistie et al. [20] revealed that electrical conductivity enhancement as a secondary solvent is added can be explained utterly by the enhancement of the structure order, mobility of the charge carriers and the density of charge carriers and the oxidation level plays no role in this enhancement. They also employed the solution processing method using various solvents such as EG, PEG, methanol, and methanoic acid and this treatment ended in the electrical conductivity as high as 640, 800, 1300, and 1900 S/cm. Also, no noteworthy alteration in the value of the Seebeck coefficient was observed. They also explained the ultra-high electrical conductivity of the sample treated with methanoic acid by the hypothesis that methanoic acid has eliminated the non-ionized dopant particles and related chains in a process called the PSS removal. The PF and the figure of merit for the latter case were  $80.6~\mu\text{W/m}~\text{K}^2$ , and 0.32 at 300K, respectively.

Wang and his colleagues [21], prepared PEDOT:Tos:PPP (polyethylene glycol-polypropylene glycol-polyethylene glycol) thin layers. They successfully removed PPP: Tos and improved the order of the PEDOT structure, which eventually resulted in the improved thermoelectric performance. They also employed secondary solvents like NaBH4 and DMSO to modify the level of oxidation. They found that the PF of dedoped coatings that have experienced a solution processing in the presence of NaBH4 or DMSO was about 98.1  $\mu$ W/m K² which was greater than the one for raw coatings. This process also reduced the thermal conductivity from 0.501 to 0.451 W/m K. Therefore, the figure of merit at 300K was raised from 0.02 to 0.064.

Improving the thermoelectric material and their performance is of great importance today. To this end, many studies have been conducted to introduce more effective methods. One of the most promising materials is the composite made of PEDOT polymer and carbon nanotubes (CNT). Carbon nanotubes due to their high electrical conductivity, high durability, and spectacular mechanical properties are very interesting alternatives. Carbon nanotubes tend to construct bundles, because of the van der Waals forces. Therefore, it's not easy to have them dispersed in aqueous media. To this end, stabilizers are used normally, and in the case of polymer/carbon nanotube composites, DMSO doped PEDOT: PSS and insulating Gum Arabic (GA) are used as stabilizers more often [22, 23]. Among CP/CNT composites involving a latex made of vinyl acetate and ethylene, the electrical conductivity measured to be greater whenever PEDOT: PSS was used as a stabilizer. The PF has been measured

to be about 25 µW/mK² for the films containing 35 wt % single-walled CNT and the same amount of PEDOT:PSS as a stabilizer. The parameter of thermoelectric performance was found to be about 0.02 at 300K. Even though this number is yet too small but since it is higher than bulk silicon and by far better than most of CPs, using carbon nanotubes has been considered as a useful ingredient for enhancing thermoelectric response [23]. After CNTs, some other dispersion candidates have been considered. Li et al. [24] prepared aqueous PEDOT: PSS solution and dispersed Graphene oxide (GO) in it, then using hydroiodic acid, successfully reduced the GO to graphene (GN). They reported PF to be about 32.6 μW/m K<sup>2</sup> for the thin layers of GN/PEDOT: PSS composites (rGO/PEDOT: PSS) when the graphene oxide was only 3 wt%. Another novel idea that has been proposed by Zhang [25] was about using more than one type of nano-fillers. They hypothesized that using hybrid nano-fillers can improve the thermoelectric response of conductive polymers. Generally, the addition of nano-fillers to the polymer structure enhances the thermoelectric performance by decreasing the thermal conductivity. This team prepared an aqueous PEDOT:PSS solution and added fullerene-functionalized graphene  $[rGO_xC_{60(30-x)}]$ . A fullerene (C<sub>60</sub>) is an allotrope of carbon whose molecule consists of carbon atoms connected by single and double bonds so as to form a closed or partially closed mesh, with fused rings of five to seven atoms. C<sub>60</sub> and GN have distributed themselves in the polymer structure by a proper ratio which ended in improvement both in thermal and electrical conductivity but the increment in the electrical conductivity was greater than the enhancement of thermal conductivity. During this process, the Seebeck coefficient also has experienced a four-fold increment, the best result was achieved for a film comprised of 21% graphene oxide (x=21 %) where electrical conductivity was 700 S/cm, thermal conductivity was 2.3 W/m K, and ZT was 0.067 at room temperature which is exhibiting a three-fold enhancement compared to the samples in which single type nano-fillers are used [25].

In spite of all of the advantages of carbon nanotubes, their high costs limit their commercial use. To overcome this problem, Jiang and his colleagues [26] proposed a novel, inexpensive, practical technique to produce PEDOT: PSS/paper composites employing Chinese calligraphy. In this technique, the prepared solution is applied on a piece of paper just like writing a normal Chinese word. The Seebeck coefficient

in this method found to be about 30.6  $\mu$ V/K at room temperature which is not too different from that of PEDOT: PSS/CNTs composite which was something between 15 and 30  $\mu$ V/K [22]. Additional treatment with ethylene glycol or dimethyl sulfoxide increased the electrical conductivity up to 54.1 S/cm and 56.9 S/cm respectively. Also, due to the extremely low thermal conductivity of these coatings (about 0.16 W/m K), ZT measured to be about 5.5 × 10<sup>-3</sup>. The possibility of using a paper as a substrate on which thermoelectric material could be applied triggered the idea of flexible wearable Thermoelectric Generators (TEGs).

#### 1.2 Organic-Inorganic Hybrid Thermoelectrics

Even though the enormous attempts have been made to enhance the thermoelectric performance of pristine thermoelectric materials, they still could not meet the industrial demands, for example in the case of wearable thermoelectric generators. Normally, the thermoelectric performance of inorganic materials due to their higher electrical conductivity and Seebeck coefficient is better than that of organic matter. Nevertheless, organic thermoelectric matters are inexpensive, easy to process, ubiquitous, eco-friendly, and they do possess great flexibility and poor thermal conductivity. Such characteristics have increased the attention to these materials [27, 28]. For thermoelectric material to be utilized commercially, their figure of merit or thermoelectric performance must exceed two and three, which is not the case today. According to Eq. (1.1), large electrical conductivity and Seebeck coefficient accompanied by small thermal conductivity are the key for a high thermoelectric response. Since pure organic and inorganic materials failed to meet the demands, maybe hybrid materials comprised of both organic and inorganic materials do the job. Hopefully, the hybrid thermoelectrics would inherit the advantages of conventional thermoelectric materials. Here, some of the recent studies on the hybrid thermoelectric material are reviewed.

#### 1.2.1 P type hybrid TE materials

There have been numerous studies on the various methods to enhance the thermoelectric response of hybrid materials. The addition of nanoparticle inorganic materials such as bismuth telluride (Bi<sub>2</sub>Te<sub>3</sub>), tellurium (Te), carbon nanotubes (CNTs), and graphene (GN) to the CPs matrix proved to be beneficial [23]. Ideally, this will end in a product having both advantages of organic (i.e. poor thermal conductivity) and inorganic (i.e. high electrical conductivity) materials. Li and his colleagues [29] produced a thin layer of Te-PEDOT:PSS coating by the drop-casting method using an ultrasonically treated suspension comprised of aqueous PEDOT: PSS and Te nanowires in the presence of ethanol as a secondary solvent. According to their outcomes, the highest power factor was 25 μW/mK<sup>2</sup> and it was achieved when 10 wt% PEDOT:PSS have been employed. During a process called PSS removal, non-conductive PSS chains can be eliminated, which results in an enhanced  $\sigma$ . This process normally takes place using acids like sulfuric acid or Phosphoric acid. Meng and his team [30] prepared a thin layer of PEDOT:PSS: PC-Te composite using a PSS removal treatment on Te (PC-Te) nanorod doped PEDOT:PSS by sulfuric acid. The best result has been achieved for a sample which was 9/10 parts comprised of PC-Te nanowires and post-treated by sulfuric acid with 12 Molar concentration. The power factor for this sample was about 142.0 μW/mK<sup>2</sup> which is 3 orders of magnitude higher than the PF of pristine PEDOT: PSS: PC-Te coating. They also reported a relationship between the amount of the inorganic fillers, and S and  $\sigma$ , but after the acid treatment took place no relationship between the inorganics content and the Seebeck coefficient was observed. Nevertheless, the direct relationship with the electrical conductivity was preserved.

Meng et al. [30] continued their work by applying the same method but this time for coating SWCNT/PEDOT: PSS films. They prepared a suspension of SWCNT/PEDOT: PSS and added Te (PC-Te) nanowires to it. They also used the vacuum filtration technique as a post-treatment. Eventually, they used sulfuric acid to eliminate not ionized PSS chains. They concluded that SWCNT addition and sulfuric acid treatment both increased the electrical conductivity but their impact on the Seebeck

coefficient was negative. Hence, the highest power factor was  $104~\mu W/mK^2$  for the thin composite layer with 70~wt~% SWCNT.

Another group prepared aqueous PEDOT: PSS solution and doped it with Te–Bi<sub>2</sub>Te<sub>3</sub> nanowires [31]. They used the spraying method to apply the hybrid suspension of Te–Bi<sub>2</sub>Te<sub>3</sub>/PEDOT:PSS on a glass surface. This way they produced a plastic TEG, thereafter an acid treatment was done. They reported an enhancement in the electrical conductivity of the Te–Bi<sub>2</sub>Te<sub>3</sub>/PEDOT:PSS film which was because of the post-treatment by sulfuric acid. They found power factor as  $60.05 \,\mu\text{W/mK}^2$  for the sample post-treated by  $60 \, \text{vol}\%$  sulfuric acid.

Hu et al. [32] prepared a composite of PEDOT and Te nanowires. They have announced that Tellurium nanorods effectively enhanced the Seebeck coefficient. The resulting thin composite layer exhibited their best performance with the power factor of 28  $\mu$ W/mK² when the added Tellurium nanorods were up to 30 wt %. Further addition of Tellurium nanorods exhibited a negative impact.

Even though the thermoelectric performance of CPs and hybrid thermoelectric material have increased when Tellurium nanostructured additives are employed but due to the scarcity of Tellurium, its commercial utilization is limited. So, it's necessary to find a procedure to reduce the Tellurium consumption while no significant drop in thermoelectric performance occurs. To this end, Wang and his colleagues [33] proposed to employ multiwalled carbon nanotubes (MWCNTs) instead of Tellurium nanowires. They checked this in the Tellurium nanowire/PANI composite. The best power factor they found for Te-MWCNT/PANI film was 54.4 μW/mK<sup>2</sup> when 16 % of multiwalled carbon nanotubes have been used beside 52 % of Tellurium. This was 2 times greater than the power factor measured for Te/PANI film when the same amount of Tellurium was consumed. Du et al. [34] employed Bi-Te based alloys instead of Tellurium to produce a Bi-Te nanosheet/PEDOT:PSS composite using a simple vacuum-assisted technique. They found that as the content of Bi-Te based alloy they have been using increases, the electrical conductivity drops, hence the power factor also drops with the increasing Bi-Te based alloy content. Therefore, the best power factor they got was 53 µW/mK<sup>2</sup> when the BTBA nanosheet content was minimum and only 10 %.

The next nano-filler that have been proposed in the literature is Tin selenide (SnSe). SnSe, due to its exceptional Seebeck coefficient, which is about 520  $\mu$ V/K, and poor thermal conductivity, which is about 0.6 W/m·K at room temperature, is considered as an interesting alternative for Tellurium [35]. According to the study conducted on the SnSe nanosheets/PEDOT:PSS composites, even though this composite exhibited an acceptable Seebeck coefficient, but it exerted a notable reduction on the electrical conductivity. They increased the power factor up to 390  $\mu$ W/mK² by finding a balance between S and  $\sigma$  when 20 wt% of SnSe nanosheets were incorporated [36].

Li and his team [37] introduced MoSe<sub>2</sub> as an alternative nano-filler to enhance the thermoelectric performance of PEDOT: PSS. They varied the MoSe<sub>2</sub> content between 0 wt % and 70 wt % to find an optimal concentration for it. The best power factor achieved for MoSe<sub>2</sub>/PEDOT:PSS composite was 48.6 µW/mK<sup>2</sup> when only 5 wt % MoSe<sub>2</sub> was incorporated. The outcomes confirmed that there exists a trade-off relationship between MoSe<sub>2</sub> content and electrical conductivity. A tradeoff relationship that has been observed in the studies above was blocking the possibility of further enhancement in thermoelectric performance. To solve this issue Wang et al. [38] introduced a technique in which they applied ce-MoS<sub>2</sub> nanosheets and PEDOT:PSS alternately over a glass substrate utilizing the spin coating method. They also have used DMSO for PSS removal, during which the PSS chains have been eliminated. This improved the electrical conductivity of the thin composite layers. Moreover, the energy filtering phenomenon has guaranteed the large Seebeck coefficient for the PEDOT: PSS/ce-MoS<sub>2</sub> film. The energy filtering phenomenon is a procedure during which the low energy electrons are scattered from a barrier while the electrons with energy greater than the height of the quantum barrier can easily pass it. The best power factor achieved was 41.6 µW/mK<sup>2</sup> for the PEDOT: PSS/ce-MoS<sub>2</sub> film with 4 layers.

#### 1.2.2 N type hybrid TE materials

As mentioned before, organic thermoelectric matters exhibit poor thermal conductivity while inorganic thermoelectric matters exhibit great electrical conductivity and high Seebeck coefficient. These properties combined are what a good thermoelectric device must possess. Also, the n-type organic thermoelectrics

must exhibit air stability otherwise they would recover their positive Seebeck coefficient as soon as they experience direct contact with airstream for a long enough duration. A Japanese group of researchers [39] studied the methods to increase the air stability of n-type thermoelectric semiconductors. In their study, n-type single-walled carbon nanotubes have been exposed to a few conventional salts such as NaCl, NaOH, KOH, and crown ethers. They found that the SWCNT which has been exposed to the potassium hydroxide (KOH) with 0.1 M concentration accompanied by 18-crown–ether, does exhibit the best power factor of 230  $\mu\text{W/mK}^2$ . The air stability for this n-type composite film has been estimated to be more than a month. Another attempt for increasing the air stability of n-type TE materials has been done by Zaia and his colleagues [40]. To this end, they used PDI which is an air durable component to cover Tellurium NWs. The resulted PDI-Te composite exhibited the best power factor was about 17.6  $\mu\text{W/mK}^2$  when 80 vol % PDI have been incorporated.

Chen et al. [41], coated Nickel NWs using the polyvinylidene difluoride (PVDF). They mixed both PVDF powder and Nickel NWs in the DMF solution to obtain an n-type thermoelectric Ni/PVDF composite film. They argued that raising the amount of Nickel NWs from 20 wt% to 80 wt% has improved the mobility of electrons and hence the electrical conductivity, while no modification on the Seebeck coefficient was observed. Eventually, they reported a significant enhancement in the thermoelectric performance of Ni/PVDF composite film as they measured the power factor to be 200  $\mu$ W/mK² when 80 wt% nickel NWs have been incorporated.

Wu et al. [42] mixed SWCNT, perylene diimide (PDINE) and naphthalene diimide (NDINE) to prepare an n-type hybrid thermoelectric composite. They chose SWCNT because of its great electrical conductivity while perylene diimide (PDINE) and naphthalene diimide (NDINE) are chosen due to their high Seebeck coefficient. The PF in the case of PDINE/SWCNT composite films were about  $112 \pm 8 \,\mu\text{W/mK}^2$  and in the case of NDINE/SWCNT composite films were about  $135 \pm 14 \,\mu\text{W/mK}^2$ . Gao and his colleagues [43] introduced a novel technique. They employed a set of tertiary amine groups of ADTA to produce an n-type SWCNT/ADTA thin composite layers. They reported that both S and  $\sigma$  depends strongly on the nature of the terminal tertiary amine group and the abundance of side chains. The best power

factor they achieved was 124.4  $\pm$  10.5  $\mu W/mK^2$  at 300K for a composite called SWCNT/ADTAb.

Despite all have been done recently, yet the thermoelectric performance of the ntype CP composites is lower than that of inorganic thermoelectrics. Nevertheless, there is a novel approach to produce a hybrid inorganic/organic superlattice. Wan et al. [44]employed this new technique to mix TBA and TA molecules as organic thermoelectric with titanium disulfide elements to produce n-type  $TiS_2(TBA)_{0.013}(HA)_{0.019}$ . The charge carrier density for this composite is lower than that of the pristine titanium disulfide. Therefore, its electrical conductivity is greater than that of the TiS2 while its thermal conductivity is lower. So, the power factor of TiS<sub>2</sub>(TBA)<sub>0.013</sub>(HA)<sub>0.019</sub> thin composite layers are about 904 μW/mK<sup>2</sup> at room temperature, which exhibits a great enhancement compared to the pristine titanium disulfide.

#### 1.3 Objective of the Thesis

It was aimed to prepare some p-type and n-type polymer-inorganic hybrid nanocomposites, which have power factor higher than  $1000~\mu\text{W/mK}^2$ .

#### 1.4 Hypothesis

The thermoelectric properties of poly (3,4-ethylene dioxythiophene) (PEDOT) can be enhanced by composing it with some inorganic nanoparticles according to literature data. Metal sulfides can be used to prepare polymer-inorganic hybrid nanocomposites since they are attractive photo-catalyst materials for electrocatalytic hydrogen generation, photo-electrochemical water splitting, batteries, and sensors. Because of this, it can be expected to improve the thermoelectric properties of the PEDOT.

Energy and environment problems are of significant importance today. More economical considerations for fossil fuel consumption are required. Also, there is a great demand for new energy sources. As a result, energy transformation and hunting for new energy sources became the subject for numerous studies. The thermoelectric (TE) energy transformation method is an example of the energy transformation methods that have gone under serious consideration. This method employs a specific sort of matter, alluded to as thermoelectric matter, that immediately transforms thermal energy into power [45-49].

The thermoelectric matters are eco-friendly solid-state coolers. They are capable of being utilized as energy propellers with no need for mechanical components. Since it's easy to put the thermoelectric matters in use, they are broadly employed in various areas such as space energy production. Most of the space missions that are conducted beyond Mars have used some kind of radioisotope thermoelectric generator. Material's radioactive decay is the source of generated electricity. Normally, radioactive decay has a slow procedure and this guarantees the durability of the thermoelectric energy conversion technique. Also, TE matter is used in luxury cars' seats' air conditioning system, mini fridges, and in semiconductor lasers' cooling systems [47, 50].

#### 2.1 History

1821–1909: It was in 1821 that the Seebeck effect had been observed for the very first time, and 23 years later the Peltier effect was discovered. The Thomson effect was empirically verified in 1851. Gustav Magnus hypothesized the existence of a relationship between the temperature gradient of the junctions of a thermocouple, and the generated electric potential gradient in 1856 [46, 51].

1910–1949: It was Altenkirch who proposed the phrase "thermoelectric figure of merit" or ZT parameter for the very first time. He argued that thermoelectric matter quality increases as electrical conductivity grows and also as Seebeck coefficient raises however it drops by any increment in thermal conductivity. The small thermal

conductivity works in favor of minimizing Ohmic heating and keeping high thermal differences. The fact that lattice vibration, as well as impurity amount, has an impact on the metals' conductivity, has been shown later. According to Wilson, the electrical conductivity of semiconductors and insulators must depend on the temperature such that, the electrical conductivity must drop by the temperature reduction due to the reduction in the density of carriers [1, 46, 52, 53].

1950-1959: Ioffe (1820-1920) [54] declared that atomic mass affects the semiconductors' thermal conductivity. Heavy elements have lower thermal conductivity due to the lower concentration of carriers. Clearly, the force on the electrons grows as the number of protons grows inside the nucleus. Also, thermal conductivity is lower in the material with lower density and this may be because of their porous structure [46, 51]. Another model has been suggested later, representing some deviations from the equilibrium state of the lattice [46, 51, 53]. Goldsmith [51] investigated the crystal structure and electron mobility's effects on the conductivity. TE characteristics of the matter are affected by the mobility and the atomic mass affects the thermal conductivity. Also, he argued that the conductivity to charge mobility ratio depends on atomic mass. Furthermore, alloys made of semiconductors and isomorphous matter possess lower thermal conductivity while their electrical conductivity is just as good as the pure semiconductor confirmed by Ioffe. Therefore, there have been found various TE applications for adjusted semiconductor composites. He also suggested a measure for the materials' TE performance called ZT [1, 46, 51, 53].

1960–1969: Chasmar et. al [52] proposed a function depending on atomic mass, electron mobility, doping element, temperature, and thermal conductivity as the material parameter also called the fit parameter. In a model suggested by Ioffe, ZT is introduced to be the function of bandgap such that as the bandgap grows wider, thermal conductivity increases however this is accompanied by a reduction in electron mobility. Later, Littman and Davidson stated that due to the irreversibility of the thermodynamics of this process, it would not be possible to estimate an upper bound for the parameter ZT.

1970–2015: Dresselhaus et. al [49] declared that layering extremely anisotropic TE matter must enhance materials' figure of merit, but due to the occurrence of various

adjustments and interfaces the thermal conductivity drops, and it may take place due to a phenomenon called the phonon scattering. The superlattices do possess a limited thermal conductivity and tunneling probability is finite for quantum wells, argued by Sofo and Mahan [55]. According to their study, the quantum mixing in the alternating superlattices can alter the density of states (DOS) from 2D to 3D, yet they predicted that ZT must raise, but not as much as the prediction made by Dresselhaus and Hicks. Bulusu and Walker [53] suggested a Green's function solution in non-equilibrium conditions to evaluate the TE performance of Silicon nanolayers, Silicon/Germanium/Silicon alternating superlattices (ASL), and Silicon nanowires. Quantum effects have been modeled using the dispersion formula for every single sub-band. They also investigated the confinement and scattering impacts on the conductivity and Seebeck coefficient in ASLs.

Studies aim to increase the power factor  $(S^2\sigma)$  and decrease the thermal conductivity using bulk TE matters, and industrially commonly used matter such as Bi<sub>2</sub>Te<sub>3</sub>, PbTe, etc. Recently, it has been found that there is a novel group of matter with similar properties [56-59]. Slack's [56] model is comprised of atoms vibrating in a quantum well structure. He also proposed the phonon-glass-electron-crystal (PGEC) concept. Many other studies have been conducted on semiconductor dopings and their impact on TE performance. Novel techniques have been developed due to the studies that took place in bandgap engineering. The most important ones are binding energy levels, energy filtering, multiple-band conduction methods, and convergence of electronic bands [60-64].

The new class of TE matters presented were the nanocomposites. The new approach was to combine band engineering with nanomaterial engineering to manufacture bulk TE materials with higher response capability recommended by Kanatzidis et al. [65-67]. There are many possible strategies for improving the TE performance of the matters using some alterations in their nanostructure such as doping some additives, employing nanocomposites, etc. A study used electrical conductive polymers to produce flexible TE matter. Another class of carbon-based nanocomposites has been introduced to manufacture light devices with a high TE response.

Thermoelectric materials have attracted so much attention in different fields recently. Air-conditioned seats, compact refrigerators and cooling systems of microprocessors are some of the examples in which TE matters are used as active refrigeration tools. Also, they used as a power generation tool in solar energy generation, and waste heat recovery [50].

## 2. 2 Some concept in the thermoelectric materials

## 2.2.1 Seebeck coefficient

The ratio of open-circuit voltage to the temperature discrepancy between the two ends is called the Seebeck coefficient. The open-circuit voltage (OCV) is obtained between the hot and cold ends of the material. Seebeck Coefficient is comprised of three different sources which are electronic, phonon and electron-phonon [68, 69]. The main element affecting the Seebeck coefficient in metallic systems is the electronic source since the metallic systems possess a high number of free electrons. Here, it's possible to excite the electrons using a heat treatment, then the excited electrons immigrate from the hot end to the cold end, creating a potential difference which is the mechanism by which electric source contributes. The explained method strongly depends on the temperature such that the Seebeck coefficient increases linearly as the temperature rises [69]. Phonon drag is a phenomenon by which phonons contribute to the Seebeck coefficient. This phenomenon normally takes place at temperatures lower than 200 K due to the phonon large mean free path(MFP) [68]. Electron-phonon scattering is important only when MFP of electron and phonon are near enough which is the case in low temperatures. It's more probable to see electron-phonon scattering in conducting polymers (CP) with high enough conductivity and ordered construction at low temperatures [23, 70].

Seebeck Coefficient for massively doped polymers such as polypyrrole, polyacetylene, polyaniline, in Temperatures about 300K is a small positive number ( $<14~\mu\text{V/K}$ ) which drops linearly by temperature [68]. However, electron-phonon interactions can exhibit an impact on the relation between the Seebeck coefficient and temperature and ruin the linearity in the case of lightly doped CPs. Also, the lightly doped CPs may represent a higher Seebeck coefficient in comparison with massively doped ones [23, 68-70]. When the Seebeck coefficient's reduction is proportional to T1/2 one can use Mott's hopping conductivity mechanism between

localized states to explain [68]. 1/T dependence is due to the fact that hopping happens only between immediate neighbors in the confined states. However, in heavily doped CPs, the Seebeck coefficient depends linearly on the temperature [26, 70]. The Seebeck coefficient is the function of various parameters such as temperature, free electron concentration, constructing elements, and interior crystalline structure of the conductor.

The Seebeck coefficient of a TE matter is measured in the following manner; first of all, for a system prepared in it's steady-state both temperature and voltage are measured simultaneously. Then, the ratio of the voltage to the temperature difference must be checked to be linear. Finally, T and V are measured at the same and single point [46, 51, 71, 72]. The Seebeck coefficient is normally more than 10  $\mu\text{V/K}$  for metals and it's greater than 200  $\mu\text{V/K}$  for semiconductors and insulators. The performance of a TE matter is measured by the Seebeck coefficient or thermopower; moreover, better performance is expected only when the ratio of the TE potential to the temperature gradient is higher [46, 51]. It is possible to enhance the Seebeck coefficient. To this end, the dependence of l(E) on energy must be stronger which can be achieved using a scattering method which heavily depends on the free electron concentration. The other possibility is to intensify the energy dependence of n(E) which can be obtained by an increment in the density of states [60].

## 2.2.2 Electrical conductivity

A firm comprehension of the transport method in CPs is vital to study their TE characteristics. The joint electrons of chemically-bonded atoms with sp3 hybridized carbons in saturated insulating polymers (SIP) are restricted to orbit in the low energy orbitals of the resulting molecule, which ends in a lower concentration of free electrons and weak electrical conductivity. Nevertheless, the carbon atoms are sp2 hybridized in conjugated polymers. Basically, In every carbon atom 3 electrons from the exterior orbit form three "sigma" ( $\sigma$ )-bonds which comprise the polymer chain skeleton while a 2p electron consequently gets delocalized in  $\pi$ -electrons with a dominant electronic concentration in the plane orthogonal to the  $\sigma$  skeleton. Succeeding carbons are connected together by the pz orbitals of sp2 since they are

intersecting, in the end, delocalized electrons can move easily along the mainline of the polymer [80,88]. Peierls instability (i.e. a result of combining electronic and elastic characteristics) in the  $\pi$ -bonded Carbon atoms splits the p-band into p-(filled) and p/ (empty) bands with the creation of energy gap (Eg) within the electronic excitation spectrum. To make a duality with the conventional concept of semiconductor, the bonding orbital (p-) can be compared with the valence band of the semiconductor while the empty orbital (p/) may be compared to the conduction band. The manner in which distribution of the energy among the electronic DOS is expressed as bands with energy gap (Eg) between Highest Occupied Molecular Orbital (HOMO) and Lowest Unoccupied Molecular Orbital (LUMO) in conjugated portions of a molecule of polymer matches that of a conventional semiconductor [6, 68]. Conjugated polymers are organic macromolecules that are characterized by a backbone chain of alternating double- and single-bonds. Their overlapping porbitals create a system of delocalised  $\pi$ -electrons. Since the electrical conductivity in conjugated polymers is weak, it can be realized that conjugation alone can't provide electrical conductivity. So to increase the conductivity in polymers doping can be useful, but the doping technique has its own downsides [23].

The electrical conductivity  $(\sigma)$  of a semiconductor depends on free electron concentration and their mobility in the following manner.

$$\sigma = e \left( \mu e. n + \mu h. p \right) \tag{2.1}$$

where  $\mu$ e,  $\mu$ h, n, and p denote the electron mobility, hole mobility, number density of electrons, and number density of holes, respectively. The electrical conductivity of semiconductors alters broadly because of the great ranges in which these parameters vary, this is depicted in Figure. 2.1.

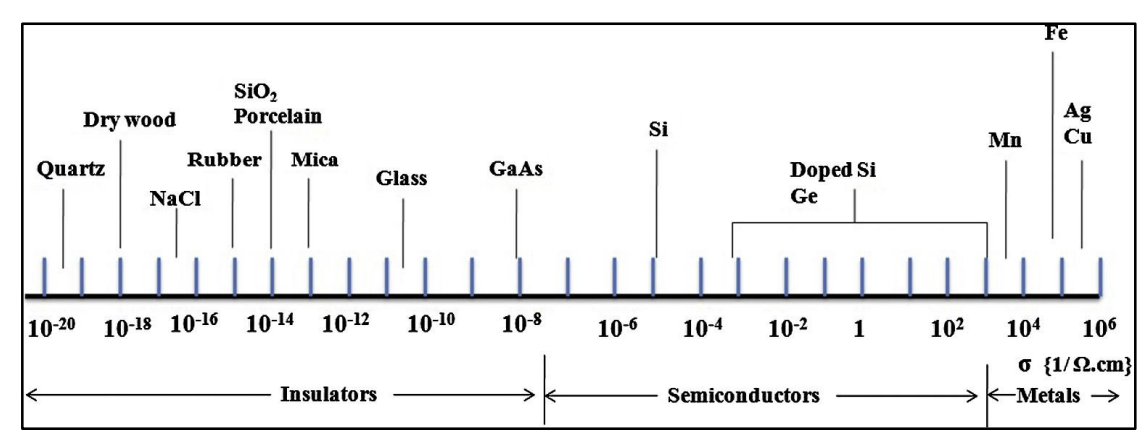


**Figure 2.1** Schematic illustration of the electrical conductivity of different compounds in 300K [73]

Conventionally, electrochemical or chemical methods are employed to dope the polymers. According to Bredas et al. [74] when it comes to polymers "doping" is a misnomer title. In fact, here, a redox reaction that converts an insulator primary polymer into an ionic compound of a polymeric cation/anion and a counterion is what we mean using doping. The counterion is the reduced/oxidized form of oxidizing/reducing agents. Those kinds of reactions are preferred via p-bonded unsaturated polymers due to the presence of p- electrons which delocalize easily without interrupting sigma bonds which keep the polymer unharmed. The doping mechanism or the process in which more free electrons got accessible in both electrochemical/chemical manner takes place in the following steps. First of all, the monomer's an oxidation/reduction reaction starts with the elimination/addition of electron from the p-system of the mainline of the chain which ends in the generation of free electrons and holes. During this process, the reduced/oxidized dopants are converted to counterions that neutralize the holes and electrons added in the pelectron system [74]. In the 2nd step, the confined charge vibration (lattice distortion) and it's ½ spin particle end in the merging of the hole with the electron and this merging is called polaron. Next, the recently formed polaron which will be either radical cation or radical anion produces lower energy electronic states in the energy gap, which have been filled by unpaired electrons. The next step is the creation of bipolaron which occurs when an electron is accepted by or removed from the polaron. Bipolaron is a spinless defect in which a radical ion pair connected with polaronic lattice distortion. Depending on the polymer's composition, bipolaron may have an interaction with 3 or 4 neighboring monomers [6].

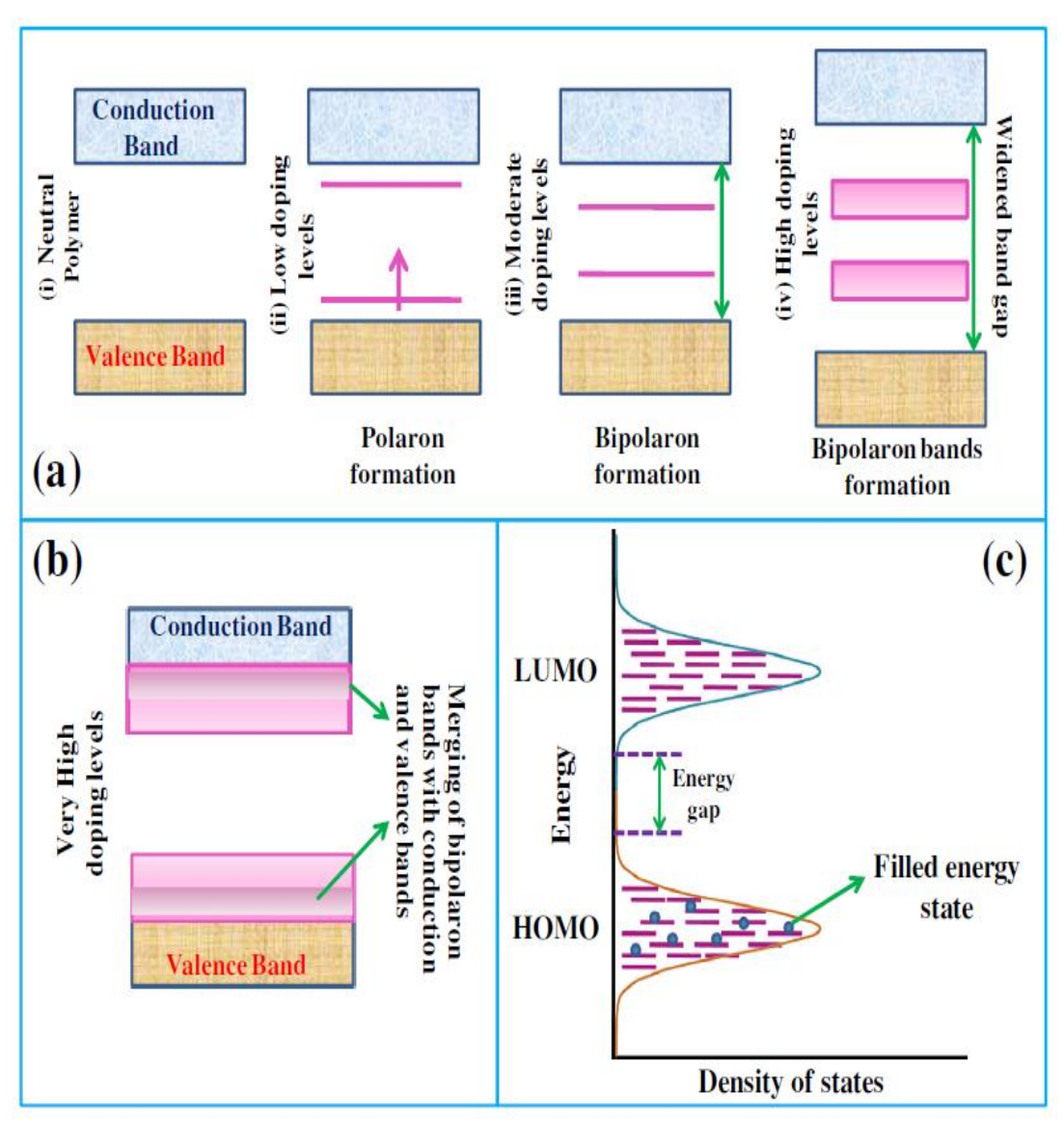


**Figure 2.2** (a) the creation of polaron, bipolaron and bipolaron bands as the doping level increases for CPs; (b) The process at extremely high doping level where the bipolaron bands merge with conduction and valence bands; (c) The distribution of confined states in the highest occupied molecular orbitals and the lowest unoccupied molecular orbitals of CPs which are Gaussian [4]

Bipolarons are thermodynamically more stable than polarons. This means that as the concentration of dopant increases, it is more probable for two polarons to join together and create a bipolaron. The formation of polaron, bipolaron and bipolaron bands as a function of the dopant concentration for different CPs is illustrated in Figure. 2.2. As has been discussed above, when the concentration of dopants is low, spin½ polarons formation is expected but as the doping amount increase, the formed polarons join together to create spinless bipolarons. As the dopant concentration increase further, the bipolarons intersect to form continuous bands.

As illustrated in Figure. 2.2 a, the formation of bipolaron bands/states makes states come forward in both valence and conduction bands which results in the enhancement of the bandgap between the valence and conduction bands. Bredas and Street [74], studied the bipolaron model and its consequences for doped polypyrrole. This model was successfully used for polythiophenes and polyparaphenylene. Nevertheless, this is not the case when the doping level is too high. In that case, upper and lower bipolaron bands join with the conduction and valence bands, respectively and form partly occupied bands just like metals, illustrated in Figure. 2.2 b. In some cases, the merging of bipolarons takes place only in the presence of remarkably large dopant concentration, for instance in the case of polypyrrole with the bandgap energy of 3.2 eV, the dopant concentration must be about a dopant per monomer unit. It can be recognized easily that for polythiophenes with the bandgap energy of 2.0 eV bipolaron bands merge with conduction and valence bands, then their electrical conductivities are comparable to the metals [68, 74].

## 2.2.3. Figure of merit (ZT)

The figure of merit (ZT) is a dimensionless parameter associated with the efficiency of thermoelectric materials which is defined in the Eq. 1.1.

Electrons/holes move by creating p-n junctions in the TE materials. Charge carriers (electrons/holes) act just like fluids in these materials, illustrated in Figure. 2.3.

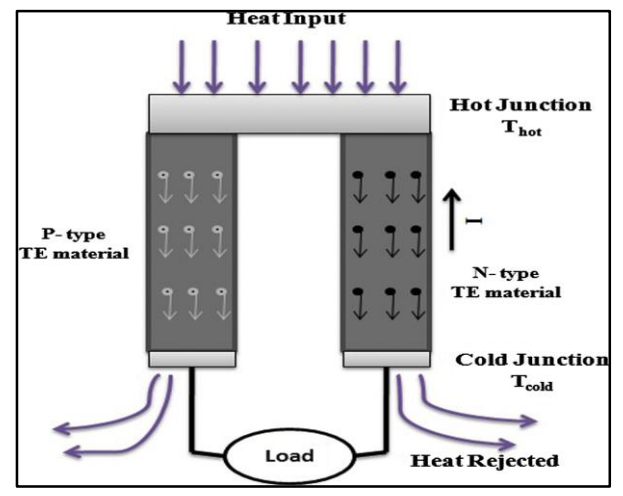


**Figure 2.3** Schematic illustration of a TE couple generating electricity in the presence of thermal gradient [75]

The electrostatic potential ( $\Delta V$ ) is generated by creating a temperature gradient between two ends of the material which in turn results in charge immigration from the hot end to the cold end. The relation between the generated TE potential and Temperature gradient ( $\Delta T$ ) is  $\Delta V$ = S.  $\Delta T$  which is obviously linear [46, 51, 52, 76]. TE transport quality depends on the nature of charge carriers and their mobility and it is evaluated by means of the figure of merit (ZT) defined by Eq. 1.1 [45, 47, 48]. This study aims to improve the figure of merit, either by raising the power factor or by decreasing the thermal conductivity. Since a high potential gradient between two ends of the device is generated when the ZT parameter is high. Hence, the best TE matters are the ones with a great Seebeck coefficient, a weak thermal conductivity, and a large electrical conductivity. Nevertheless, the Ohmic heating phenomenon must be minimized to preserve the temperature difference [46, 52, 77]. The ZT for some materials has been illustrated in Figure. 2.4.

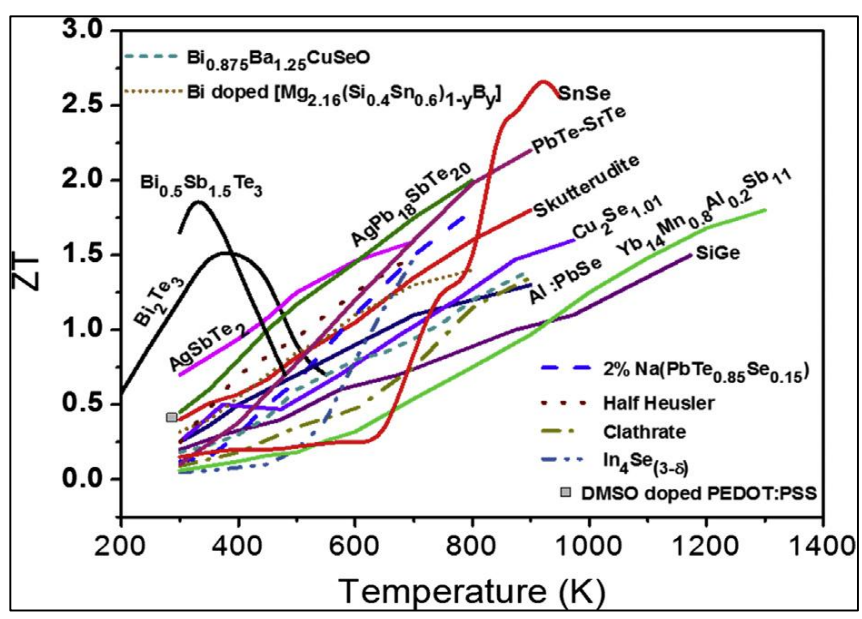


**Figure 2.4** The figure of merit for various classes of matters and their dependence on T [47]

## 2.2.4 Applications of thermoelectric materials

Thermoelectric materials possess lots of interesting applications. Extracting energy from the cars' exhaust is certainly one of them. This is mainly interesting for automaker companies since the customers prefer cars with lower gas consumption and it is possible to use this method to decrease gas consumption. TE materials also can be used to increase the combustion efficacy of wood stoves used in third world countries. Using TE matter can reduce the amount of the required wood and the produced smoke [136]. Another interesting application for TE materials is solar thermal energy conversion. It is possible to produce electricity using solar energy to create a temperature gradient across a TE material [78-81].

## 2.3 The kinds of thermoelectric materials

## 2.3.1 Inorganic thermoelectric materials

Due to their higher TE performance, conventionally thermoelectric material industries employed inorganic materials more than organic materials. Usually, Inorganic materials are categorized as skutterudites, rare earth chalcogenides, pnictogens, oxides, nitrides, Zintl phase materials, and intermetallics. There have been extensive studies on the physical characteristics, inner structure, and TE response of inorganic matter [1].

## 2.3.2 Organic thermoelectric materials

According to the figure of merit (Eq. 1.1), TE material must be electrically conductive. Although conductive organic materials are not that common, yet some classes of electrically conductive organic materials have been found recently. Conducting Polymers (CPs) such as doped polyacetylene which has been produced by Shirakawa et al. were the very first class of conductive organic materials [82]. Today, there are various CPs available. These materials are employed in electrical modules lately. The chemical formations of main CPs are demonstrated in Figure. 2.5. The 2nd class of conducting organic materials is the donor-acceptor complexes. Even though this class of conducting organic materials has been known for a longer time and there exist numerous articles on their TE performance but the studies on their applications are rare [83]. The most common donor-acceptor complex is Tetrathiafulvalene-tetracyanoquinodimethane (TTF-TCNQ) as shown in Figure.

2.6a. The charge transfer complexes don't show high conductivity. This accompanied by their low durability limits their industrial application as thermoelectric materials. However, Sun et. al [84] studied poly (metal 1,1,2,2-ethylene-tetra thiolate (PETT)) complexes as illustrated in Figure. 2.6b and reported promising thermoelectric performance.

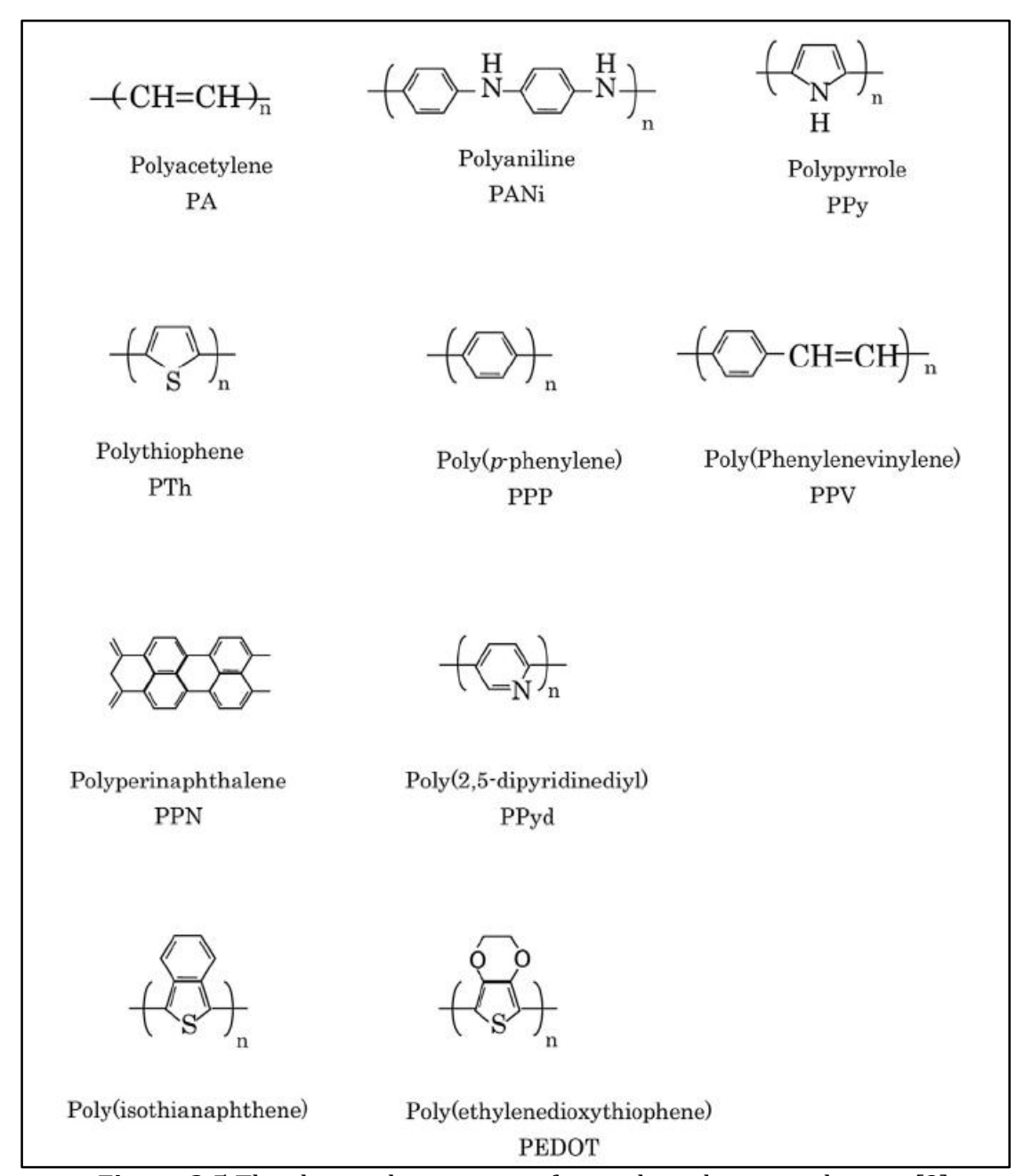


**Figure 2.5** The chemical structures of typical conducting polymers [2]

The 3rd class of organic conductive materials is carbon materials. Graphite and compressed non-crystalline carbon have been employed as a binder for electric modules. The main problem with carbon materials is their high thermal conductivity. Even though these materials show great electrical conductivity but

according to Eq. 1.1, the high thermal conductivity decreases the ZT parameter. Fullerene, graphene, and carbon nanotubes (CNTs) as shown in Figures 2.6c-e respectively, belongs to a novel class of carbon materials called nano-carbon material which has attracted great attention recently [101-104]. The electrical conductivity is high in the case of a single carbon nanotube (104–105 S/cm) however its thermal conductivity is more than 3000 W/m K, which is extremely high for a thermoelectric material. Nevertheless, the condition changes totally when carbon nanotubes gather and construct a structure called the buckypapers, which are thin layers comprised of several carbon nanotubes. The electrical conductivity for buckypapers is high just like single CNT but the thermal conductivity, in this case, is low enough to be used as organic thermoelectric material. For instance, the electrical conductivity and thermal conductivity for buckypapers composed of usual CNTs that have been produced using an arc plasma sintering are 690±16 S/cm and 0.15 W/mK, respectively [85, 86].

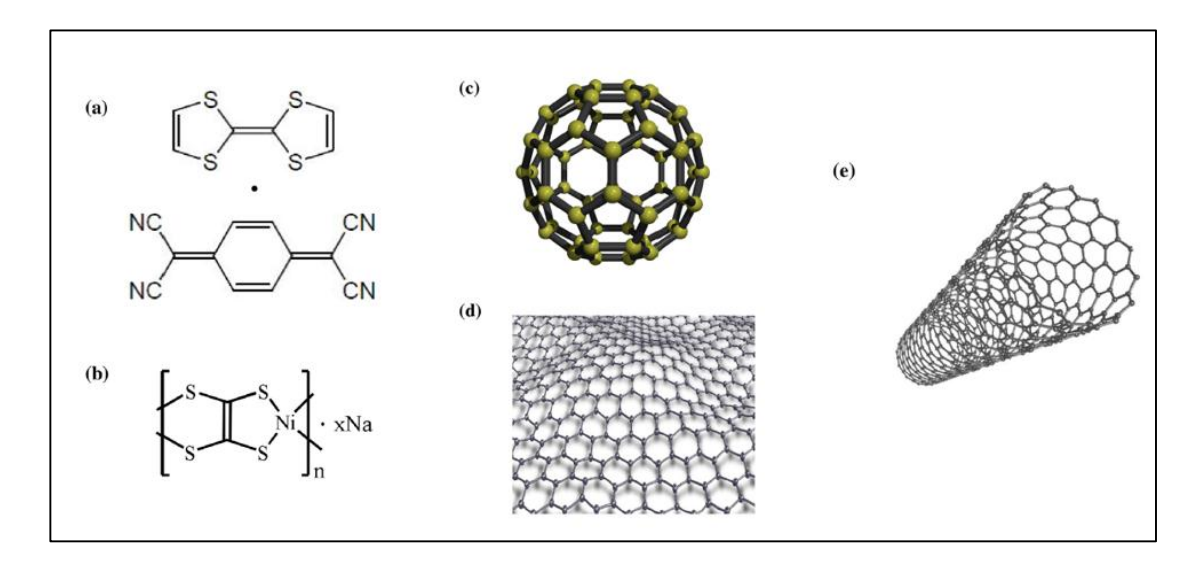


**Figure 2.6** Chemical Structures of TTF-TCNQ (a), PETT (b), Fullerene (c), Graphene (d), and CNT (e) [2]

Organic thermoelectric matters, particularly the ones which are made of CPs and vinyl polymers, show some benefits in comparison with inorganic thermoelectric matters. For instance, from the physical perspective, most of the organic thermoelectrics are thermally insulating, in the other words, their thermal conductivities are less than 1 W/mK, which is not the case for metals and in general for inorganic thermoelectrics [87]. The Wiedemann–Franz law states that the ratio of the electronic contribution of the electrical conductivity ( $\sigma$ ) to the thermal

conductivity ( $\kappa$ ) of metals and degenerate semiconductors with high charge carrier density is proportional to the temperature [88].

$$\frac{\kappa}{\sigma} = LT \tag{2.2}$$

Here L is the Lorenz constant. Since the main element of organic thermoelectric materials is carbon and carbon is abundantly found in nature, so there is no resource problem in this case. In the Figure 2.7, we can observe the evolution in the value of ZT in recent years, especially for PEDOT and Polyaniline polymers.

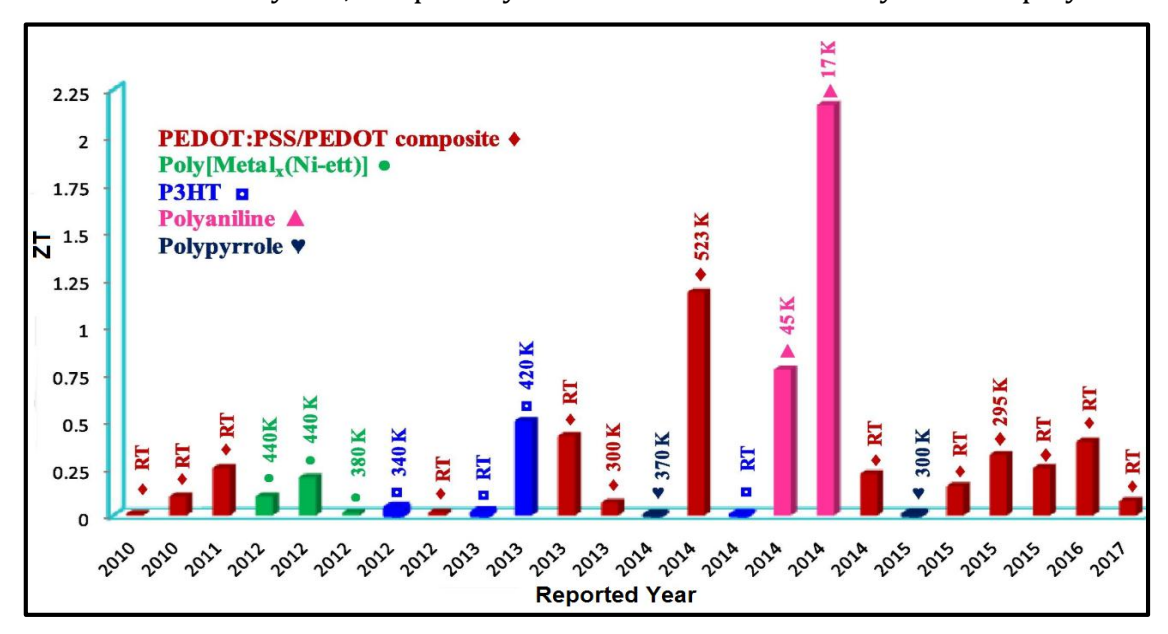


**Figure 2.7** The graphical representation shows Progress in the ZT of various conducting polymers over the years (RT is room temperature) [4].

Also, organic TE materials have flexible chemical structure and it is possible to alter the TE properties employing appropriate chemical reactions. This is another positive point for organic TE materials.

Other than that, since most of the organic thermoelectrics are eco-friendly and not harmful to mankind, it is possible to apply the devices which are made of organic thermoelectrics to the human body. On the other hand, they can be removed and destroyed without any harm to the environment after their mission is done [2].

Last but not least, due to the high plasticity of organic thermoelectrics, it's possible to manufacture components with difficult shapes. Large foils of organic thermoelectrics can be fabricated only using the printing technique, which diminishes the module manufacturing costs and enhance their utility. So using

organic TE materials can be beneficial from both economic and engineering perspectives [2].

## 2.3.2.1 Polyacetylene

Polyacetylene (PA) or polyethyne is an organic polymer with the main chain unit (C<sub>2</sub>H<sub>2</sub>)n . It's been reported that doping PA with the halogen group elements and with arsenic pentafluoride (AsF<sub>5</sub>) results in great improvements in the electrical conductivity. This process not only enhances the electrical conductivity but gives the ability to produce materials within the full range of conductivity, from nonconductive materials to material with high conductivities such as metals. Basescu et. al [90], studied the PA thin layers doped with iodine in 300K and found its electrical conductivity about 20,000 S/cm. They repeated their study in an extreme condition with T = 0.48 K and p= 10 kbar and reported the promising value of 9000 S/cm for its electrical conductivity. Park and his colleagues [91], investigated the polyacetylene doped with ZrCl<sub>4</sub>, FeCl<sub>3</sub>, NbCl<sub>5</sub>. They have measured the Seebeck coefficient and electrical conductivity in each case. The best electrical conductivity has been obtained for the polyacetylene doped with FeCl<sub>3</sub>, and it was about 28500 S/cm. Some studies have confirmed higher electrical conductivities for polyacetylene. The best has been reported is  $\sigma = 44,247$  S/cm, but the fact that polyacetylene is not soluble in most of the usual solvents and it's not stable in the air limits its utility as a TE matter. This has lead studies to investigate other polymers in order to find polymers with more durability in contact with air. Recently, some new polymers have been introduced [82, 90-92].

## 2.3.2.2 Polyaniline

Polyaniline (PANI) is a conducting polymer of the semi-flexible rod polymer family. Semi-flexible rod polymers are a kind of organic polymers that may be converted to conductive polymers using appropriate doping techniques. Polyaniline is another conductive polymer that has attracted wide attention as a promising TE material since it's cheap and does not require a high technique preparing process. Nevertheless, processing conditions and structural defects can have a great impact on the electrical conductivity of polyaniline. Polyaniline is comprised of leucoemeraldine, emeraldine, and pernigraniline. These structures are illustrated in

Fig. 2.8. Despite its low TE performance, PANI has been used in plastic and cheap TE components [93-95].

Figure 2.8 Chemical structure of PANI

Various parameters such as degree of oxidation, internal structure, and doping level can affect the electrical conductivity of polyaniline. The internal structure itself is a function of the separation between the chains, crystallinity ratio, and molecular structure. Polyaniline just like polyacetylene has shown a great enhancement of its thermoelectric response in the presence of appropriate dopants [93-95]. For instance, in the case of polyaniline doped with HCl, it has been reported that increasing the HCl concentration raises the figure of merit and electrical conductivity but, decreases the Seebeck coefficient. A group of reseachers manufactured polyaniline nanotubes doped with b-naphthalene sulfonic acid to study the influence of the disorders introduced in the molecular structure of PANI. They have found the electrical conductivity of PANI to be 7.7×10<sup>-3</sup> S/cm. They concluded that the introduced disorder interferes with the electrical conductivity through modification in the mean free path of charge carriers [96]. Due to the promising properties of both inorganic matters and CPs, the studies based on producing nanocomposites using these materials have been extended recently [96]. The resulting nanocomposites will be utilized in manufacturing flexible TE components with extremely high TE response [94].

## 2.3.2.3 Poly(2,7-carbazole)

Polycarbazole (PCB) is an electrically conducting polymer obtained by the polymerization of carbazole. Due to the existence of oxidized nitrogen in the backbone of PCBs and the fact that charges are localized in them, PCBs enjoy a large Seebeck coefficient, but simultaneously these properties result in low electrical conductivity. The molecular arrangement of poly (2,7-carbazole) is depicted in

Figure.2.11 The effects of doping have been investigated in a study by a group leading by Aich in which they have prepared doped poly(2,7-carbazole). According to their study, a secondary alkyl chain is added to the carbazole along the backbone due to the presence of a doping agent. This will raise both conductivity and Seebeck coefficient to 500 S/cm and 70  $\mu$ V/K, respectively. They also found an enhancement in the air stability of polycarbazole after the doping, with PF about 19  $\mu$ W/mK² [97].

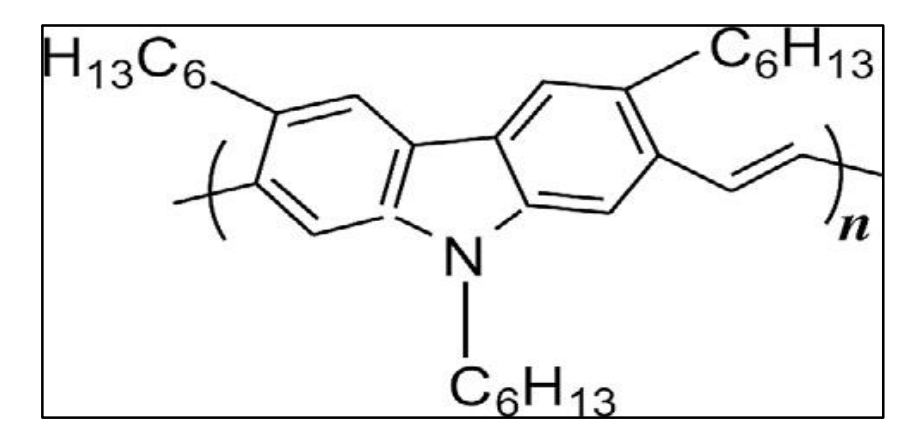


**Figure. 2.9** Chemical structure of poly (2,7-carbazole) [97]

## 2.3.2.4 Poly (3-hexylthiophene) (P3HT)

The next group of organic conductive polymers is regionegular (RR) P3HT. The rrP3HT because of its ubiquity, easy processing techniques and ensuring conductivity is an excellent semiconducting polymer [98, 99]. Despite its promising properties, there are too few studies conducted upon rrP3HT. Crispin et al. [100] studied the TE characteristics of drop-casted P3HT thin layers doped with acetonitrile (NOPF6). They have reported, an increment in power factor (PF) from  $10^{-10}$  W/m K<sup>2</sup> to  $1.4 \times 10^{-7}$  W/m K<sup>2</sup> for the dopant concentration in the range of 20 to 30 percent. Another team repeated the experiments using benign ferric as a dopant and they observed power factor increases tremendously up to 20 μW/m K², which is the greatest PF recorded in doped P3HT thin layers. For triflimide (TFSI)-doped P3HT thin layers, figure of merit is measured to be about 0.04 at T=340K and assuming  $k \sim 0.2$  W/mK which indicates that an optimized CP can be used as an economic plastic TE material [101]. The energy filtering effect of nanocomposites comprised of inorganic materials and organic conductive polymers has been proposed as a technique for increasing the Seebeck coefficient and power factor. According to basic quantum mechanics, it is possible to scatter low energy particles using a potential step with appropriate height. In this case, the P<sub>3</sub>HT/Bi<sub>2</sub>Te<sub>3</sub> interface has been used as a potential step for scattering low energy electrons. This technique has improved the power factor up to 13.6 μW/m K<sup>2</sup>, which is much greater than the power factor for pure P3HT which was about 3.9 μW/m K<sup>2</sup>. Muller et al. [102] revealed that the TE response of conductive polymers can be improved by manufacturing nanocomposites comprised of CPs and CNTs accompanied by optimized p-doping. They have reported, the power factor for a nanocomposite layer of multi-wall CNT and P3HT doped with ferric chloride is found to be about 6  $\pm 2 \mu W/m K^2$  which has been increased a lot in comparison with 0.2  $\pm$  0.1  $\mu W/m K^2$ of pure CP composite layers. It has been found the same pattern in the case of nanocomposite layers of single-wall CNT and P3HT doped with ferric chloride, where PF was measured to be about  $95 \pm 12 \,\mu\text{W/m}$  K<sup>2</sup> at 300K. Also, ZT was about 0.015 in the latter case while this parameter's value is much smaller for an undoped film  $(7 \pm 2 \times 10^{-4})$ . Lee and his colleagues [103] studied the influence of different coating techniques and ink(single-wall Carbon nanotubes or SWCNTs) concentration on the TE performance of the nanocomposites made of CPs and carbon nanotubes. They used spiral drawdown rod coating also known as Wire Bar Coating (WBC) which is an excellent method to apply a coating film on thin and flexible materials. The main advantage of WBC to the drop-casting method is that in WBC the doping stage has been removed from the process. Eventually, this team applied a solution of SWCNT as a coating on P3HT polymer using WBC which increased the power factor up to 105 μW/m K<sup>2</sup> at 300K. Endrődi and his team [99] studied the thermoelectric properties of the nano threads of P3HT doped with silver perchlorate (AgClO<sub>4</sub>). Their best result was something about  $6.84 \pm 0.64 \,\mu\text{W/m}$  K<sup>2</sup> of power factor which has been achieved only by controlling the nanostructure of the P3HT and deposition of the dopants. They also reported an increment in the figure of merit up to 0.0026 at 25 °C. Xu et. al [104] have studied the possibility of using P3HT as a TE energy generator. They reported an improvement both in thermal expansion and electrical conductivity of Phenyl-C<sub>61</sub>-butyric acid methyl ester (PCBM) doped P3HT material with increasing dopant concentration and photoexcitation, separately. Both together have increased the figure of merit to the highest reported value of 0.5 at 420K.

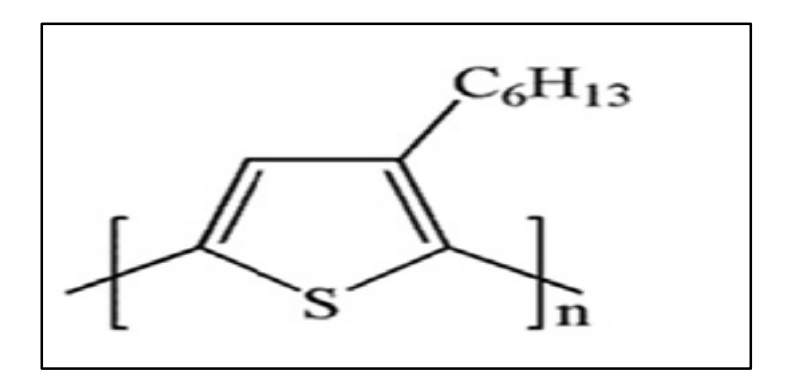


Figure. 2.10 schematic illustration of P3HT

## 2.3.2.5 Poly (3,4-ethylene dioxythiophene) (PEDOT)

Poly (3,4-ethylene dioxythiophene) is one of the most promising CPs as a thermoelectric material. PEDOT is highly conductive highly stable and easy to process. Doping poly (3,4-ethylene dioxythiophene) with poly (styrene sulphonate) simplifies the processing of PEDOT in the aqueous phase. Poly (styrene sulphonate) (PSS) is used because of its ion-exchange properties. PEDOT: PSS is used extensively in electric components such as solar cells as an organic TE material. PEDOT: PSS is comprised of the coupled poly (3,4-ethylene dioxythiophene) with a positive charge and negative poly (styrene sulphonate) depicted in Figure.2.11 PSS is used as a dispersing agent and stabilizer for PEDOT to increase its durability in aqueous media.

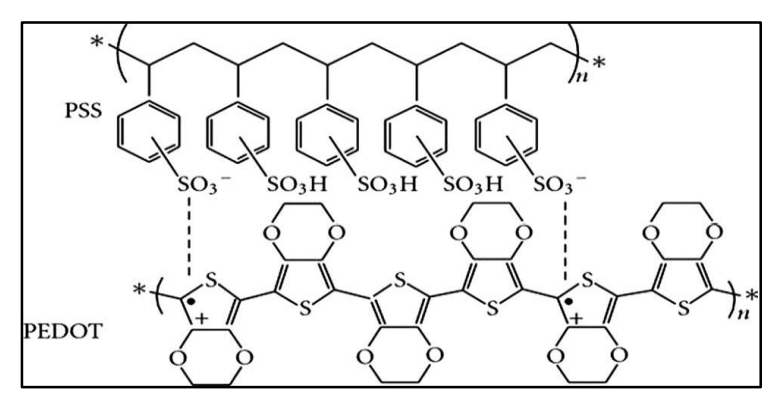


Figure. 2.11 Chemical structure of PEDOT: PSS

PEDOT: PSS is the most commercially employed CP. It is mostly seen in the aqueous dispersion form which is a dark blue transparent suspension. PEDOT: PSS can be

applied easily over any kind of surface by several aqueous coating methods. Some of the methods which have been utilized in literature are: spin casting, wire bar coating, spraying, etc. The PEDOT:PSS thin layer coating is smooth and depending on the coating method and quality, its roughness is about 5 nm. Also, the thin enough layer of this coating is transparent for the wavelength range between 380 nm and 700 nm. The transmittance (T) for a film of PEDOT: PSS with 100 nm thickness is 90 percent for the green light. The electrical conductivity of PEDOT:PSS depending on the solution processing, doping agent and its concentration can be anywhere between 10<sup>-2</sup> and 103 S/cm. The work function is the next property that has been studied for PEDOT:PSS which is something between 5.0 and 5.2 eV that it is a great number for a polymer. The great conductivity accompanied by high work function makes PEDOT:PSS films proper catalyst. Accelerated charge transfer is the phenomenon that is allowed for material with high conductivity and work function. PEDOT: PSS films are stable in direct contact with air stream which was a problem for most of the conductive polymers discussed before. Because of the named characteristics, PEDOT: PSS and even pure PEDOT have been used widely in thermoelectric devices.

# 2.4 Strategies for Improvement of the Thermoelectric Performance 2.4.1 Doping.

Appropriate doping can increase the electrical conductivity of polymers but it also diminishes the Seebeck coefficient. So doping has its own advantages and disadvantages regarding thermoelectric performance. Dopants such as halogens, FeCl<sub>3</sub>, MoCl<sub>5</sub>, etc have been used widely in thermoelectric polymers [105]. PEDOT: PSS as an organic conductive polymer has been studied more than most of the CPs due to it's promising thermoelectric properties, great durability in required media, and its high electrical conductivity. Its utilization in the organic light-emitting diodes is one of the most known examples [15, 106, 107]. TE response of PEDOT: PSS heavily depends on the number of ionized doping agents, since ionized dopants can decrease the electrons mean free path and in turn the TE performance. Nevertheless, PSS usually has a neglectable ionizing ratio. Recently, a group leading

by Kim [16] achieved the highest ever figure of merit for organic CPs of 0.42 using the appropriate solution in which PSS is ionized even less.

## 2.4.2 Doping Mechanisms of conjugated polymers

According to the IUPAC gold book, a dopant is a charge-transfer agent that generates positive or negative charges in natural CPs by oxidation or reduction. So doping can be used to modify the electron/hole concentration. There are mainly two mechanisms in which doping affects the charge carriers' concentration. First is redox doping which transports electrons and creates a donor-acceptor complex. The second one which is called acid-base doping transports cations and anions in the polymers' skeleton's mainline. Doping methods are illustrated schematically in Figure.2.12. The charge neutrality is preserved due to the creation of counterions in the case of acid-base doping [108].

During doping, it is observed that the structure of the polyaromatics is modified locally accompanied by a more quinoidal conformation. Doping efficacy is measured by the highest occupied molecular orbital and the lowest unoccupied molecular orbital levels of conjugated polymers, and by the parameter that demonstrates the number of created electrons and holes due to the addition of a molecule of dopant [109-111].

Environmental factors such as light, air, and temperature can affect the doping level. It is possible to limit materials' contact with light and air using various techniques such as isolation, but since thermoelectric materials' working foundation is based on the temperature difference, temperature differences are not avoidable. Consequently, the doped state must be highly stable in thermally hazard conditions, in addition to the factors which have been named before, otherwise, the thermoelectric device will experience progressive corrosion during the process [108].

The acid-base doping is the addition of a H+ to the backbone of a CP, during which a p-type semiconductor is produced. One of the most well-known examples is an emeraldine base of polyaniline. An emeraldine doped with Camphorsulfonic acid (CSA) or 4-Dodecylbenzenesulfonic acid (DBSA) is a highly conductive semiconductor with  $\sigma > 100$  S/cm.

Acid-base doping is a method that can be used on various polymers such as Poly(3-hexylthiophene) known as P3HT and Poly[2,5-bis(3-alkylthiophen-2-yl)thieno(3,2-b)thiophene] known as PBTTT. Today, there are several practical doping methods. For instance, exposing polythiophene(PT) to the perfluorooctyltrichlorosilane (FTS) steam is the one in which chlorosilane (SiH<sub>3</sub>Cl) hydrolyzes and creates HCl during the doping process [108].

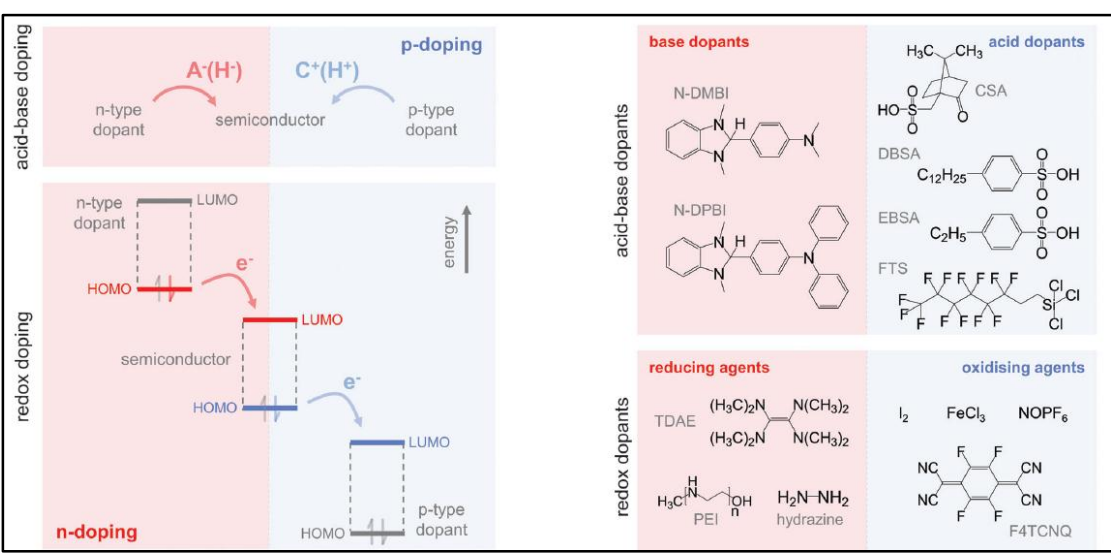


**Figure 2.12** illustrates the both doping methods (left) and the common dopants used in those methods (right) [108]

A similar thing happens in the case of N-DMBI and N-DPBI, but in this case H- is added to the backbone of the conjugated polymer. This is a method called base doping during which an n-type semiconductor is produced. N-DMBI and N-DPBI are created from benzimidazole Figure.2.12 these compounds are stable in direct contact with the airstream. Schlitz et al. [112], applied the base doping method on the napthalenedicarboximide-bithiophene copolymer P(NDIOD-T<sub>2</sub>) using both N-DMBI and N-DPBI as dopant, successfully.

## 2.4.3 Addition of Carbon Nanotubes (CNTs)

Carbon nanotubes are identified with their stable 1D nanostructure and unique electrical characteristics. So they can enhance the TE performance of CPs when they are added to their structure. A study conducted by Kim and his colleagues [113] confirmed that PEDOT: PSS mixed with CNTs due to the enhanced electron mean path may exhibit better conductivity. Also, Since CNTs and PEDOT: PSS particles have different vibration frequencies, the heat transfer is troubled in their mixture and this leads to a reduced thermal conductivity [114, 115]. The max figure of merit

obtained was 0.02 which was when 35 weight percent of carbon nanotubes were added to the PEDOT: PSS chemical structure. But exceeding this threshold can decrease thermoelectric performance heavily. Adding further CNTs will result in reduced electrical conductivity and the Seebeck coefficient while it increases the thermal conductivity [115].

## 2.4.4 Polymer Composite.

Doping with the inorganic matter has utterly different consequences. Inorganic dopants such as Tellurium used mostly in the form of nanotubes but  $Bi_2Te_3$  and  $Ca_3Co_4O_9$  have been used in the form of powder [116-118]. The reason these compounds have been chosen is their high Seebeck coefficient. Tellurium nanotubes' effects on thermoelectric materials have been studied by See and his team and they observed fairly similar behavior to the CNTs as the electrical conductivity was improved and thermal conductivity was reduced. They tried to explain the shockingly positive Seebeck coefficient by considering holes only as a charge transporting agent which does not take place through the polymer entirely. The best result they got was ZT=01 at 300K.

## 2.4.5 Addition of Semiconducting Stabilizer

Carbon nanotube (CNT) is a hydrophobic compound so it's not stable in aqueous media and its' dispersion in water is so limited [119, 120]. To stabilize the CNT composites in the aqueous media normally stabilizers are employed. Surfactants are widely used to help the CNT dispersion in an aqueous medium. The other option to help CNTs to disperse in water are CPs which can enhance the electrical conductivity [113, 121-123]. Moriarty et al. [124] studied the thermal conductivity of polymercarbon nanotube solutions doped with DOC and TCPP, separately and reported a reduction in thermal conductivity. Moriarty claimed that during this process tube-to-tube joints have been blocked and this, in turn, has hindered the phonon motion which is the reason for the observed reduction of thermal conductivity. On the other hand, the stabilizing agent works as a scattering barrier for the phonons since it's been implanted in the composite adjacent to the carbon nanotubes. There other parameters that may be responsible for the reduction of thermal conductivity such as the morphology of the CNTs, the distance between two neighboring tubes and the

defects which have been created in the nanostructure due to the presence of carbon nanotubes [113, 121-123].

## 2.4.6 Nanostructured Thermoelectric Materials

Using nanofibers may improve the performance of TE devices. Since the nanofibers are considered as a one-dimensional material, they are useful as they reduce the thermal conductivity while leaving electrical conductivity unchanged, which can increase the figure of merit. There are many studies conducted on increasing ZT by modifying the thermal and electrical conductivities [125].

It may be possible to enhance electrical conductivity by quantum confinement effects that describe electrons in terms of energy levels, potential wells, valence bands, conduction bands, and electron energy band gaps. An example of these effects is Quantum dots (QDs) which are some artificial nanoscale crystals that can transport electrons. When UV light hits these semiconducting nanoparticles, they can emit light of various colors. Using QDs one can increase the concentration of electrons around the Fermi energy [124]. On the other hand, there are some practical methods to diminish the thermal conductivity. These methods mechanism mainly is phonon scattering using superlattices. An optimized Superlattice can both enhance the electrical conductivity and decrease thermal conductivity. Usually, electrical and thermal conductivity are entangled in CPs [126]. Normally, this is because of the fact that while the rise in the number of charge carriers can be beneficial for electrical conductivity, in the meantime it increases the number of collisions between the particles and with the walls of crystalline structure, therefore it raises the thermal conductivity. The nanostructures can help to improve this condition. They can disentangle thermal and electrical conductivities as they can block the phonons while helping electron transportation. This way they decrease the thermal conductivity and increase the electrical conductivity in CPs which is in favor of the thermoelectric performance of TE materials [127, 128].

Besides, it is possible to disentangle the impacts of thermal and electrical conductivity, if the characteristics of the heat transfer through phonons and electrical conductivity by electrons are understood. Since it is known that the MFP for phonons is in the order of 100 nm while this number for electrons is normally

less than 10 nm, it is possible to limit the mean free path of phonons without affecting electrons. Also, due to the fact that electrons and phonons do possess a different range of energies and phonons' energy is much less than electrons. So, it is possible to introduce some scattering steps for phonons, without bothering electrons. With electrical conductivity not changed and thermal conductivity reduced, the figure of merit which is a parameter to measure thermoelectric performance is improved [129].

During this chapter, we have investigated the potentials of CPs as a TE material. Due to their poor thermal conductivity and the possibility of developing electrical conductivity using appropriate dopants, they have been identified as a potential thermoelectric material. This potential can be investigated more and more by evaluating the TE response of CPs in the nanoscale using the electrospinning method, chemical vapor deposition method, electrodeposition method, etc. [130]

## 3.1. Instruments

## 3.1.1 Conductivity Meter (Four Point Probe)

Four-point technique was used for conductivity measurements of thin films and pellets prepared from synthesized polymers. In this technique, four ends with a certain distance from each other are placed on the surface of the sample to be measured. When alternating current or direct current is applied, voltage drops between the two points in proportion to the sample resistance and voltage difference occurs between the two inner ends. The device converts it to resistance and electrical conductivity using the corresponding equations. The photograph of the Four Point Probe measurement device of Entek brand FPP 470 used in this study is given in Figure 3.1.



**Figure 3.1** Four point probe measuring device

#### 3.1.2. Seebeck Coefficient Meter

Seebeck coefficient measurement from thin films and pellets prepared by pouring into the microscope glass of the synthesized polymers was taken from the Entek brand SC 001 model device given in Figure 3.3.



Figure 3.2 Seebeck coefficient measuring system.

## 3.1.3 X-Ray Photoelectron Spectroscopy (XPS)

The testing of the synthesized polymers by providing atomic and molecular information about this steady by used Thermo Scientific K - Alpha X - Heat Photoelectron Spectrometer was used. Tests were provided the levels of the photoelectrons billet and electrostatic level of the film sample information by XPS analysis. Separation of each element examined by XPS analysis after obtaining the raw crude XPS data, this experimental data is the best the binding energy values were determined by the curve fitting method.

## 3.1.4 Scanning electron microscope (SEM)

The morphology of the samples were characterized using a field –emission scanning electron microscope (FE-SEM; PhilipsXL30FEG, FEL Co., Hillsboro, OR, USA) with an accelerating voltage of 5 kV and high resolution transmission electron microscope (HRTEM; JEOL JEM-2100 F, JEOL Ltd., Akishima, Tokyo, Japan).



Figure 3.3 Scanning electron microscope (SEM)

## 3.1.5 X-Ray Diffractometer (XRD)

Rigaku's D / Max-Ultima + / PC XRD device was used to determine the crystal structure. The diffraction pattern of the crystal is given as a result of q, 2q and 2q / q scans with the copper targeted x-ray tube and detector movement of the device. After X-ray is sent to the sample in XRD analysis, samples are obtained at an atomic level from the diffraction pattern obtained by breaking the beam at different angles and intensity according to the crystal structure. XRD analysis enables reliable and very precise data collection, for example, about the crystal structure.

## 3.1.6 Infrared-Reduced Total Reflection Spectroscopy with Fourier Transform

In Perkin Elmer Spectrum One FT / IR, Perkin Elmer Universal ATR was used for structure determination of synthesized polymers with Fourier transform infrared spectrophotometer (FTIR) with sample accessories. FTIR-ATR spectra were taken from the solid state of the polymer samples.

## 3.1.7 Ultraviolet-Visible Region Spectroscopy

UV spectra were taken with Shimazdu brand A109351 05066 model UV mini-1240 UV-vis spectrophotometer, which is shown in Figure 3.1. The absorbance values read from the UV-vis spectrophotometer were obtained as a result of the calculation made by using the logarithm according to the "e" base of the device. Dilute aqueous solutions of polymer samples were prepared and measured in quartz cuvettes.



**Figure 3.4** Ultraviolet-Visible Region Spectroscopy

## 3.1.8 Sonicated homogenizer.

The composites were prepared in various proportions of PEDOT:PSSA and TiS<sub>2</sub> powder by either non-sonicating (just mixing) or sonicating with a sonicated homogenizer.



**3.5 Figure** Ultrasonic homogenizer

## 3.2 Materials

3,4-Ethylene dioxythiophene (EDOT), poly (4-styrene sulfonic acid) (PSSA), Polyvinyl alcohol (PVOH), hydrogen peroxide (H<sub>2</sub>O<sub>2</sub>), Zinc chloride (ZnCl<sub>2</sub>), Zinc acetate dehydrate (Zn(CH<sub>3</sub>COO)<sub>2</sub>.2H<sub>2</sub>O), Glucose (C<sub>6</sub>H<sub>12</sub>O<sub>6</sub>), Cesium carbonate (Cs<sub>2</sub>CO<sub>3</sub>), Titanium sulfur (TiS<sub>2</sub>), Thiourea (CH<sub>4</sub>N<sub>2</sub>S), Tetra-n-butyl ammonium bromide (TBAB) ((CH<sub>3</sub>CH<sub>2</sub>CH<sub>2</sub>CH<sub>2</sub>)<sub>4</sub>NBr), Ethylene glycol (C<sub>2</sub>H<sub>6</sub>O<sub>2</sub>), copper (I) chloride (CuCl) and copper nitrate hydrate (Cu(NO<sub>3</sub>)<sub>2</sub>.H<sub>2</sub>O) were purchased as analytical reagent grade from Sigma-Aldrich Company Ltd. and used without purification.

## 3.3 Methods

## 3.3.1 Synthesis of the samples PEDOT:PSSA

The samples PEDOT:PSSA were synthesized using a similar technique but with different amounts of 3,4-Ethylene dioxythiophene (EDOT), poly (4-styrene sulfonic acid) (PSSA), hydrogen peroxide (H<sub>2</sub>O<sub>2</sub>), copper nitrate hydrate (Cu(NO<sub>3</sub>)<sub>2</sub>.H<sub>2</sub>O) and water.

## 3.3.1.1 Synthesis of the samples PP 1 (PEDOT:PSSA 1)

To create this sample, first, we prepared a PSSA solution using 1.035g PSSA (30%) and 10 milliliters of deionized water. Then we put 0.11 g EDOT into the solution and stirred it for half an hour before adding 0.073 g  $H_2O_2$  drop by drop to the resulting solution. Eventually, we added 0.0007 g ( $Cu(NO_3)_2.8H_2O$ ) to the solution and it has been stirred for 4 hours. The resulting solution's color was dark blue.

## 3.3.1.2 Synthesis of the samples PP 2 (PEDOT:PSSA 2)

This time, the PSSA solution was prepared using 1.76 g PSSA (30%) and 10 milliliters of deionized water. Then 0.11 g EDOT was put into the solution, and the solution was stirred for 24 hours before 0.3 g  $H_2O_2$  was put drop by drop into the solution. Eventually, 0.0001 g ( $Cu(NO_3)_2.8H_2O$ ) was added to the solution and again it has been stirred for 4 hours. Yet, the final PEDOT:PSSA solution was dark blue.

## 3.3.1.3 Synthesis of the samples PP 3 (PEDOT:PSSA 3)

To prepare this sample, the PSSA solution was prepared employing 1.76 g PSSA (30%) and 10 milliliters of deionized  $H_2O$ . Then 0.11 g 3,4-Ethylenedioxythiophene (EDOT) was put into the solution, and the solution was stirred for half an hour before 0.3 g  $H_2O_2$  was put drop by drop into the solution. Eventually, 0.0007 g ( $Cu(NO_3)_2.8H_2O$ ) was added to the solution and again it has been stirred for 24 hours. Once again, the final PEDOT:PSSA solution was dark blue.

## 3.3.1.4 Synthesis of the samples PP 4 (PEDOT:PSSA 4)

For the 4th sample, 15 milliliters of deionized water were used to prepare the PSSA solution instead of 10, and instead of 1.76 g PSSA, 1.1 g PSSA (30%) was put in. Yet the solution was stirred for half an hour before 0.3 g Hydrogen peroxide was added drop by drop into the solution. Eventually, 0.0001 g (Cu(NO<sub>3</sub>)<sub>2</sub>.8H<sub>2</sub>O) was added to the solution, and it has been stirred for 24 hours. No alteration was detected in the color of the final solution.

## 3.3.1.5 Synthesis of the samples PP 5 (PEDOT:PSSA 5)

Since the concentration of the initial PSSA solution plays an important role in the quality of the final product, in the 5th specimen, 1.54 g PSSA (30%) was dissolved in only 8 milliliters of deionized  $H_2O$ , while other parameters were completely fixed

compared to the 4th specimen. The solution was stirred for half an hour before 0.3 g Hydrogen peroxide was added drop by drop into the solution. Eventually, 0.001 g (Cu(NO<sub>3</sub>)<sub>2</sub>.8H<sub>2</sub>O) was added to the solution, and it has been stirred for 24 hours. Yet, no alteration was detected in the color of the final solution.

## 3.1.6 Synthesis of the samples PP 6 (PEDOT:PSSA 6)

To prepare this sample, the PSSA solution was prepared using 1.76 g PSSA (30%) and 12 milliliters of deionized  $H_2O$ . Then 0.11 g 3,4Ethylenedioxythiophene (EDOT) was put into the solution, and the solution was stirred for half an hour before 0.3 g Hydrogen peroxide was put drop by drop into the solution. Eventually, 0.003 g ( $Cu(NO_3)_2$ .  $XH_2O$ ) was added to the solution and again it has been stirred for 24 hours. Once again, the final PEDOT:PSSA solution was dark blue.

## 3.3.1.7 Synthesis of the samples PP 7 (PEDOT:PSSA 7)

0.11 g EDOT was added to the 1.76 g PSSA (30 %) solution, and adding to 54 ml deionized water then the mixture was stirred vigorously for 1 hour and 0.3 g  $H_2O_2$  was added drop by drop as the oxidation solution, finally 0.001 g (Cu ( $NO_3$ )<sub>2</sub>.8H<sub>2</sub>O) was put into the above mixture, then the mixture was stirred vigorously for 24 hours, then the PEDOT:PSSA was obtained as a dark blue solution.

## 3.3.1.8 Synthesis of the samples PP 8 (PEDOT:PSSA 8)

0.11 g EDOT was added to the 0.9 g PSSA (30 %) solution, and adding to 33 ml deionized water then the mixture was stirred vigorously for 1 hour and 0.3 g H<sub>2</sub>O<sub>2</sub> was added drop by drop as the oxidation solution, finally 0.001 g (Cu (NO<sub>3</sub>)<sub>2</sub>.8H<sub>2</sub>O) was put into the above mixture, then the mixture was stirred vigorously for 24 hours, then the PEDOT:PSSA was obtained as a dark blue solution.

## 3.3.1.9 Synthesis of the samples PP 9 (PEDOT:PSSA 9)

0.11 g EDOT was added to the 0.275 g PSSA (30 %) solution, and adding to 15 ml deionized water then the mixture was stirred vigorously for 1 hour and 0.3 g  $H_2O_2$  was added drop by drop as the oxidation solution, finally 0.001 g (Cu ( $NO_3$ ) $_2.8H_2O$ ) was put into the above mixture, then the mixture was stirred vigorously for 24 hours, then the PEDOT:PSSA was obtained as a dark blue solution.

## 3.3.1.10 Synthesis of the samples PP 10 (PEDOT:PSSA 10)

0.11 g EDOT was added to the 1.76 g PSSA (30 %) solution, and adding to 20 ml deionized water then the mixture was stirred vigorously for 1 hour and  $0.32 \text{ g H}_2O_2$  was added drop by drop as the oxidation solution, finally 0.007 g Cu (NO<sub>3</sub>)<sub>2</sub>.8H<sub>2</sub>O was put into the above mixture, then the mixture was stirred vigorously for 24 hours, then the PEDOT:PSSA was obtained as a dark blue solution by means of oxidation of EDOT with a mild oxidant, hydrogen peroxide, and a small amount catalyst, Cu(NO<sub>3</sub>)<sub>2</sub>.

## 3.3.1.11 Synthesis of the samples PP11 (PEDOT:PSSA 11)

The same previous method as for preparing the PP11 polymer was used but there is a difference in the value of the power factor.

## 3.3.1.12 Synthesis of the samples PP12 (PEDOT:PSSA 12)

The same previous method as for preparing the PP11 polymer was used but there is a difference in the value of the power factor.

## 3.4. Synthesis of ZnS

The zinc sulfide (ZnS) samples were synthesized using a similar technique but with different amounts of reductants or surfactants.

## 3.4.1 Synthesis of ZnS-PVOH

Polyvinyl alcohol (PVOH) which is a water-soluble synthetic polymer has been used as a dispersant. PVOH (2%) was prepared by mixing 2 milliliters of 10 % stock solution of PVOH and 18 milliliters deionized  $H_2O$ , then the resulting solution was stirred using a magnetic apparatus. Next, the main solution was prepared by mixing 0.5 g ( $Zn(CH_3COO)_2.2H_2O$ ) with 50 mL deionized  $H_2O$  and adding it to PVOH solution, then 0.99 g thiourea ( $CH_4N_2S$ ) adding to 5 mL deionized  $H_2O$ , then we were adding it to main solution drop by drob.

Eventually, the pH of the solution was adjusted to be 9 applying ammonia solution drop by drop. In the end, the thiourea solution was mixed with the main solution. A magnetic treatment, and a heat treatment, which have been conducted in 70 C, were used, and a milky solution was achieved.

## 3.4.2 Synthesis of ZnS-G

Glucose (G) was employed as a capping agent which primarily acts as a stabilizing agent and provides colloidal stability along with preventing agglomeration and stopping uncontrolled growth. By mixing 0.76 g of thiourea with 10 milliliters deionized H<sub>2</sub>O, a thiourea solution was made. Then 1.8 g of glucose has been put in 20 mL deionized water and a solution of glucose was prepared. Mixing these two solutions and adding a solution that is comprised of 2.195 g (Zn (CH3COO)<sub>2</sub>.2H<sub>2</sub>O) and 10 mL deionized water would result in a raw solution that was demanded. Eventually, it is stirred and heated at 50 C for 6 hours.

## 3.4.3 Synthesis of ZnS-TBAB

Tetra-n-butyl ammonium bromide (TBAB) was used as a capping agent and surfactant which is used to lower the surface tension between two liquids, between a gas and a liquid, or between a liquid and a solid. Just like the previous solution, a thiourea solution was prepared by the addition of 0.07 g thiourea to 10 milliliters deionized H<sub>2</sub>O, then in contrast with the last sample, a solution of TBAB was prepared by the addition of 0.02 g of TBAB to 5 mL deionized water. Mixing these two and adding another solution comprised of 0.22 g (Zn(CH<sub>3</sub>COO)<sub>2</sub>.2H<sub>2</sub>O) in 10 mL deionized water, would result in a raw solution that was demanded. Eventually, it was stirred using magnetic stirrer and heated at 60 C for 4 hours.

## 3.4.4 Synthesis of ZnS -EG

ZnS-EG solution was prepared in the following steps; first, the ZnS NPs were prepared by dissolving 1.3628~g of  $ZnCl_2$  in 15 milliliters of EG, then it was stirred using a magnetic stirrer. Next, a thiourea solution was synthesized by the addition of 3.806~g of it to 20~mL EG, and the thiourea solution was added to the ZnS solution drop by drop. Eventually, the final solution was heated to  $80~^{\circ}C$  gradually, then a stirring process took place under nitrogen gas for 4~hours. The outcome of this process was a cloudy solution.



**Figure 3.6** Method for preparing Zinc sulfide.

# 3.5. Synthesis of the $Cu_{1.8}S$

2.500 M thiourea solution in EG including glucose was added dropwise into the 0.333 M copper (I) chloride solution in EG, which is kept at reaction vessel at 80  $^{\circ}$  C under nitrogen gas. After the addition of thiourea is completed, the mixture is heated to 140  $^{\circ}$  C by continuing to stir. The Cu<sub>1.8</sub>S particles were obtained as a black solution after 5 hours of reaction at 140  $^{\circ}$  C under nitrogen gas. The solutions were prepared only in dried EG and no water was used throughout the synthesis process.

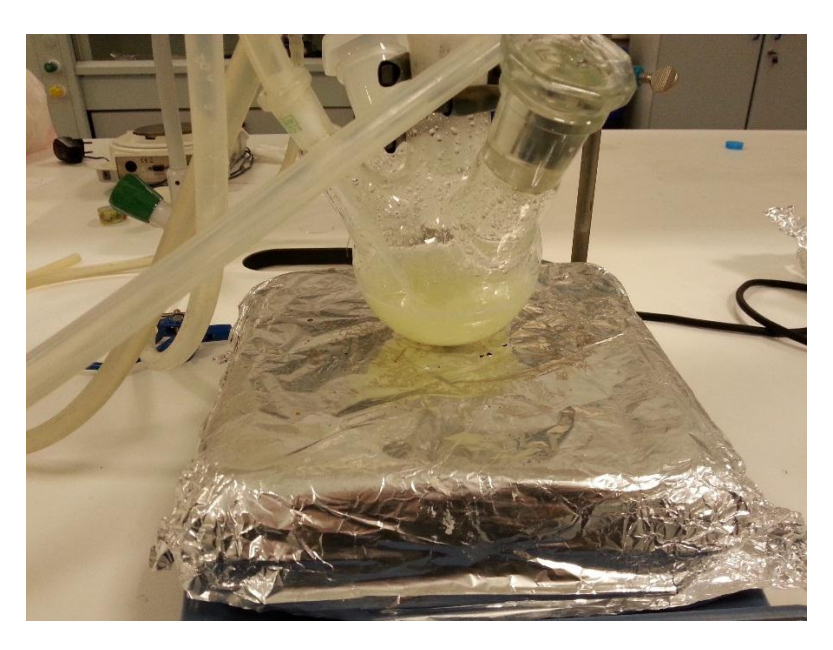


Figure 3.7 Method for preparing copper sulfide

## 3.6 Preparation of the films for composites

## 3.6.1 Preparation of the films for composite 1

The glass substrates were cleaned in the concentrated sulfuric acid solution then successively transferred to water, pure water and acetone. Later they were ultrasonically cleaned in isopropyl alcohol, finally with deionized water. The films of PEDOT:PSSA or the certain proportions of PEDOT:PSSA solutions and ZnS-PVOH were prepared by drop coating of 1 mL solution on the cleaned glass substrate. Thin films on the glass substrates were also dried at 60 °C for 1hour after drying at ambient conditions.

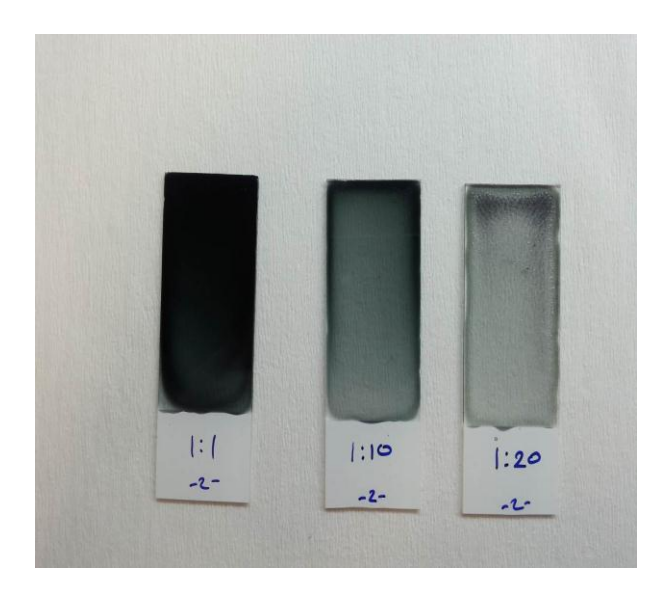


Figure 3.8 PEDOT:PSSA/ZnS-POVH films

## 3.6.2 Preparation of the films for composite 2

The glass substrates were cleaned in the concentrated sulfuric acid solution then successively transferred to water, pure water and acetone. Later they were ultrasonically cleaned in isopropyl alcohol, finally with deionized water. The films of PEDOT:PSSA or the certain proportions of PEDOT:PSSA solutions and  $\text{Cu}_{1.8}\text{S}$  particles in EG were prepared by drop coating of 1 mL solution on the cleaned glass substrate . Thin films on the glass substrates were also dried at 120 °C for 15 min at ambient conditions.



**Figure 3.9** PEDOT:PSSA/Cu<sub>1.8</sub>S films.

## 3.6.3 Preparation of composite 3

The glass substrates were cleaned in the concentrated sulfuric acid solution then successively transferred to water, pure water and acetone. The films of PEDOT:PSSA and/or composites were prepared by drop casting on the cleaned glass substrate. The composites were prepared in various proportions of PEDOT: PSSA and TiS<sub>2</sub> powder by either non-sonicating (just mixing) or sonicating with a ultra-sonicator homogenizer. Thin films on the glass substrates were then dried at 60 oC for 1 hour after drying at ambient conditions.



**Figure 3.10** PEDOT:PSSA/TiS<sub>2</sub> films.

## 3.6.4 Preparation of composite 4

The glass substrates were cleaned in the concentrated sulfuric acid solution then successively transferred to water, pure water and acetone. The films of PEDOT:PSSA and/or composites were prepared by drop casting on the cleaned glass substrate. The composites were prepared in various proportions of PEDOT: PSSA and TiS<sub>2</sub> powder and Cs<sub>2</sub>CO<sub>3</sub> powder by either non-sonicating (just mixing) or sonicating with a ultra-sonicator homogenizer. Thin films on the glass substrates were then dried at 60 oC for 2 hours after drying at ambient conditions.



**Figure 3.11** PEDOT:PSSA/TiS<sub>2</sub>-Cs<sub>2</sub>CO<sub>3</sub> films.

#### 4.1 Pristine PEDOT:PSSA

Table 4.1 shows the Seebeck coefficients and Electric conductivity and power factor which is calculated by using the equation PF=S $^2\sigma$ , of the PEDOT:PSSA samples synthesized in this thesis. The synthesis conditions of the samples are described in the experimental section. They were synthesized at different time zones and used to prepare different amount of the raw materials. The PEDOT:PSSA samples given in the Table 4.1 are pristine, i.e. no solvent treatment or reducing agent is used to increase their thermoelectric properties. The positive signs of the Seebeck coefficients indicate that all of the synthesized PEDOT:PSSA samples show p-type conductivity. The magnitude of PF indicates the efficiency of the sample as a thermoelectric material. The PF value should be higher than  $1000~\mu\text{W/mK}^2$  for an efficient thermoelectric material. The results suggest that pristine PEDOT:PSSA samples are not a good candidate to be useful thermoelectric materials.

**Table 4.1** Thermoelectric parameters measured at room temperature of the PEDOT:PSSA samples synthesized using different amount of EDOT and PSSA

PEDOT:PSSA	Seebeck coefficient S (µV/C)	Electric conductivity σ (S/cm)	Power factor PF (µW/mK²)
PP1	323	0.03	0.3
PP2	845	0.8	57
PP3	333	6	67
PP4	237	0.7	39
PP5	198	0.1	0.4
PP6	463	0.3	6
PP7	1100	0.3	36
PP8	812	0.5	35
PP9	423	4	72
PP10	1125	1	137
PP11	1087	0.9	103
PP12	1119	0.6	75

In Table 4.2, PEDOT samples with higher thermoelectric parameters reported in the literature are given for comparison. The samples in the Table 4.2 are not pristine, i.e. they were reduced and/or solvent treated to increase their thermoelectric properties. By comparing the tables, it can be seen that the Seebeck coefficients of our PEDOT samples are quite high but their conductivity is very low according to the literature. As a result, PF values of our pristine PEDOT:PSDA samples are lower than those reported in the literature. For the additive-free PEDOT, the highest power factor achieved so far is 469  $\mu W$  /  $mK^2$ .

**Table 4.2** Thermoelectric parameters of the various PEDOT samples, reported in the literature.

Sample	S (µV/K)	σ (S/cm)	κ (W/mK)	PF (μW/ mK²)	ZT	Ref.
PEDOT ClO <sub>4</sub> - doped hydrazin treated	35	230	0.35	41	-	[131]
PEDOT PF <sub>6</sub> -doped hydrazin treated	34	312	0.22	60	-	[131]
PEDOT BTFMSI doped hydrazin treated	42	708	0.19	147	0.22 (RT)	[131]
PEDOT:Tos TDAE trated	-	-	0.37	324	0.25 (RT)	[15]
PEDOT:PSS DMSO mixed, EG post treated	73	880	0.32(κ <sub>⊥</sub> ) 0.31(κ <sub>//</sub> )	469	0.42 (RT)	[132]
PEDOT:PSS (PH750) DMSO 5%	13.5	570	0.34	10.4	0.00 92 (RT)	[9]
PEDOT:PSS (PH1000) DMSO 5%	22.2	945	-	46.57	-	[9]
PEDOT:PSS (FET) DMSO 5%	30.3	320		29.39	-	[117]

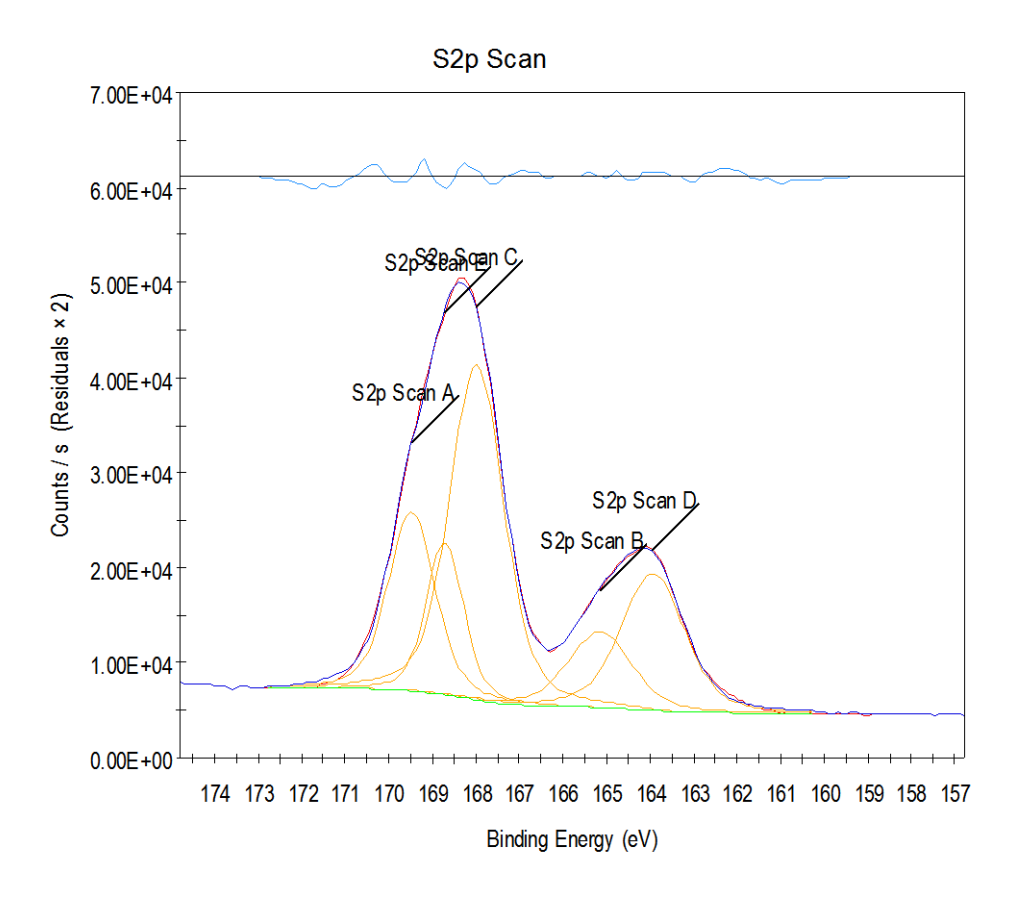


Figure 4.1 XPS survey spectra of PEDOT:PSSA

The peaks for the S 2p spectra can be fitted by two component peaks corresponding to the S in PEDOT (centered at 165.2 eV and 163.8 eV) and another three component peaks corresponding to the sulfur atom in PSSA (centered at 169.5 eV, 168.9 eV and 167.9 eV), respectively [133].

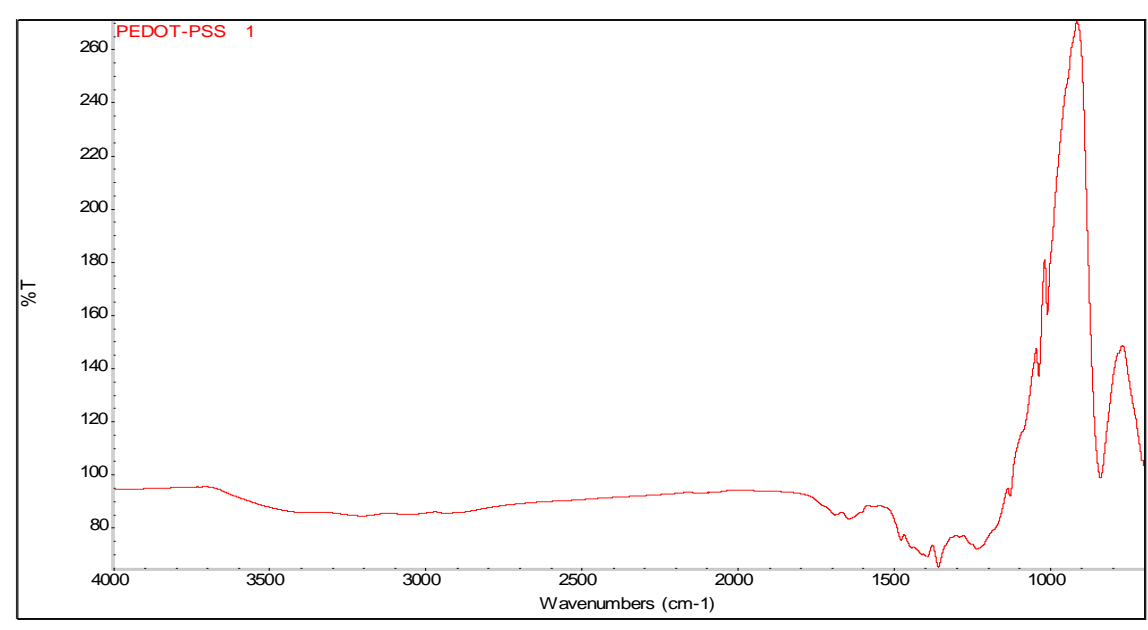


Figure 4.2 FTIR of pristine PEDOT:PSSA (PP2)

The FTIR spectrum of PP2 was given in the Figure 4.2 The peaks around 1400, 1250 and), 836 cm<sup>-1</sup> were assigned as stretching vibrations of C=C, C-C and C-S of thiophene ring of PEDOT, respectively [134]. The absorption band at 1630 cm<sup>-1</sup> is contributed by the C=C stretching of the phenyl side group of PSS and the quinoid EDOT of PEDOT.

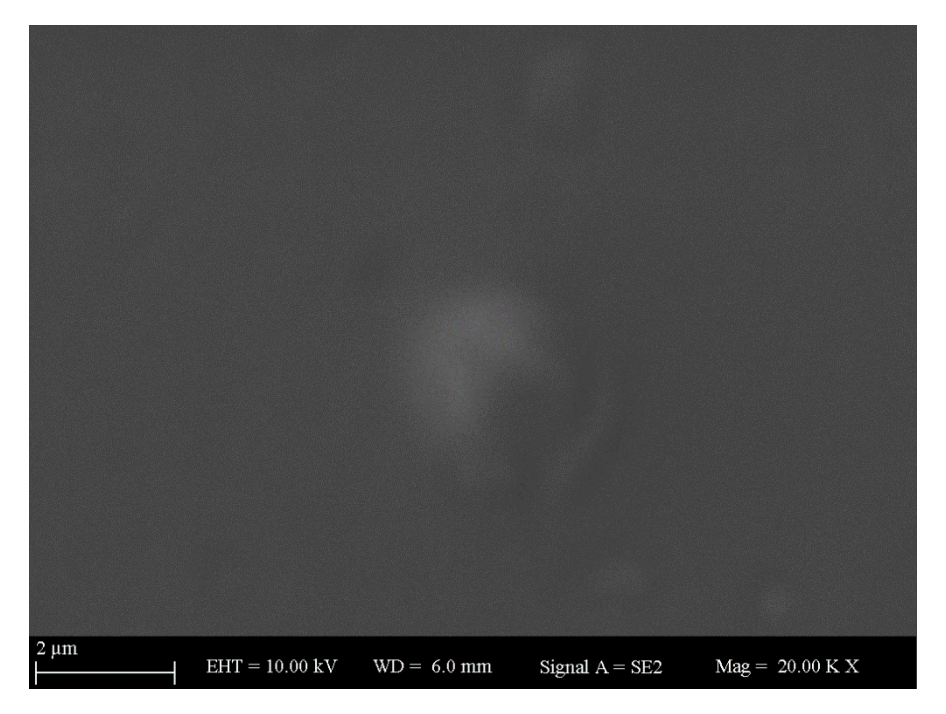


Figure 4.3 SEM image of PP2

The PP2 gives smooth and homogenous films as seen in the Figure 4.3 The films were also transparent and blue color.

### 4.2 PEDOT:PSSA/ZnS-PVOH Composites

In order to enhance the power factor of PEDOT, ZnS nanoparticles prepared in the PVOH solution were introduced into the sample PP2 which has the highest power factor synthesized at the earlier stage and the results were given in Table 4.3. However, it was observed that the thermoelectric parameters of these composites were not found high enough. The highest power factor was found as  $287~\mu\text{W/mK}^2$  for the composite which has equi mass composition.

**Table 4.3**: Thermoelectric parameters measured at room temperature, of the composites of ZnS at different weight ratios with PP2

PP2/ZnS-PVOH w/w	S (µV/K)	σ (S/cm	PF (μW/mK <sup>2</sup> )
1/0	845	0.8	57
1/1	2821	0.6	287
1/1.5	140	0.6	1
1/2	230	0.6	3
1/2.5	20	10	0.6
1/3	18	1.3	0.04
1/3.5	-38	0.5	0.07

Inadequate power factors were also obtained for the composites of ZnS-PVOH with PP7, PP8 and PP9 as can be seen from Tables 4.4-4.6. The power factors of the composites were found lower than those of the corresponding pristine PEDOT:PSSA.

**Table 4.4**: Thermoelectric parameters measured at room temperature, of the composites of ZnS at different weight ratio with PP7

PP7/ZnS-PVOH w/w	S (μV/K)	σ (S/cm)	PF (μW/mK <sup>2</sup> )
1/0	1100	0.3	36
1/0.2	870	0.1	8
1/0.5	1011	0.09	9
1/1	989	0.06	6

**Table 4.5** Thermoelectric parameters measured at room temperature, of the composites of ZnS at different weight ratio with PP8

PP8/ZnS-PVOH w/w	S (μV/K)	σ (S/cm	PF (μW/mK
1/0	812	0.5	35
1/0.2	611	0.3	13
1/0.5	853	0.1	9
1/1	463	0.08	2

**Table 4.6** Thermoelectric parameters measured at room temperature, of the composites of ZnS at different weight ratio with PP9

PP9/ZnS-PVOH w/w	S (µV/K)	σ (S/cm	PF (µW/mK
1/0	423	4	72
1/0.2	309	2	21
1/0.5	340	1	12
1/1	538	0.7	20

The power factors of the PEDOT:PSSA/ZnS-PVOH composites were found lower compared to the literature data given in Table 4.7. It was concluded that ZnS does not increase the power factor of PEDOT:PSSA.

**Table 4.7** Thermoelectric parameters of the various PEDOT/inorganic hybrid

composites, reported in the literature

PEDOT Sample	S (µV/K)	σ (S/cm)	κ (W/mK)	PF (μW/mK <sup>2</sup>	ZT	Ref.
PEDOT:PSS(PH1 000)/p-Bi <sub>2</sub> Te <sub>3</sub> 10%HCl rinsing of Bi <sub>2</sub> Te <sub>3</sub>	149	59	-	131	-	[117]
PEDOT:PSS (PH1000)/n-Bi <sub>2</sub> Te <sub>3</sub> 10%HCl rinsing of Bi <sub>2</sub> Te <sub>3</sub>	-125	58	-	91		[117]
PEDOT:PSS (PH1000)/p-Bi <sub>2</sub> Te <sub>3</sub> 30% HCl rinsing of Bi <sub>2</sub> Te <sub>3</sub>	110	65	-	70	-	[117]
PEDOT:PSS (PH1000)/n-Bi <sub>2</sub> Te <sub>3</sub> 30% HCl rinsing of Bi <sub>2</sub> Te <sub>3</sub>	-80	60	-	40		[117]
PEDOT:PSS/Sb <sub>2</sub> Te <sub>3</sub> composite	175	130-110	0.15 (300- 523K)	-	1.18 (523 K)	[135]
PEDOT:PSS/Te nanocomposite	163.4±4	19.3±2.3	0.22- 0.30	70.9	0.1 (RT)	[116]
PEDOT:PSS/Te 80% .vol H <sub>2</sub> SO <sub>4</sub> treated	114.97	214.86	0.22 estimatio n	284	0.39 estimati on	[136]
PEDOT:PSS/Te composite 70% wt	26	650	0.197- 0.218	51.4	0.076 (292 K)	[137]
PEDOT:PSS/Cu <sub>1.75</sub> Te	220	-	-	84	-	[138]

The XPS survey analysis of ZnS-PVOH synthesized in our laboratory was given in the Figure 4.4. The XPS spectrum of Zn2p represents the binding energies of Zn 2p3/2 at about 1022.0 eV and Zn 2p1/2 centered at 1045.1. The XPS results indicate the ZnS was synthesized successfully since the binding energies of Zn2p electrons are in agreement with literature [139].

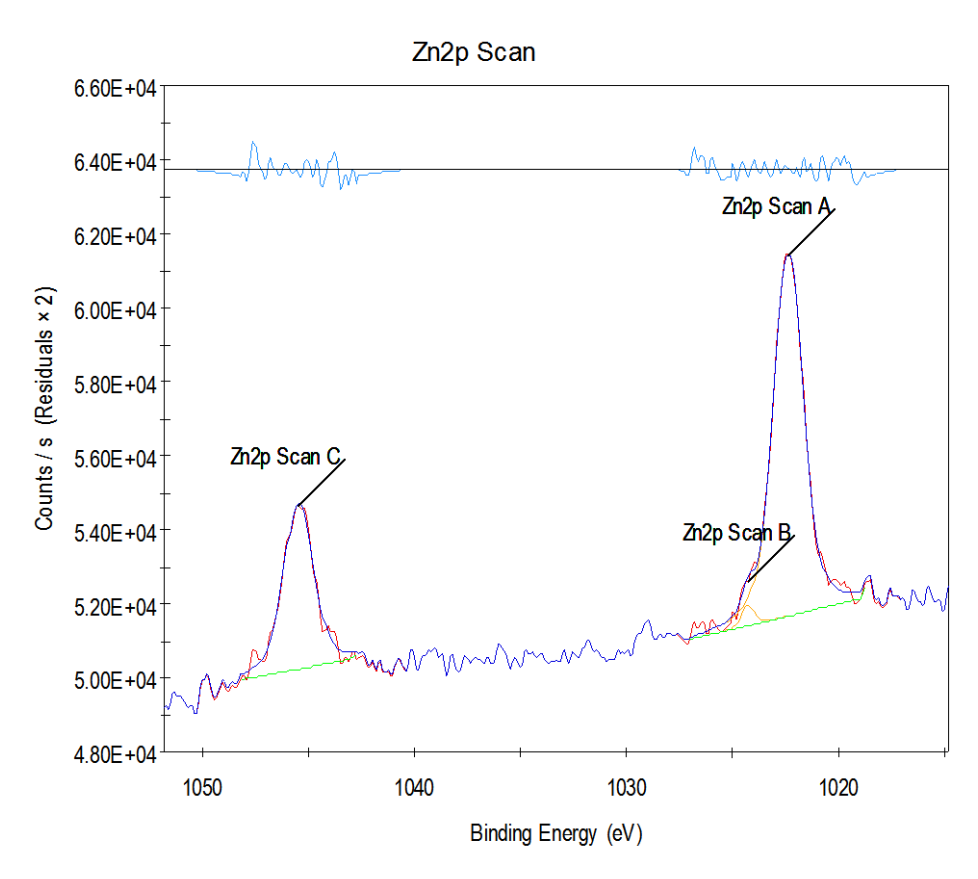
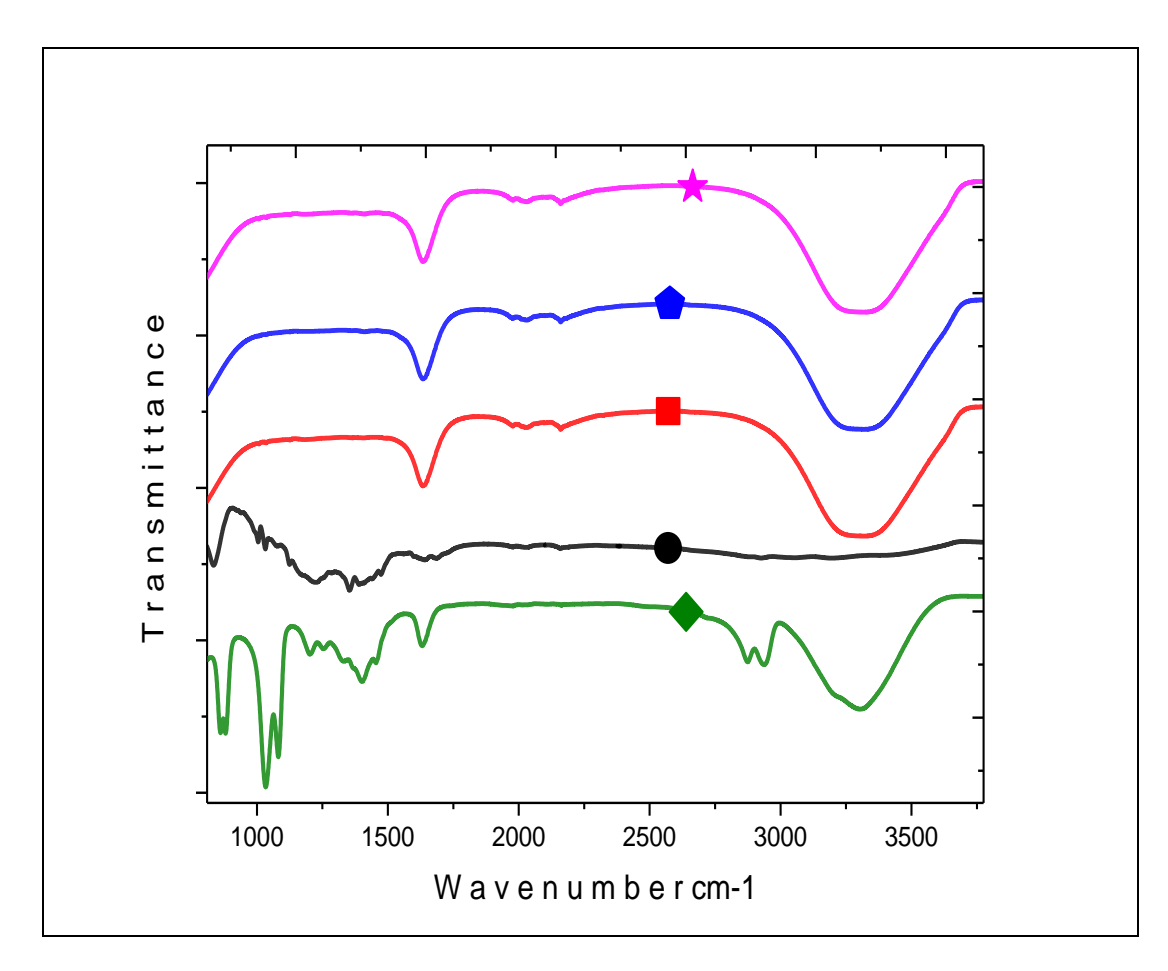


Figure 4.4 XPS survey spectra of-ZnS-PVOH synthesized



**Figure 4.5** FTIR absorption spectra. The ZnS-PVOH nanoparticle (diamond), and bottom line (circle) belongs to pristine PEDOT:PSSA and their composites in the ratio of PEDOT:PSSA/ZnS-PVOH are 1/1 (square), 1/1.5 (pentagram), 1/2 (star)

Figure 4.5 demonstrates the ambient temperature situation for the FTIR spectrum of ZnS nanoparticles. The aforementioned spectrum represents the IR absorption related to the different vibration modes. The detected characteristic main peaks for ZnS were in an appropriate agreement with the reported results of the other researchers (about 1124, 998, and 624 cm<sup>-1</sup>).

The detected peaks at 1550 cm<sup>-1</sup>–1750 cm<sup>-1</sup> are allocated to the C=O stretching modes, as well as the broad absorption peaks at 3100 cm<sup>-1</sup>–3600 cm<sup>-1</sup> refer to O–H stretching modes coming from the absorption of water on the surface of nanoparticles via –COOH cluster. The major IR bands of PEDOT are observed under 1550 cm<sup>-1</sup> [140].

### 4.3 PEDOT:PSSA/Cu<sub>1.8</sub>S composites

Since He et al. showed that the TE performances of CuxS (x = 1.97, 1.98, and 2) are very high ZTs of 1.4–1.7 at 1000 K in 2014 [141]. The composites were prepared by using PP10 and copper sulfide nanoparticles synthesized in ethylene glycol using a method improved in our laboratory. The XRD spectrum of powder copper sulfide is recorded in order to determine its phase structure. The pattern is given in the Figure 4.6. The phase structure of synthesized copper sulfide was identified as digenite phase ( $Cu_{1.8}S$ ) according to the PDF#47-1748 card and Zhao's report [142, 143].

 $Cu_{1.8}S$  has not attracted enough attention since it has a low Seebeck coefficient (about 10  $\mu$ V/K) [142] although it possess a band gap of 1.5 eV and a high electrical conductivity.

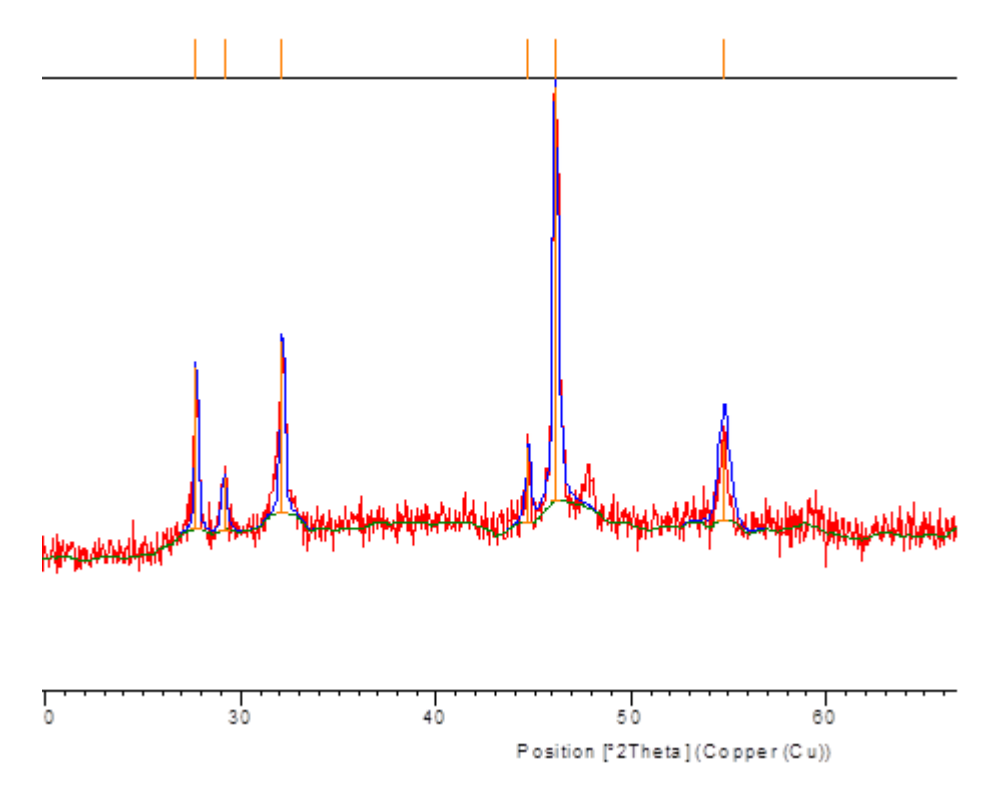


**Figure 4.6** XRD pattern of the Cu<sub>1.8</sub>S nanoparticles powders

Among these copper sulfides, digenite ( $Cu_{1.8}S$ ) is known as a steady phase and their high ZTs are mainly attributed to the ultralow lattice thermal conductivities (0.3-0.5 W/mK) caused by the liquid-like copper ions [144]. When temperature of the digenite rises over 364 K, the position of the Cu atom in the crystal structure changes

from ordered states to confused states. The  $Cu_{1.8}S$  could be used as a p-type semiconductor originated from the high mobility of copper ions in the lattice.

The thermoelectric parameters of PEDOT:PSSA/Cu<sub>1.8</sub>S composites were given in Table 4.8. Their estimated figure-of-merits given in the Table 4.8 were calculated for 300 K by assuming as  $\kappa$ =0.4 W/mK.

It can be seen from the thermoelectric properties of the pristine PEDOT:PSSA (PP10) in Table 4.1, its electrical conductivity is significantly low ( 1 S/cm) but Seebeck coefficient is positive and significantly large (1125  $\mu$ V/K) compared to those of PEDOT:PSS reported in the literature, given in the Table 4.2. The reason for the high Seebeck coefficients may be that the PEDOT is mildly oxidized with hydrogen peroxide, resulting in a lower charge carrier concentration. It can be concluded that the composites are p-type since their Seebeck coefficients are positive.

The magnitude of PF indicates the efficiency of the sample as a thermoelectric material. The results suggest that our three PEDOT:PSSA/Cu<sub>1.8</sub>S samples are a good candidate to be useful thermoelectric materials since their power factors are higher than  $1000~\mu\text{W/mK}^2$ . Compared with the Seebeck coefficients of the nanocomposites given in Table 4.7, it is seen that Seebeck coefficients of nanocomposites containing 0.25 g of Cu<sub>1.8</sub>S per g PP10 is much higher than those of the nanocomposites in Table 4.7, which are reported up to now. Consequently, the composite containing 0.25 g of Cu<sub>1.8</sub>S per g PP10 has the highest power factor reported up to now. This may also be due to the high mobility of copper ions in the crystal structure of Cu<sub>1.8</sub>S. In addition, the ethylene glycol in the Cu<sub>1.8</sub>S nanoparticle dispersion may also behave as a secondary dopant by extending the PEDOT chains. It is also possible that all of these reasons work concurrently.

**Table 4.8** Thermoelectric parameters measured at room temperature, and power factor (PF) calculated by means of PF=  $S^2\sigma$ , and figure-of merit (ZT) estimated at 300 K by assuming as  $\kappa$ =0.4 of PEDOT:PSSA (PP10) and its nanocomposites with Cu<sub>1.8</sub>S synthesized in this study

PP10/Cu <sub>1.8</sub> S w/w	S (µV/K)	σ (S/cm)	PF (μW/mK²)	Estimated ZT at 300 K
1/0	1125	1	137	~ 0.10
1/0.11	3900	0.8	1232	~ 0.92
1/0.25	7000	0.5	2646	~ 1.98
1/0.33	5000	0.8	2000	~ 1.50
1/0.67	1000	0.9	93	~ 0.07

In order to see the electronic transitions in the visible region, the UV-Vis. absorption spectra of the aqueous dispersions of the pristine PEDOT:PSSA and its nanocomposites were given in the Figure 4.7. The spectrum at the bottom (black line) belongs to pristine PEDOT:PSSA and the others are ranked upward according to the increasing amount of Cu<sub>1.8</sub>S. A broad absorption band between 600 nm and 900 nm originates from the p - p\* transition of the polarons or bipolarons in the samples. The absence of tailing at the pristine PEDOT:PSSA and nanocomposites low amount of Cu<sub>1.8</sub>S indicates that the charge carriers cannot move freely. The polaron band becomes a free carrier tail by increasing amount of Cu<sub>1.8</sub>S dispersion including ethylene glycol. This indicates that charge carriers can move freely in the chains extended by ethylene glycol. This is in agreement with the electrical conductivity data given in the Table 4.8.

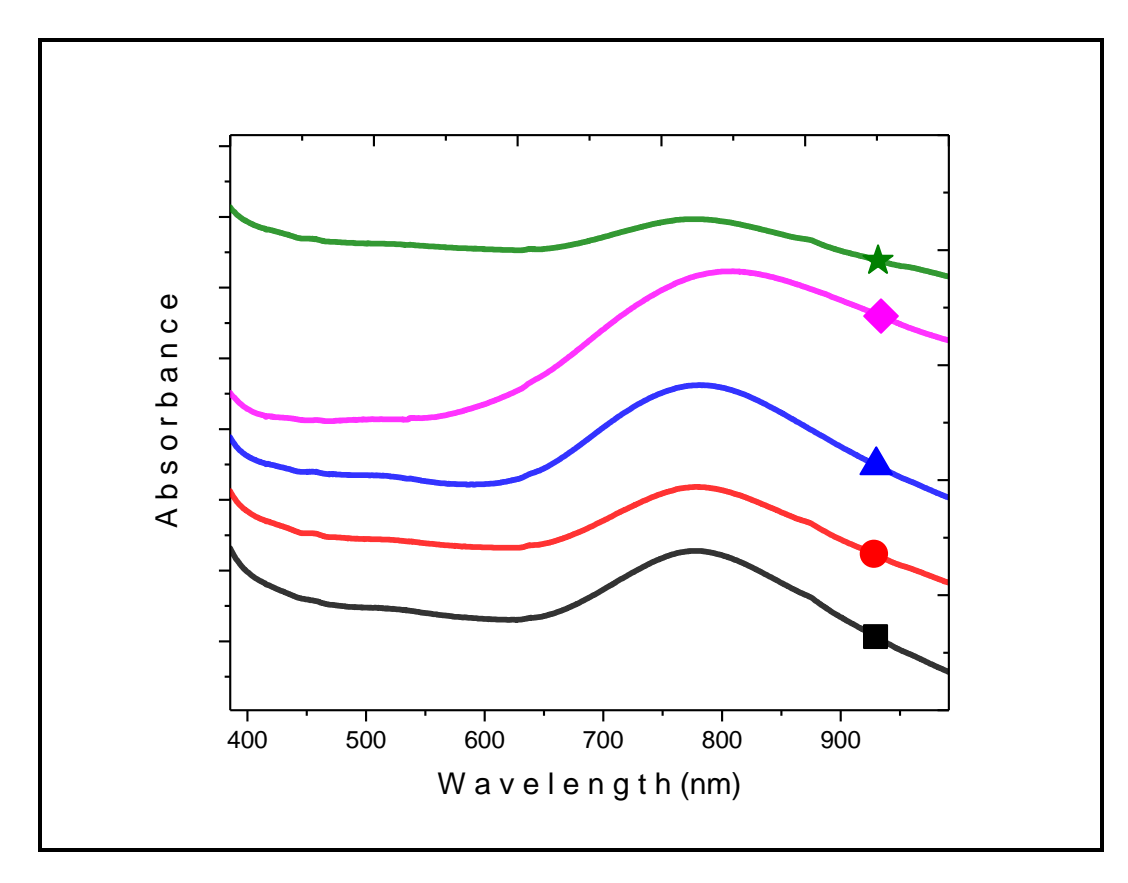
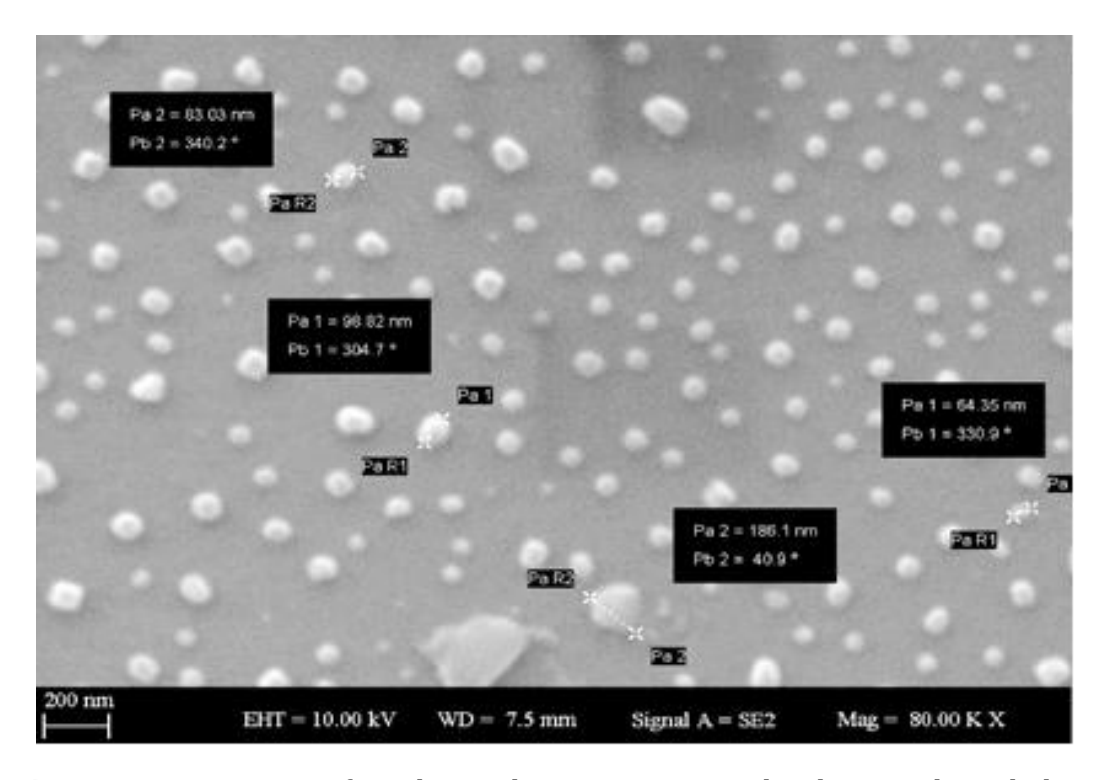


**Figure 4.7** UV absorption spectra of the PEDOT:PSSA and its nanocomposites. The curves are shifted artificially. (The bottom line (square) belongs to pristine PEDOT:PSSA and upward lines belong to the PEDOT:PSSA/Cu<sub>1.8</sub>S nanocomposites in the following ratios: 1/0.11 (circle), 1/0.25 (triangle), 1/0.33 (diamond), 1/0.67 (star), respectively)

As seen in Figure 4.8, the morphology of the synthesized dignity nanoparticles can be described as a mixture of nanosized cubic and spherulitic particles although they are not monodisperse. It can be assumed that the nanoparticles do not contain oxidized copper compounds because they are synthesized in an anhydrous and nitrogen atmosphere. The synthesized Cu<sub>1.8</sub>S nanoparticles were used as dispersions in ethylene glycol without purification in preparation of their nanocomposites with PEDOT:PSSA. Figures 4.9, 4.10 and 4.11 show the morphology of PEDOT:PSSA/Cu<sub>1.8</sub>S nanocomposites.



 $\label{eq:curve_series} \textbf{Figure 4.8} \ \text{SEM image of synthesized Cu}_{1.8} S \ nanoparticles \ dispersed \ in \ ethylene \\ glycol$ 

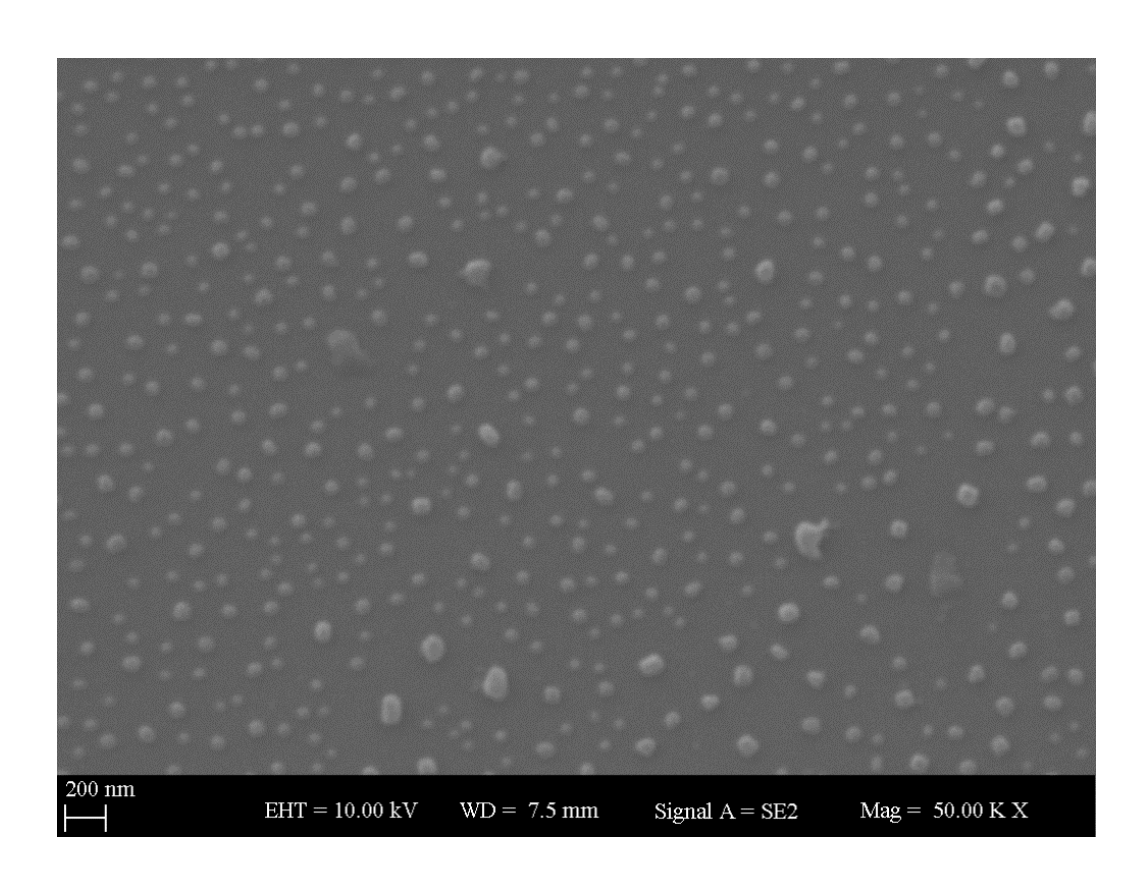


Figure 4.9 SEM images of composite of PEDOT:PSSA / Cu1.8S (1:0.25)

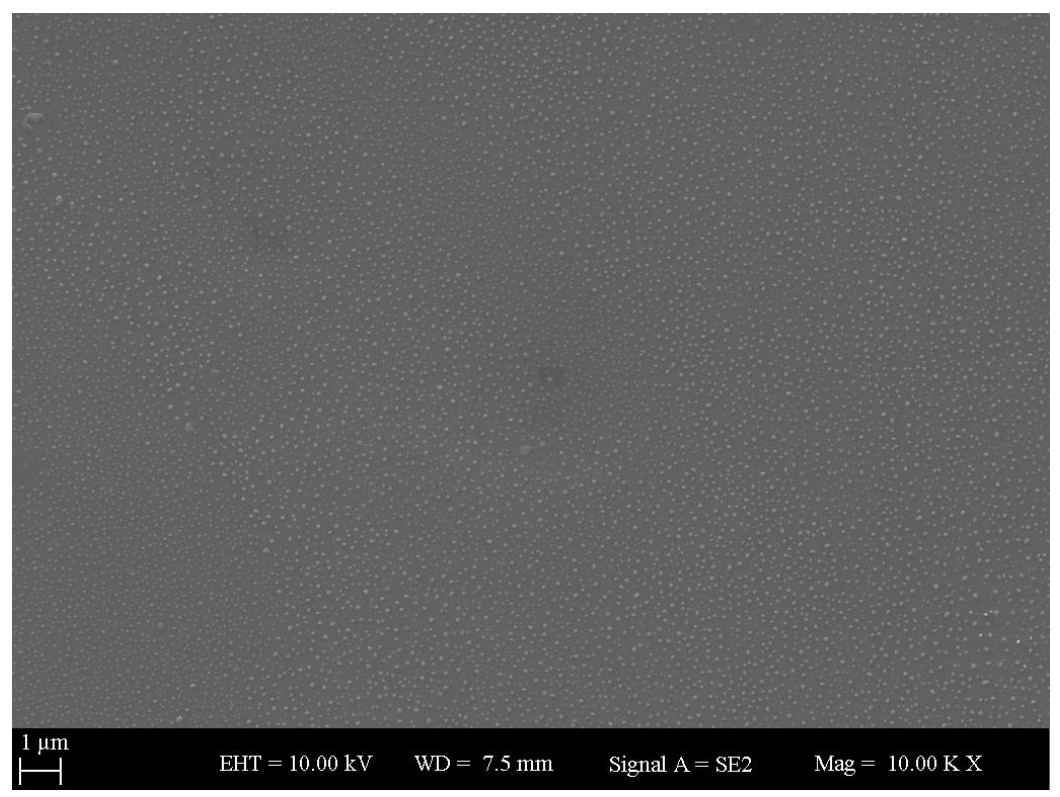


Figure 4.10 SEM images of composite of PEDOT:PSSA / Cu1.8S (1:0.33)

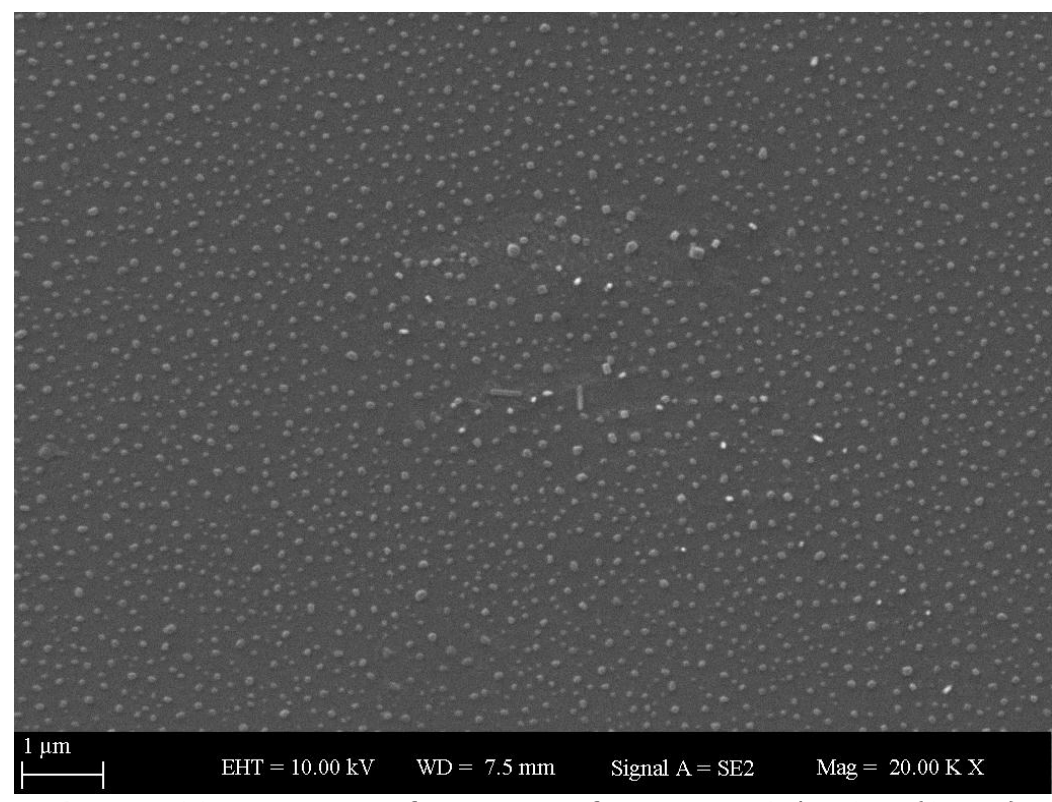


Figure 4.11 SEM images of composite of PEDOT:PSSA / Cu1.8S (1:0.66)

### 4.4 PEDOT:PSSA/TiS<sub>2</sub> composites

Later, in order to prepare n-type thermoelectric material, PEDOT:PSSA/TiS2 composites were studied. PEDOT:PSSA (PP11) which displays p-type conductivity with considerably large Seebeck coefficient. The TiS2 used was purchased from the market i.e. it was not synthesized in our laboratory. The PF of 103  $\mu$ W/mK² was found for pristine PEDOT:PSSA. However, TiS2 is n-type material with large S (-250  $\mu$ V/K and high conductivity (580 S/cm) in agreement with the reported values in the literature [145].

In the Table 4.9, the thermoelectric parameters of the composites prepared using the  $TiS_2$  as received were given. The values of Seebeck coefficient (with positive sign) and  $\sigma$  increased at lower concentrations and PF reached to 461  $\mu$ W/mK² with increase of  $TiS_2$ . The composites maintained the p-type conductivity up to  $TiS_2$  concentration reached to 1.8 per gram of PP11. The sign of S changed to negative at this concentration indicating the conversion of n-type conductivity. S of -2400  $\mu$ W/m  $K^2$  was measured without a significant decrease in electrical conductivity.

Power factor of 305  $\mu$ W/mK<sup>2</sup> was calculated at this concentration. The change of the sign of the S is a common phenomenon with the change of the proportion of two components of the composites (Table 4.9). As TiS<sub>2</sub> amount increase, the composites maintained the n-type conductivity although absolute values of the S decreased.

**Table 4.9**. Thermoelectric parameters measured at room temperature, power factors (PF) calculated and figure-of-merits (ZT) estimated at 300 K by assuming as  $\kappa$ =0.4  $\mu$ W/mK of PEDOT:PSSA (PP10) and its nanocomposites with TiS2 as received .  $\kappa$ ~ 6.8 W/mK was used in the estimation of ZT for TiS2 tablet

PP11/TiS <sub>2</sub> w/w	Seebeck coefficient (µV/K)	Electric conductivity σ (S/cm) <sup>[b]</sup>	Power factor PF (µW/mK²)	ZT estimated at 300 K <sup>[b]</sup>
1/0	1087	0.87	103	0.08
1/0.05	1200	3.2	461	0.34
1/0.11	220	18	87	0.065
1/0.18	1000	0.7	70	0.05
1/0.25	-2400	0.53	305	0.23

**Table4. 9**. Thermoelectric parameters measured at room temperature, power factors (PF) calculated and figure-of-merits (ZT) estimated at 300 K by assuming as  $\kappa$ =0.4  $\mu$ W/mK of PEDOT:PSSA (PP10) and its nanocomposites with TiS<sub>2</sub> as received .  $\kappa$ ~ 6.8 W/mK was used in the estimation of ZT for TiS<sub>2</sub> tablet (continued)

1/0.33	-467	3	65	0.05
1/0.43	-630	3	119	0.09
0/1 (tablet)	-250	580	3625	0.16

Using another batch of the PEDOT:PSSA, the composite samples were ultrasonicated for 30 minutes in an ice bath in in order to homogenize them. The results of the thin films of the ultra-sonicated composites were given in Table 4.10. The S of  $\pm 2400 \, \mu V/K$  was measured for the pristine PEDOT:PSSA. Its ZT value was estimated as 0.26 by assuming the thermal conductivity is 0.4 W/mK which is a mean value of the measured  $\kappa$  values for PEDOT:PSSA in the literature [145].

The S of + 2300  $\mu$ V/K was measured for the composite containing 0.05 TiS<sub>2</sub> per PEDOT:PSSA. The sign of S turns negative when the concentration of TiS<sub>2</sub> becomes 0.11 TiS<sub>2</sub> per PEDOT:PSSA Then, both S and  $\sigma$  increase as TiS<sub>2</sub> increase. The maximum S of -1080 was measured when the TiS<sub>2</sub> concentration reaches to 0.25 TiS<sub>2</sub> per PEDOT:PSSA. The highest PF of 1516 ( $\mu$ W/mK<sup>2</sup>) was calculated for the composite containing TiS<sub>2</sub> in the composite containing 0.25 TiS<sub>2</sub> per PEDOT: PSSA. The highest ZT of 1.14 was estimated for this composite by assuming  $\kappa$  equals to 0.4 W/mK.

The highest ZT achieved in this study is higher than that of Bi<sub>2</sub>Te<sub>3</sub> (0.97), which is the most efficient state-of-the art inorganic thermoelectric material at ambient conditions. The  $\sigma$  values of the composites continues to increase but S starts to decrease when the concentration of TiS<sub>2</sub> is continued to increase. It seems that the optimum concentration of TiS<sub>2</sub> should be 0.25 TiS<sub>2</sub> per PEDOT:PSSA for the maximum performance. The PF of 1516 is the highest value reported up to date for the n-type materials [146] . It is noteworthy to say that values of S and  $\sigma$  do not change for one month.

**Table 4.10.** Thermoelectric parameters measured at room temperature, power factors (PF) calculated and figure-of-merits (ZT) estimated at 300 K by assuming

PP11/TiS <sub>2</sub> w/w	Seebeck coefficient (µV/K)	Electric conductivity σ (S/cm) <sup>[b]</sup>	Power factor PF (µW/mK²)	ZT estimated at 300 K <sup>[b]</sup>
1/0	2400	0.6	346	0.26
1/0.05	2300	0.7	370	0.28
1/0.11	-296	1.0	9	0.007
1/0.18	-312	1.5	15	0.011
1/0.25	-1080	13	1516	1.14
1/0.43	-380	16	231	0.17
1/0.67	-294	23	199	0.15
1/1	-286	28	229	0.17
1/1.5	-345	34	405	0.30
1/2.3	-280	4.3	34	0.025
1/4	-243	6	35	0.027

as  $\kappa$ =0.4  $\mu$ W/mK of PEDOT:PSSA (PP11) and its nanocomposites with TiS<sub>2</sub> sonicated .

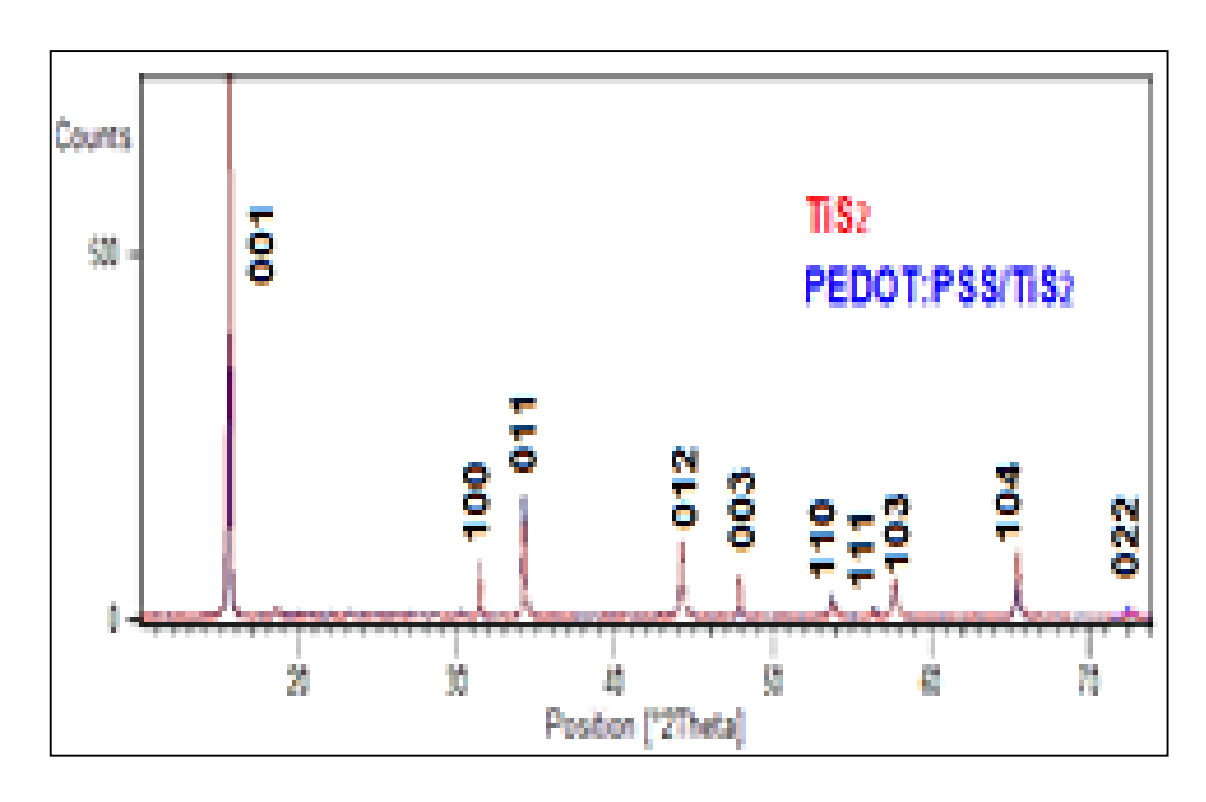


**Figure 4.12** X- ray powder diffraction patterns of TiS<sub>2</sub> as-received (the red line) and its composite with PEDOT:PSSA (blue line)

X-ray diffraction (XRD) spectra of the  $TiS_2$  powder as-received is shown in Figure. 4.12 together with its PEDOT:PSSA composite . The peaks at 15.640, 31.490, 34.260, 44.180, 47.960, 53.850, 57.740, 65.540, 72.100 for  $TiS_2$  correspond to the planes <001>, <011>, <012>, <003>, <110>, <111>, <103>, <104>, <022> [147] which agrees with the previous reported results [148]. These diffraction peaks can be coefficiented in the hexagonal  $TiS_2$  phase (Space Group, S.G. P-3m1). It can be seen in Figure 4.12 that no diffraction peak is appeared belonging to the PEDOT:PSSA in the composite. It can be seen also that  $TiS_2$  does not include any impurity in crystalline state.

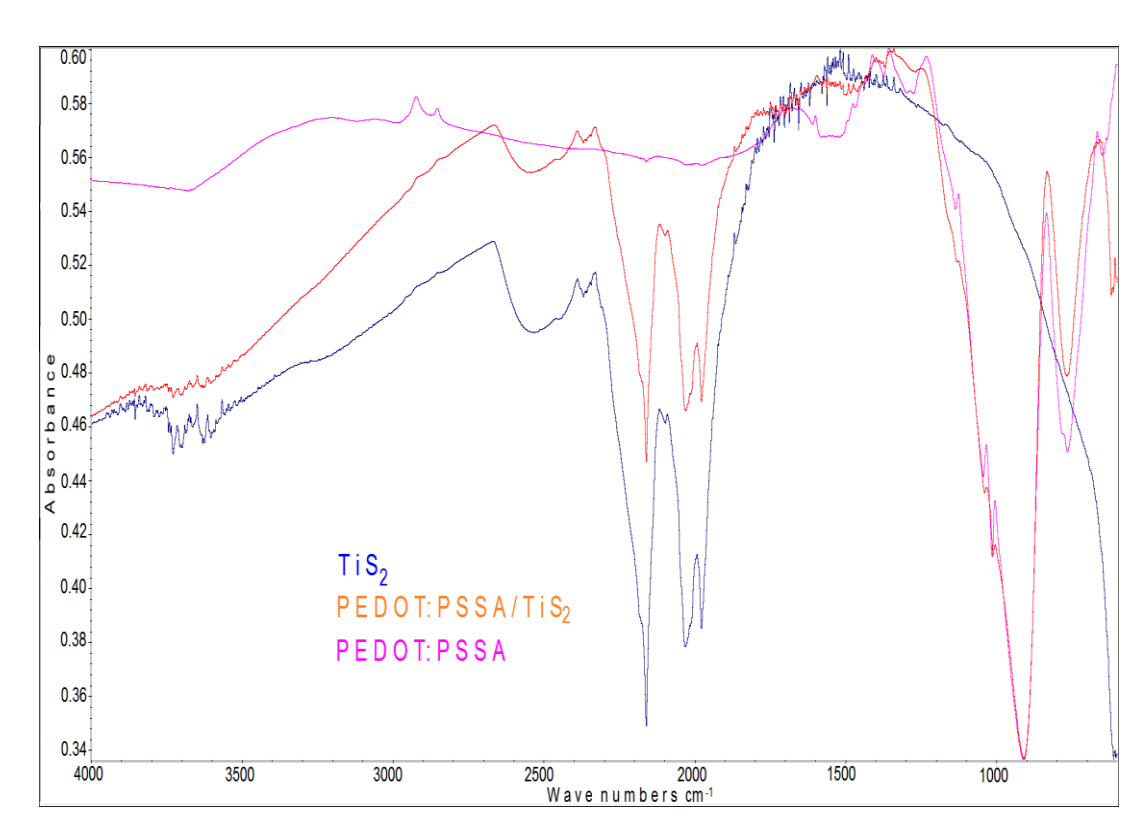


**Figure 4.13** FTIR spectra of TiS<sub>2</sub> as-received (the blue line), PEDOT:PSSA (redline) and the composite (orange line)

The FTIR spectra of PEDOT:PSSA, TiS<sub>2</sub> and their composite are given in the Figure 4.13. The bands of the PEDOT:PSSA are as follows: 1650, 1465, 1355, 1231, 1124, 832 cm<sup>-1</sup>. The broad band centered at 1650 cm<sup>-1</sup> was assigned as the C=C stretching of quinoid EDOT ring. The weak peaks appearing at around 1465 cm<sup>-1</sup> and 1355 cm<sup>-1</sup> are assigned to asymmetric stretching mode of C=C and inter-ring stretching vibration of C-C of the EDOT ring, respectively [149]. The bands at around 1231, 1124 cm<sup>-1</sup> can be attributed to the C-O-C bending vibration of ethylene dioxy group of the EDOT. The bands at 832 cm<sup>-1</sup> and 664 cm<sup>-1</sup> are stretching vibrations of C-S-C group in the thiophene group. It can be seen in the FTIR spectrum of the composite that the C=C stretching band was blue shifted from 1650 to 1780 cm<sup>-1</sup>. This can be attributed to the increase of effective π-electron delocation due to linear conformation of the quinoid EDOT [150]. It can be speculated that PEDOT chains

becomes more linear by intercalation into van der Waals gap between the S-Ti-S layers of TiS<sub>2</sub>.

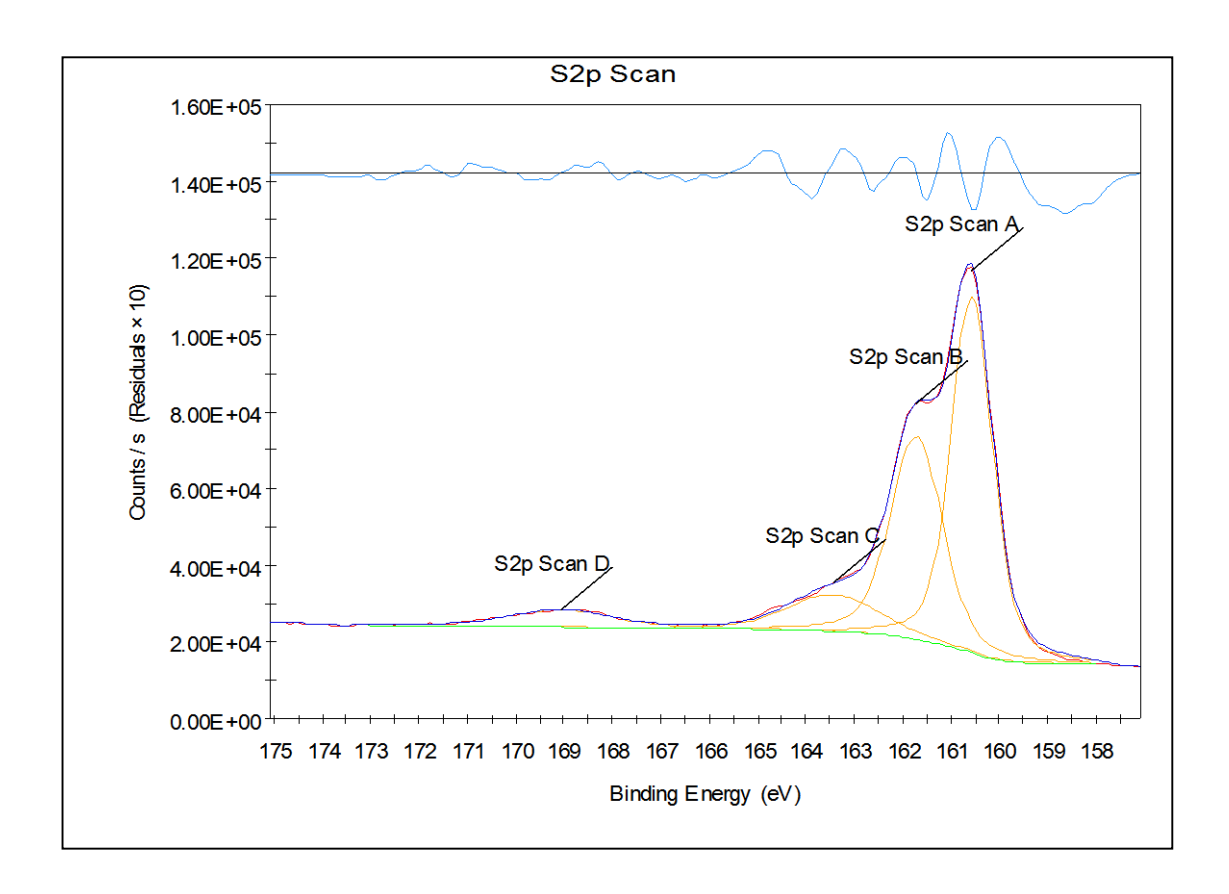


Figure 4.14 XPS survey scan of titanium sulfide as received

We performed x-ray photoelectron spectroscopy (XPS) measurements for the  $TiS_2$  as received and was given in the Figure 4.14 The binding energies at 160.6 eV and 161.8 eV correspond to S2p3/2 and 169.0 eV corresponds to S2p1/2 of  $TiS_2$ . It is in agreement with literature [151].

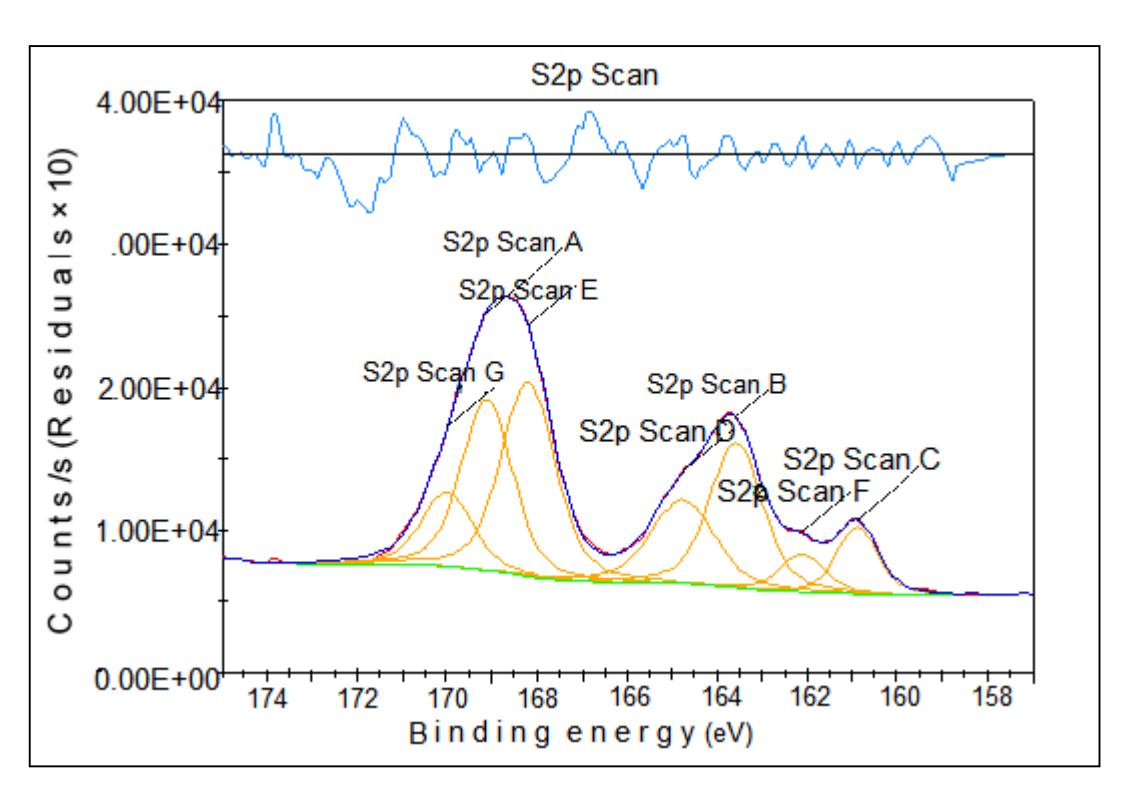


Figure 4.15 XPS survey spectra of the composite of TiS2 and PEDOT:PSSA

We performed x-ray photoelectron spectroscopy (XPS) measurements for the composite Figure.4.15 The binding energy values were determined by the curve fitting method from the raw data. The peaks for the S2p spectra can be fitted by two component peaks corresponding to the sulfur atom in PEDOT (centered at 165.0 eV and 163.8 eV) and the three component peaks corresponding to the sulfur atom in PSS centered at 169.9 eV and 169.1 eV and 168.1 eV) [152] and the two component peaks corresponding to the sulfur atom in TiS2 (162.2 eV and 160.8 eV). The two non-equivalent states with different binding energies of sulfur S2p spectra is shifted toward higher energies compared to values given compared to that of TiS2 as received. This shift may be caused by a change of the TiS2 bond angle due to intercalation of positively charged PEDOT molecules between the interlayered sections of TiS2.

The layered structure of  $TiS_2$  as received can be seen clearly in the Figure.4.16 It can be stated that the deviations of S and  $\sigma$  values of the composites might be resulted from the anisotropic structure of  $TiS_2$ . We used ultrasonic homogenizer to break down titanium sulfide as received in order to obtain a smaller size within the nanometer range.

Then it is possible to know the size of the titanium sulfide particles and the surface condition of the film after cracking using ultrasonic homogenizer, through the SEM images [133], given in the Figures 16-18. Figure 4.19 represents a composite polymer film with titanium sulfide, which shows that the polymer completely covered the titanium sulfide molecules after their homogenization, and therefore we could not know their exact size.

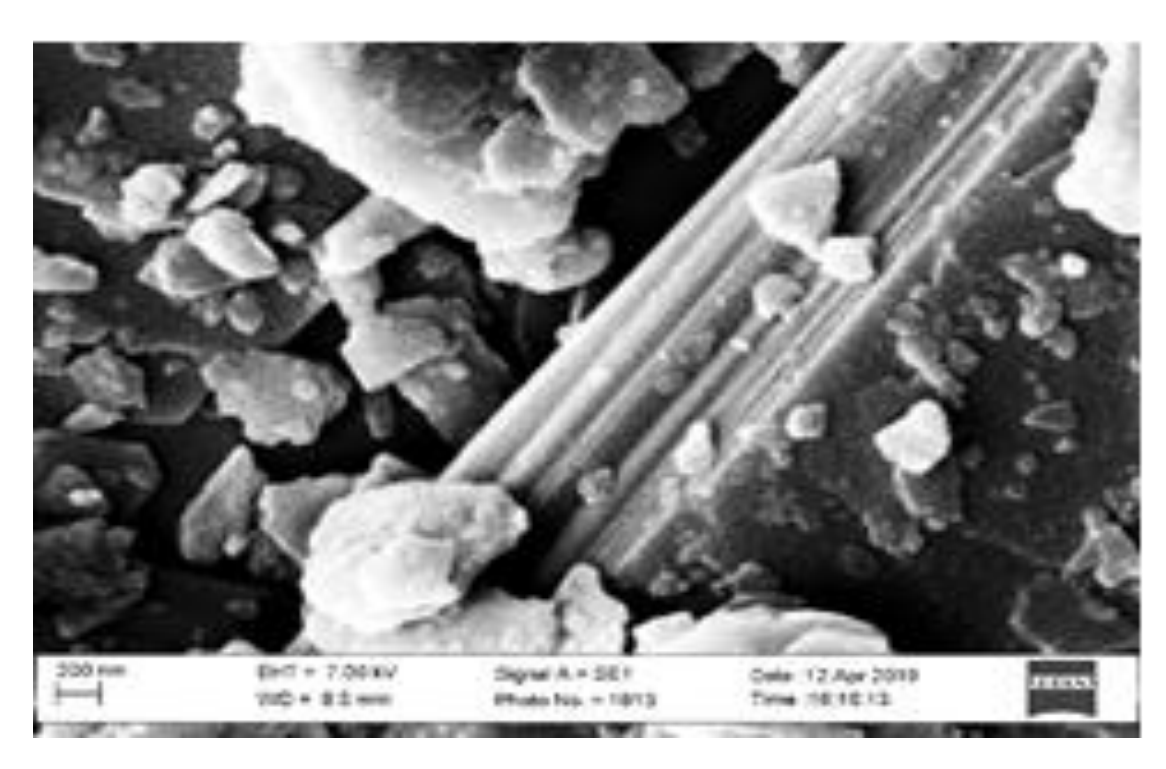
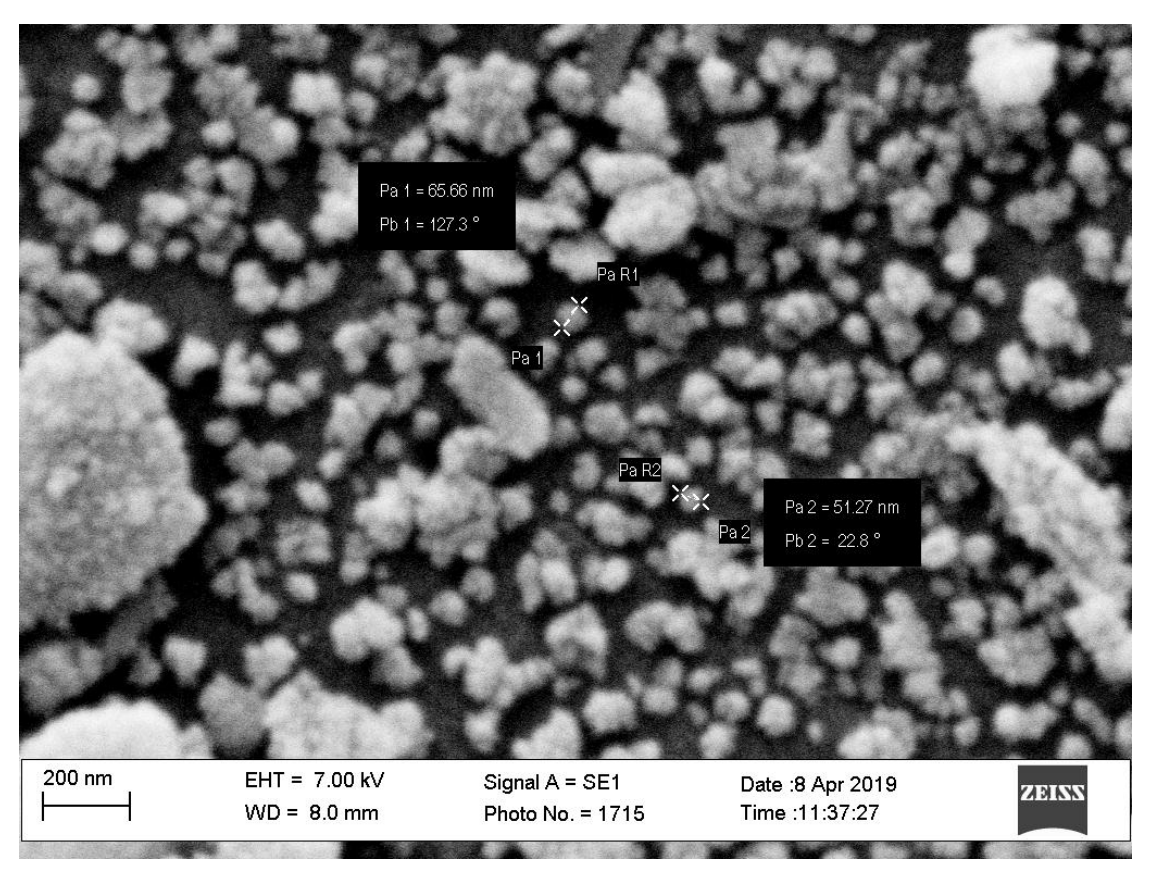


Figure 4.16 SEM image of the TiS2 as received



 $\textbf{Figure 4.17} \ \mathsf{SEM} \ \mathsf{image} \ \mathsf{of} \ \mathsf{the} \ \mathsf{TiS_2} \ \mathsf{sonicated}$ 

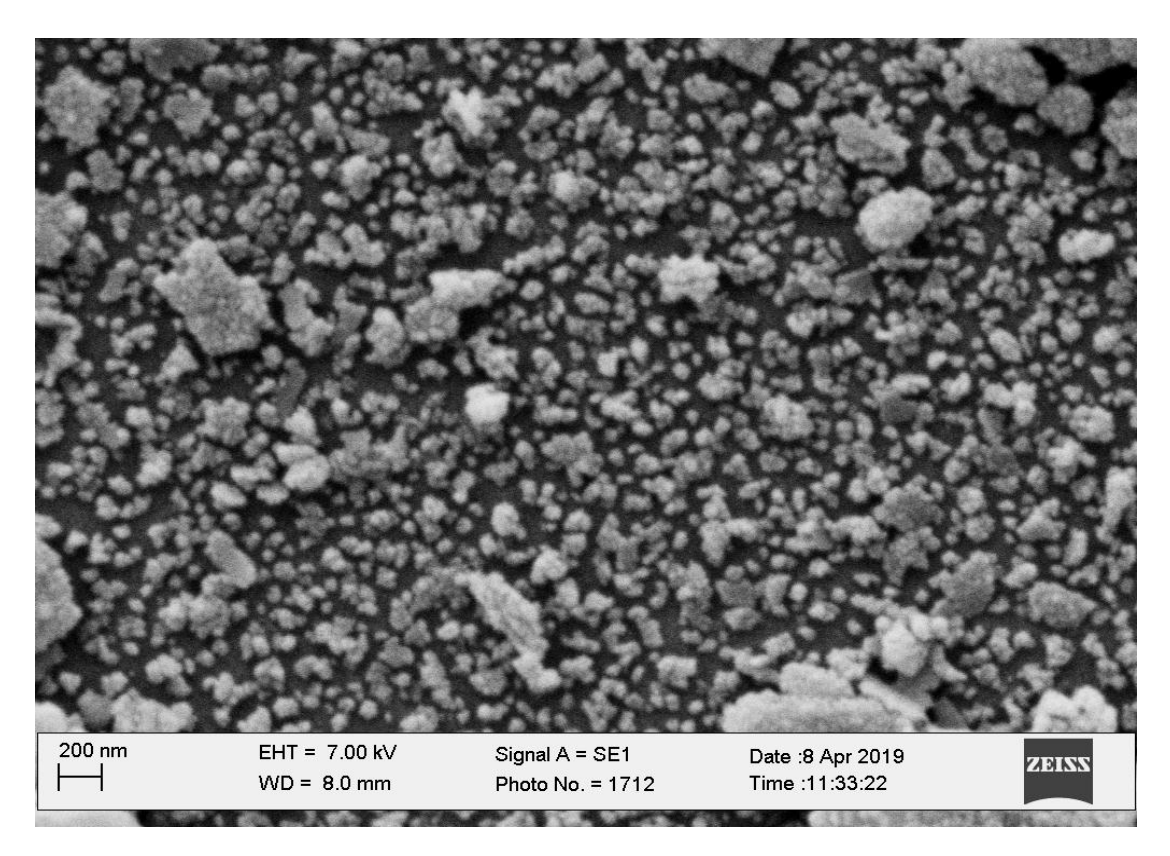


Figure 4.18 SEM image of the  $TiS_2$  as sonicated

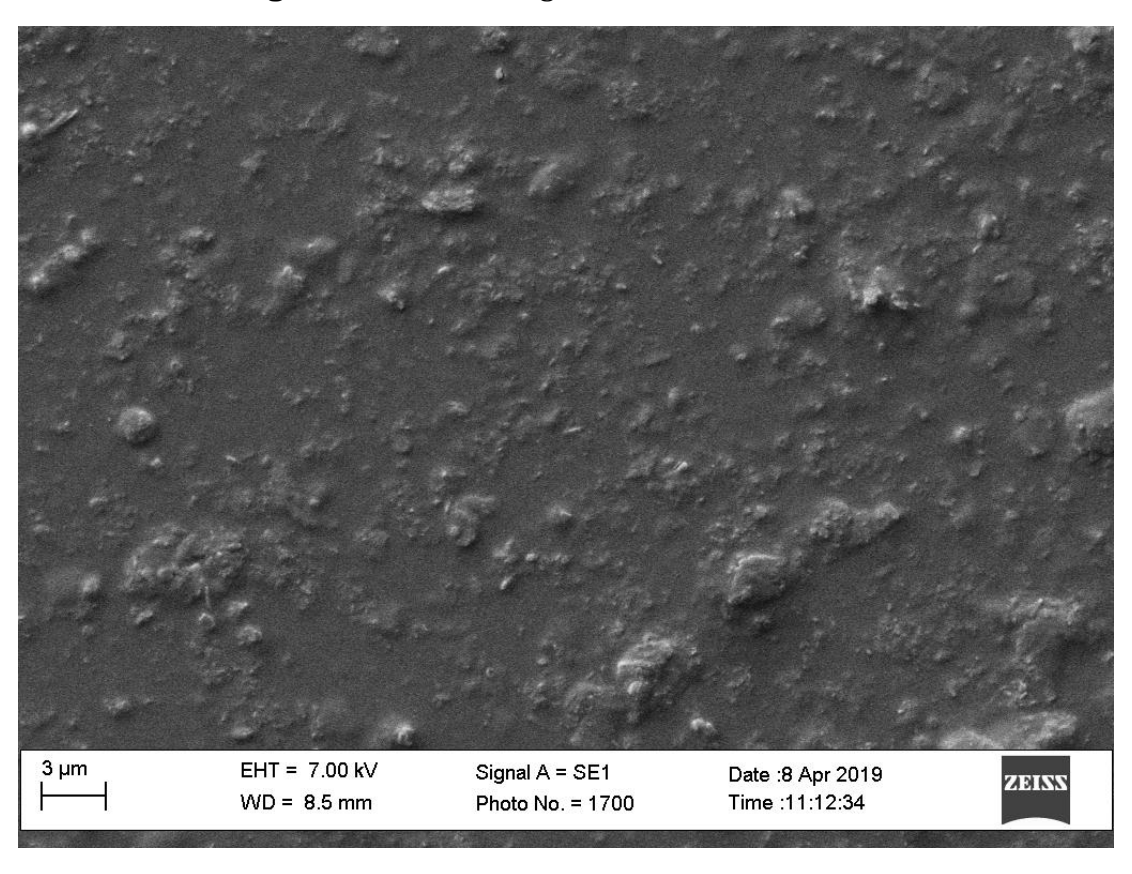


Figure 4.19 SEM image of the PEDOT:PSS/TiS2 composite sonicated

## 4.5 PEDOT:PSSA/TiS<sub>2</sub>/CS<sub>2</sub>CO<sub>3</sub> composites

Finally, it was tried to increase the power factor of the  $TiS_2$  composites by introducing another basic n-type inorganic material,  $Cs_2CO_3$ . The samples were prepared by ultrasonication of PP12,  $TiS_2$  and  $Cs_2CO_3$  in water. However, it was not possible to obtain smooth and homogeneous films with this ternary composite. The results were given in Table 4.11. It can be seen from Table 4.11, the PP12 turns to n-type material by introduction of  $Cs_2CO_3$  and  $TiS_2$ . However, the magnitudes of Seebeck coefficient and conductivity of the samples are not high enough. It was concluded that the ternary composites of PEDOT:PSSA,  $TiS_2$  and  $Cs_2CO_3$  are not promising thermoelectric materials probably because of the immiscibility of the components.

**Table 4.11** Thermoelectric parameters measured at room temperature, of the composites of Cs<sub>2</sub>CO<sub>3</sub>-TiS<sub>2</sub> at different weight ratio with PP12

PP12/Cs <sub>2</sub> CO <sub>3</sub> /TiS <sub>2</sub>	Seebeck coefficient S (µV/K)	Electric Conductivity σ (S/cm)	Power factor PF (µW/mK²)
1/0/0	1119	0.6	75
1/0.14/0.3	1062	1	135
1/0.3/0.3	-553	2	55
1/0.2/0.8	-433	2	43
1/0.5/1	312	2	23

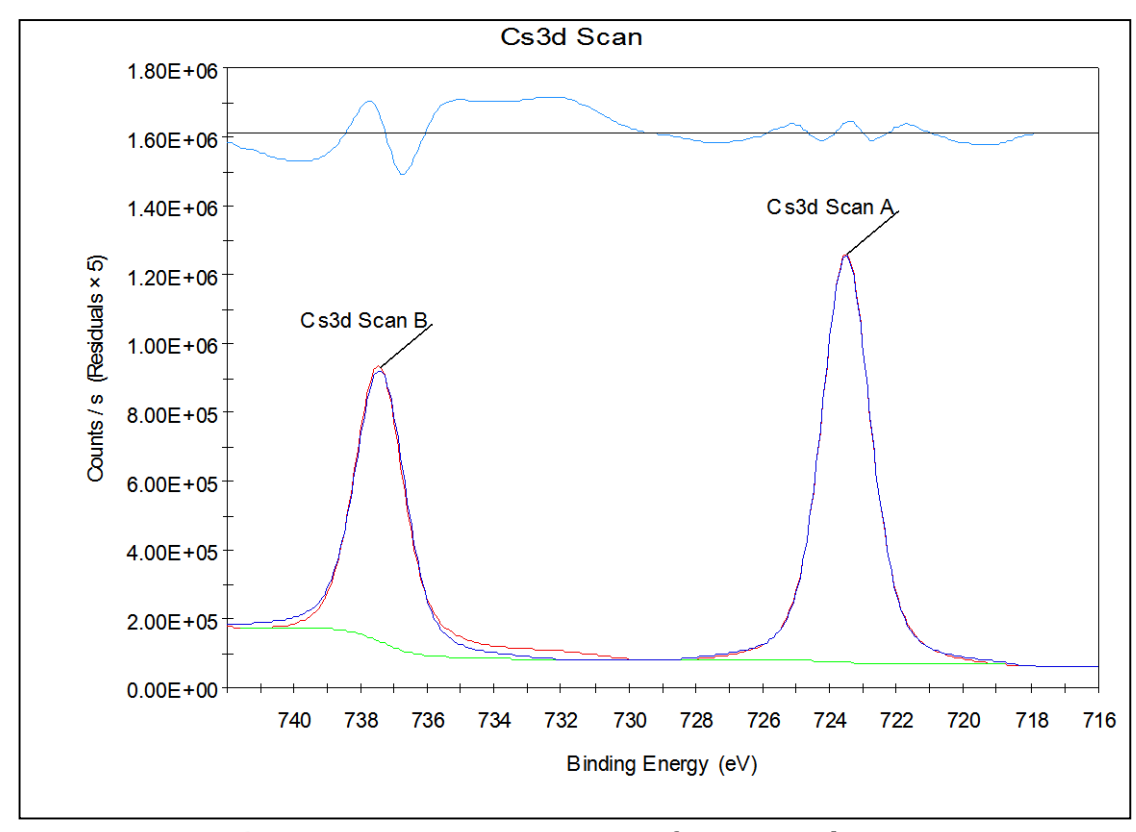
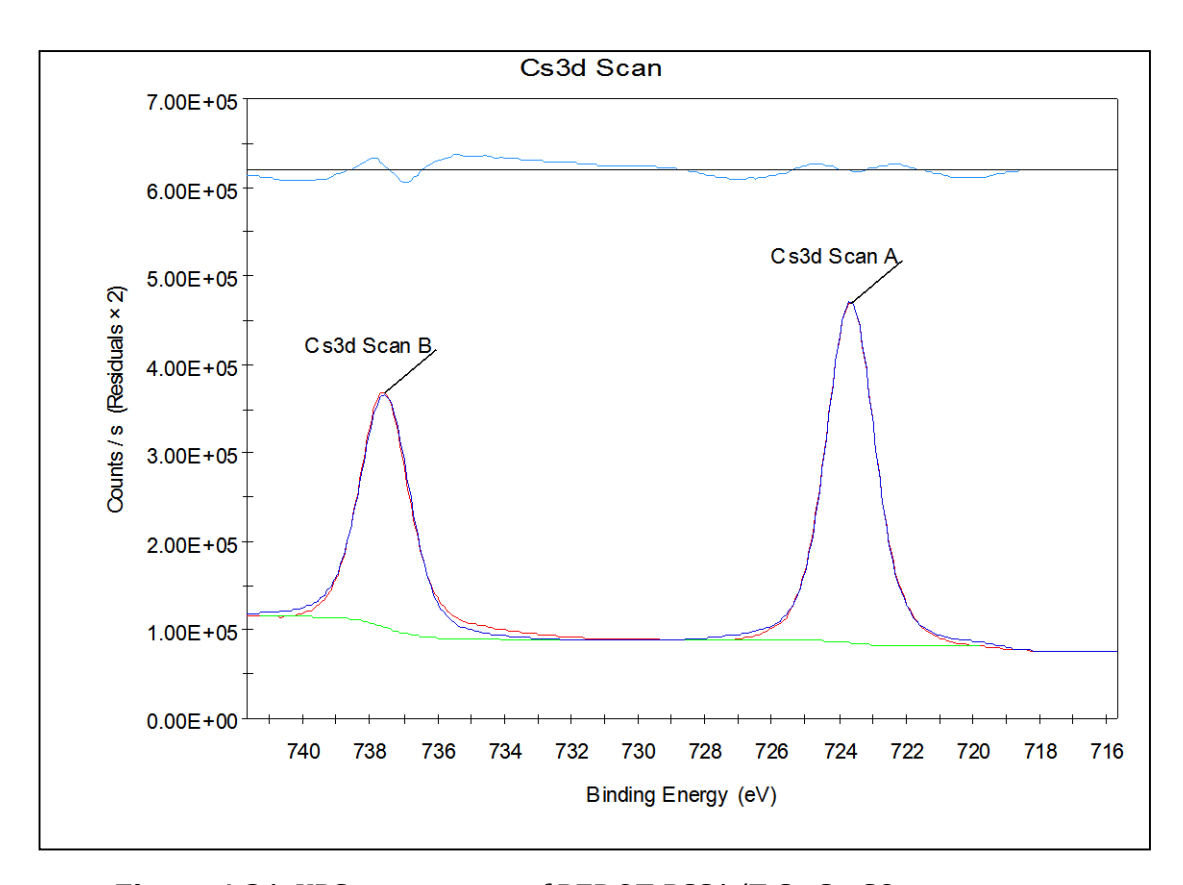


Figure. 4.20 XPS survey scan of cesium carbonate



**Figure.4.21** XPS survey scan of PEDOT:PSSA/TiS<sub>2</sub>-Cs<sub>2</sub>CO<sub>3</sub> composite

We performed x-ray photoelectron spectroscopy (XPS) measurements for cesium carbonate as received and PEDOT:PSSA/titanium sulfur/cesium carbonate composite. In the Figures 4.20 and 4.21, the binding energies of Cs3d electrons are found as 723.5 and 737.5 eV in both pristine cesium carbonate and in the composite. It can be stated that cesium did not undergo any structural change in the composite. Figure 4.22 shows the binding energy of S2p spectra in the composite. The peaks for the S2p electrons can be fitted by two component peaks corresponding to the S in the PEDOT (centered at 164.4 eV and 163.6 eV). The peak for the S2p electrons can be assigned as S in the TiS<sub>2</sub> (centered at 162.8 eV). The three component peaks responding to the S in PSSA (centered at 169.5 eV, 168.3 eV and 167.4 eV [133]. It seems that the binding energies of the S2p electrons in the PEDOT and PSSA decrease but the binding energy of the 2p electrons of TiS<sub>2</sub> increase. The decrease the binding energy of S2p electrons of PEDOT and PSS can be attributed to the cohesive energies between the components decreased in the ternary component compared to the binary component. The increase of the binding energy of S2p electrons of TiS<sub>2</sub> can be attributed to the increase of the cohesive energy between

the S atoms in the  $TiS_2$  in the ternary composite compared to that of its binary component. These XPS analysis suggest that the layers of  $TiS_2$  became closer by decreasing their interlayer gaps.

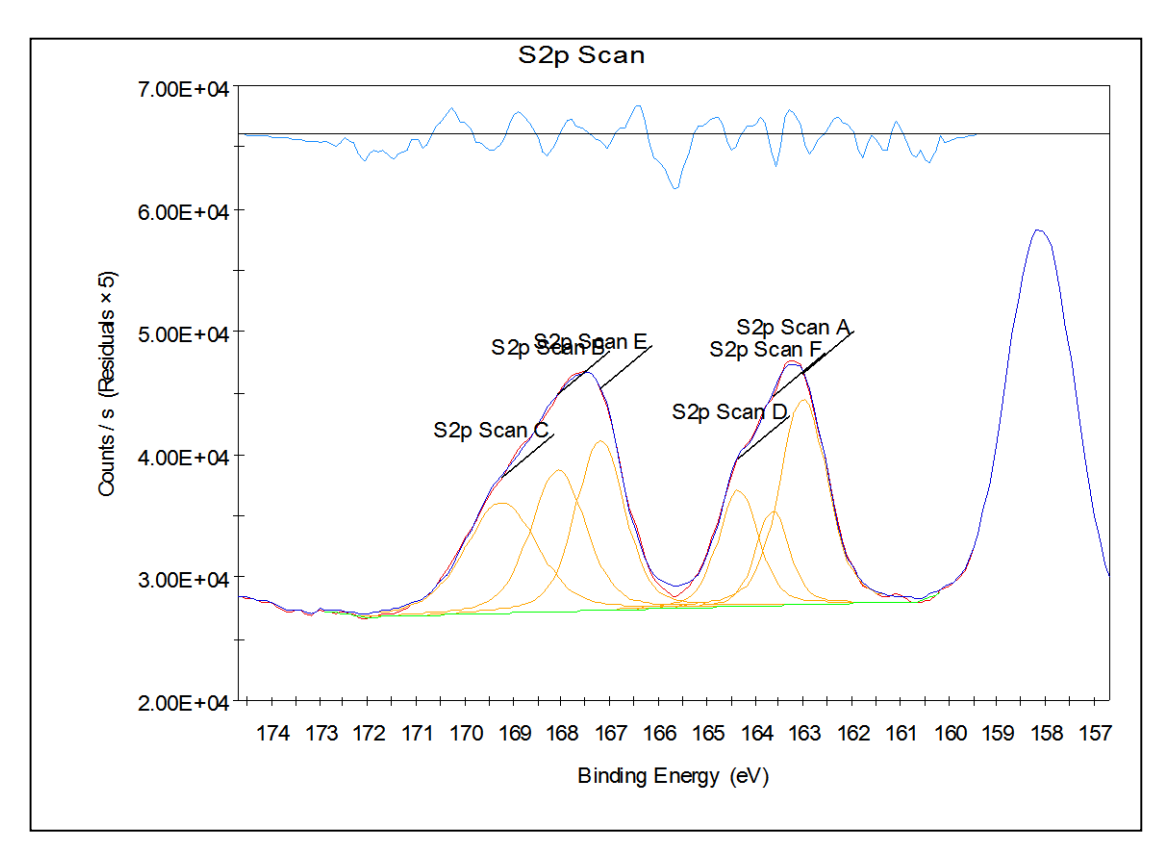
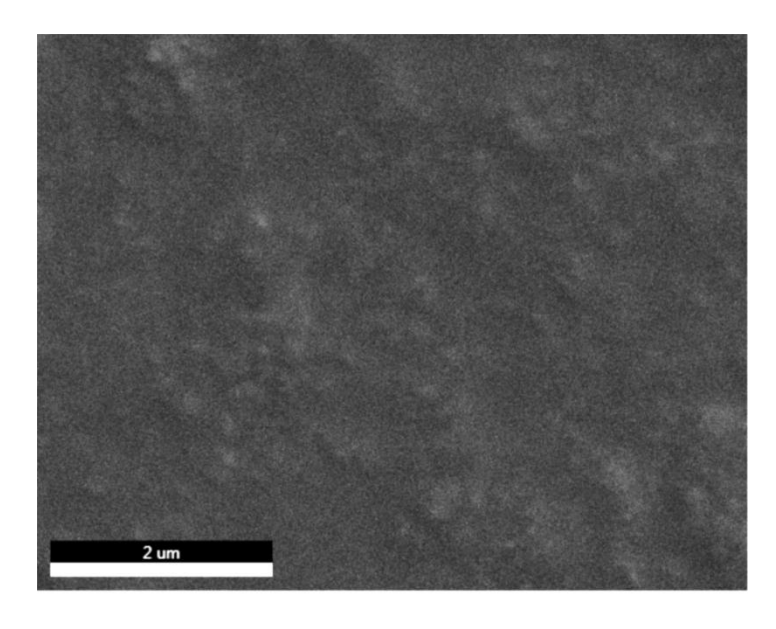


Figure 4.22 XPS survey scan of PEDOT:PSSA/TiS2-CsCO3

Figure 4.23 show he SEM morphology of the pristine PEDOT:PSSA and, then the Figures 4.24, 4.25 and 4.26 show morphology of ternary composite whereas respective distributions of the elements in the polymer C (4.24, present in the PEDOT:PSSA), O (4.25, represents the oxygen content of the compound) and S (, Shows the ratio of sulfur in the compound measured by EDAX. It seems that the homogeneity of the elements is good in the scale of micro-size [153].



**Figure 4.23.** SEM image of PEDOT:PSSA

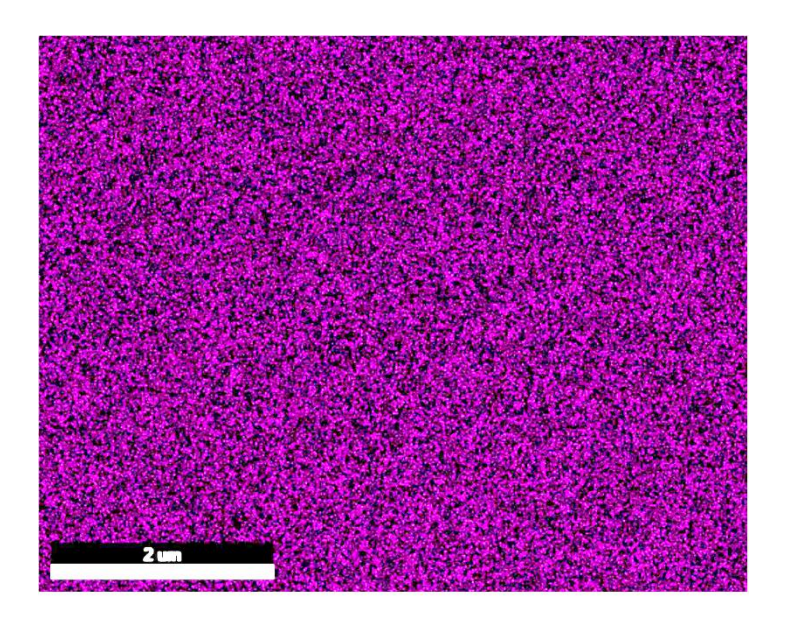
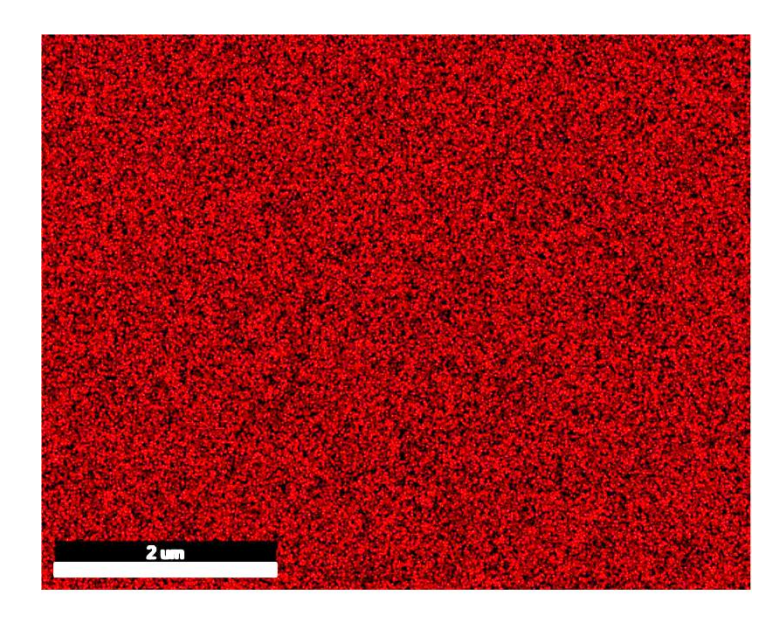


Figure 4.24 The percentage of carbon in the PEDOT:PSSA



**Figure 4.25** The percentage of oxygen in the PEDOT:PSSA

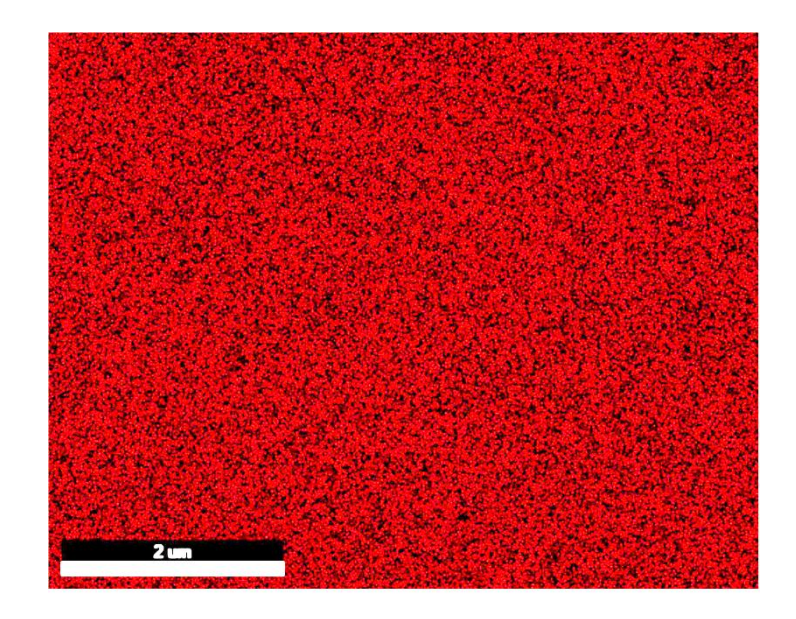


Figure 4.26 The percentage of sulfur in the PEDOT:PSSA

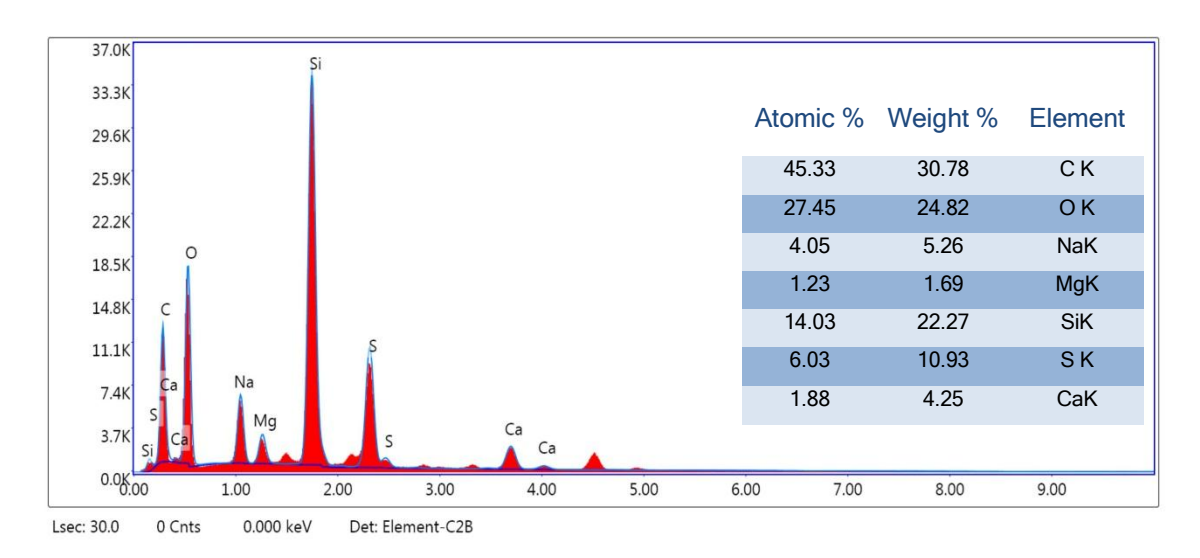
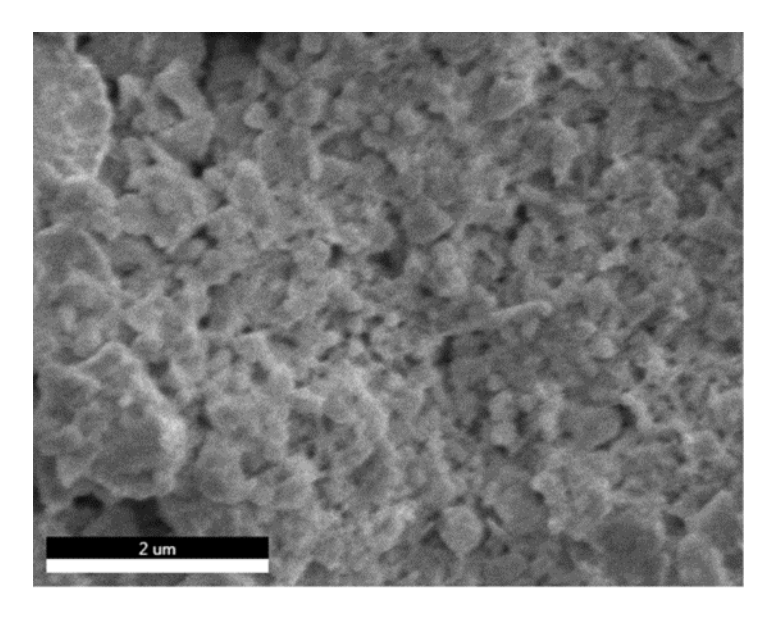


Figure 4.27 EDAX analysis of the PEDOT:PSSA

Figure 4.27 shows quantitative analysis by EDAX indicating with C loadings of 30.7 wt.%, O 24.82 wt.% and S loadings of 10.93 wt.% as against the desired loadings of the total amount from PEDOT:PSSA [153].



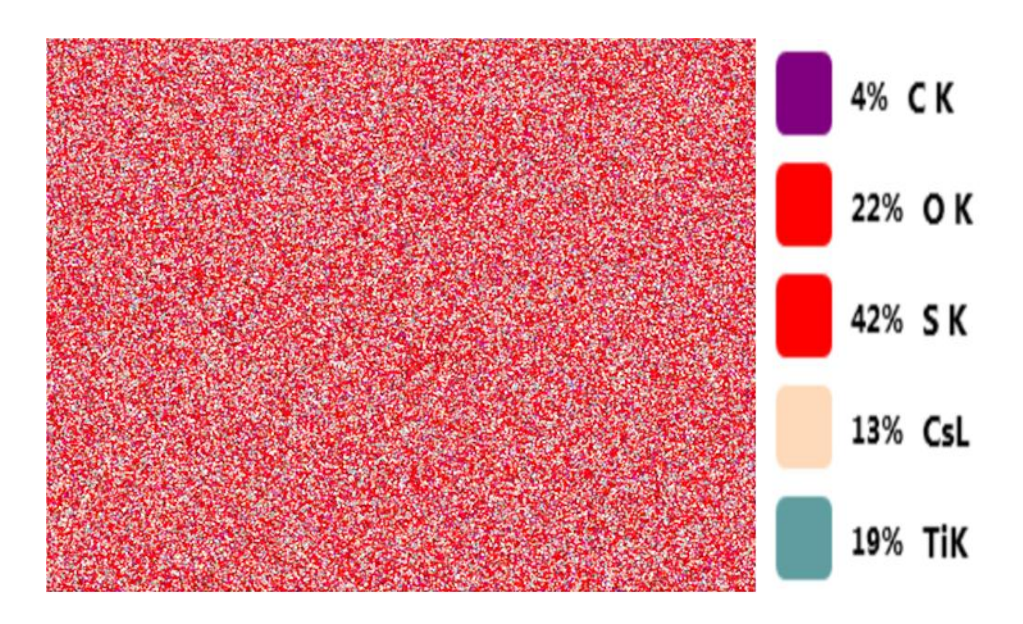
**Figure 4.28** SEM image of the composite PEDOT:PSSA/ Cs<sub>2</sub>CO<sub>3</sub> /TiS<sub>2</sub>= 1/0.14/0.3

Figure 4.28 shows the SEM morphology of the composite PEDOT:PSSAA/TiS<sub>2</sub>-CsCO<sub>3</sub> and then the Figures 4.29, 4.30, 4.31, 4.32, 4.33 and 4.34 show PEDOT:PSSA/Cs<sub>2</sub>CO<sub>3</sub>/TiS<sub>2</sub>= 1/0.14/0.3.

The respective distributions of the elements in the composite is given in the Figure 4.29 (with back-content), and the distribution the elements C, O, S, Cs and Ti are

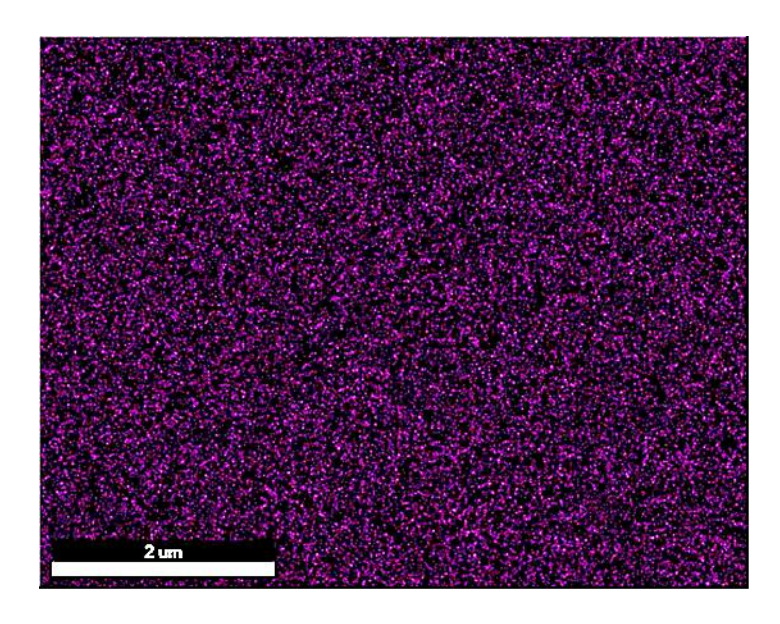
given in the Figures 4.30, 4.31, 4.32, 4.33 and 4.34, respectively. It is clear that the homogeneity of the elements is not good among themselves within the composition of the compound and this may be due to the accuracy in preparing the sample [153].

Figure 4.35 shows quantitative analysis by EDAX indicates C loadings of 7.89 wt.%, O 28.62 wt.%, S loadings of 20.82 wt.%, Cs loadings of 27.5 wt.% and Ti loadings of 15.42 wt.%, as against the desired loadings of the total amount from PEDOT:PSSAcomposite-1 [153].



**Figure 4.29** EDAX image of respective distributions of the elements of the composite PEDOT:PSSA/  $Cs_2CO_3$  / $TiS_2$ = 1/0.14/0.3

.



**Figure 4.30** Percentage of carbon in the composite PEDOT:PSSA/  $Cs_2CO_3$  / $TiS_2 = 1/0.14/0.3$ 

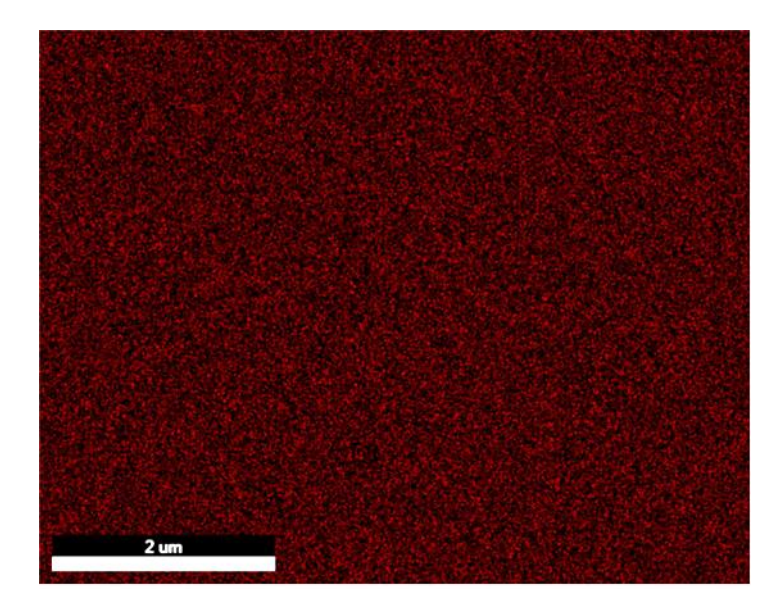


**Figure 4.31** Percentage of oxygen in the composite PEDOT:PSSA/  $Cs_2CO_3$  / $TiS_2 = 1/0.14/0.3$ 

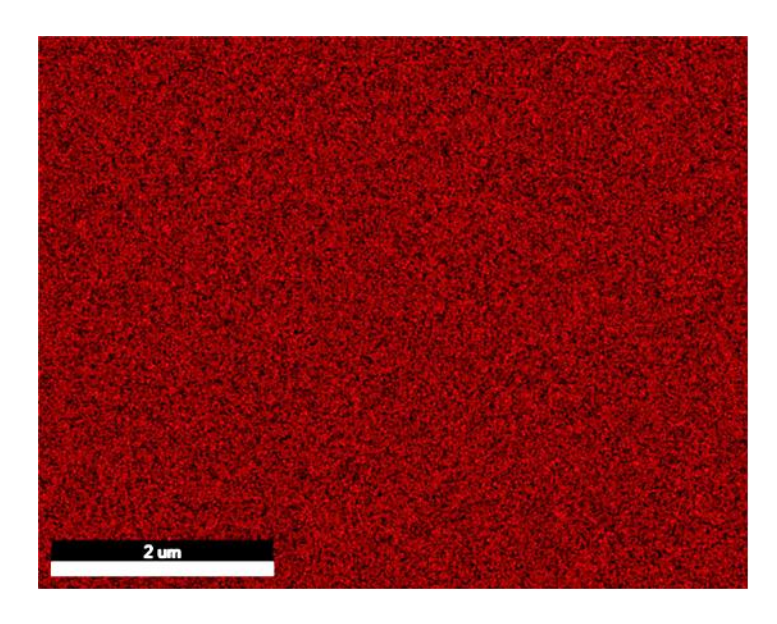


**Figure 4.32** Percentage of sulfur in the composite PEDOT:PSSA/  $Cs_2CO_3$  / $TiS_2 = 1/0.14/0.3$ 

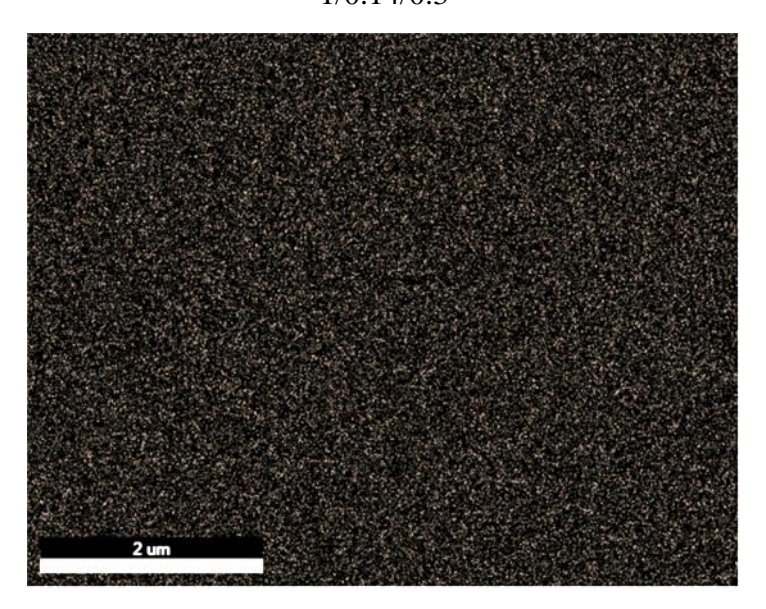


**Figure 4.33** Percentage of cesium in the composite PEDOT:PSSA/  $Cs_2CO_3$  / $TiS_2 = 1/0.14/0.3$ 

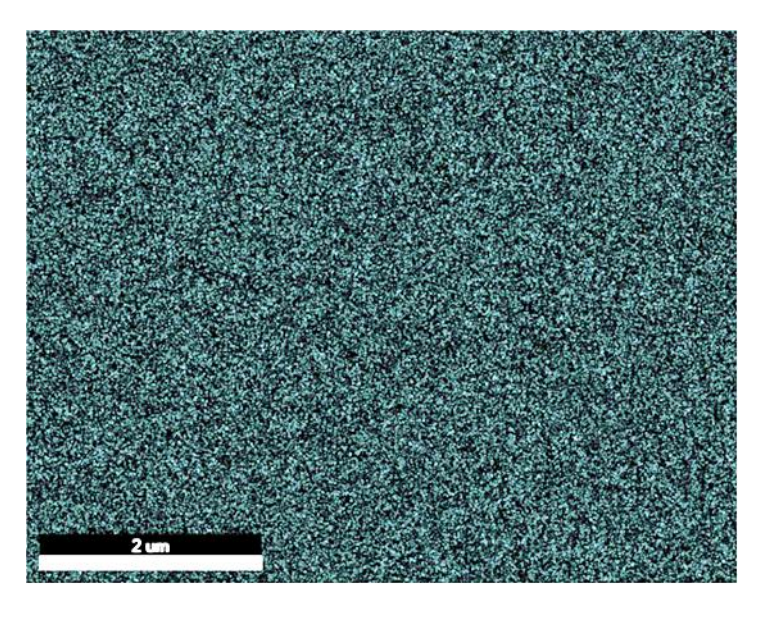


**Figure 4.34** Percentage of titanium in the composite PEDOT:PSSA/  $Cs_2CO_3$  / $TiS_2 = 1/0.14/0.3$ 

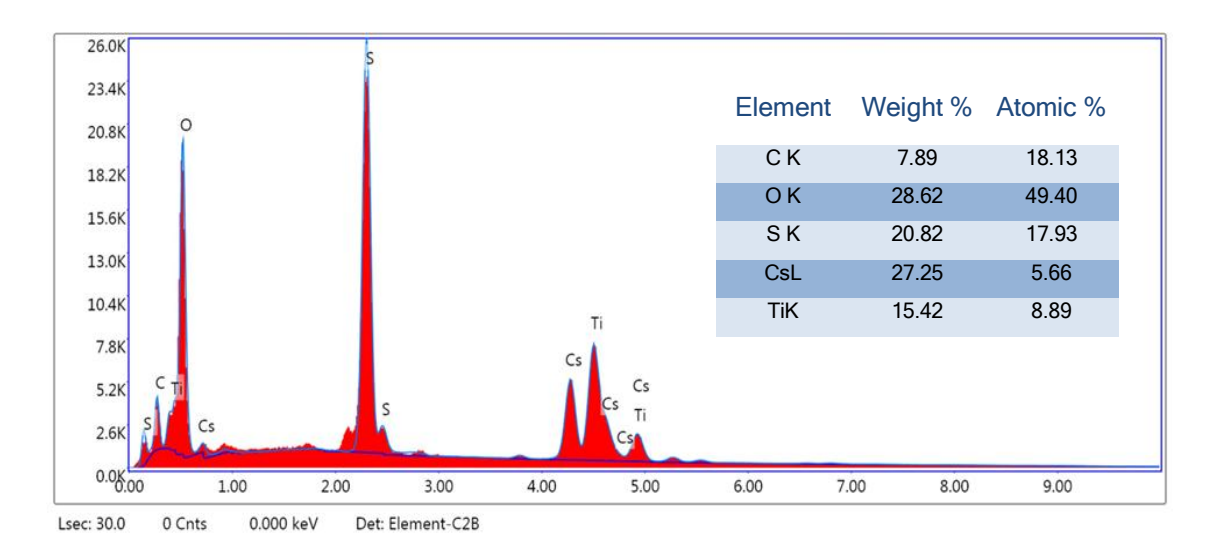


**Figure 4.35** EDAX analysis of the composite PEDOT:PSSA/  $Cs_2CO_3$  / $TiS_2 = 1/0.14/0.3$ 

# 4.6 Conclusions

- 1. PEDOT:PSSA synthesized in this study has the highest positive Seebeck coefficient reported so far in the literature for the pristine PEDOT.
- 2. The thermoelectric properties of the PEDOT:PSSA/ZnS-PVOH are not high enough.
- 3. Cu1.8S nanoparticles can be readily synthesized by the reaction of copper (I) chloride and thiourea in ethylene glycol as described in this work.
- 4. The nanocomposite containing 20%  $Cu_{1.8}S$  and % 80 PEDOT:PSSA has the largest Seebeck coefficient (i.e., 7000  $\mu V/K$ ) and highest power factor (i.e. 2646  $\mu W/mK^2$ ) reported so far for conducting polymer composites in the literature.
- 5. Since PEDOT:PSSA and Cu<sub>1.8</sub>S are abundant and nontoxic materials, PEDOT containing 20 % Cu<sub>1.8</sub>S is suitable thermoelectric material to fabricate cheap, environment friendly and efficient thermoelectric devices.
- 6. High performance and stable n-type polymer based thermoelectric materials can be simply prepared by introduction of  $TiS_2$  into the PEDOT:PSSA dispersions. The maximum PF of 1516  $\mu$ W m<sup>-1</sup> K<sup>-2</sup> was obtained for the composite containing 20 % of  $TiS_2$ . To the best of our knowledge, this is the highest PF reported at room temperature so far in the literature. Also its estimated ZT value is higher than that of  $Bi_2Te_3$  which has the highest performance (ZT=0.96) TE material used in commercial modules. Therefore,  $TiS_2/PEDOT:PSSA$  composites can be used to fabricate safer, cheaper, flexible, stable and efficient polymeric TE modules.
- 7. The thermoelectric properties of the PEDOT:PSSA/TiS<sub>2</sub>/Cs<sub>2</sub>CO<sub>3</sub> are not high enough probably because of the immiscibility of its components .

- [1] C. Gayner and K. K. Kar, "Recent advances in thermoelectric materials," *Progress in Materials Science*, vol. 83, pp. 330-382, 2016.
- [2] N. Toshima, "Recent progress of organic and hybrid thermoelectric materials," *Synthetic Metals*, vol. 225, pp. 3-21, 2017/03/01/ 2017.
- [3] Y. Zhang, Y. Zhao, D. Gosselink, and P. Chen, "Synthesis of poly(ethylene-oxide)/nanoclay solid polymer electrolyte for all solid-state lithium/sulfur battery," *Ionics*, vol. 21, pp. 381-385, 2015/02/01 2015.
- [4] M. Bharti, A. Singh, S. Samanta, and D. K. Aswal, "Conductive polymers for thermoelectric power generation," *Progress in Materials Science*, vol. 93, pp. 270-310, 2018/04/01/2018.
- [5] S. Johnsen et al., "Nanostructures boost the thermoelectric performance of PbS," Journal of the American Chemical Society, vol. 133, no. 10, pp. 3460-3470, 2011.
- [6] O. Bubnova, Z. U. Khan, A. Malti, S. Braun, M. Fahlman, M. Berggren, et al., "Optimization of the thermoelectric figure of merit in the conducting polymer poly(3,4-ethylenedioxythiophene)," *Nature Materials*, vol. 10, pp. 429-433, 2011/06/01 2011.
- [7] X.-F. Lu, L.-F. Gu, J.-W. Wang, J.-X. Wu, P.-Q. Liao, and G.-R. Li, "Bimetal-Organic Framework Derived CoFe2O4/C Porous Hybrid Nanorod Arrays as High-Performance Electrocatalysts for Oxygen Evolution Reaction," *Advanced Materials*, vol. 29, p. 1604437, 2017.
- [8] M. Culebras, C. Gómez, and A. Cantarero, "Review on polymers for thermoelectric applications," *Materials*, vol. 7, pp. 6701-6732, 2014.
- [9] M. Scholdt, H. Do, J. Lang, A. Gall, A. Colsmann, U. Lemmer, *et al.*, "Organic semiconductors for thermoelectric applications," *Journal of electronic materials*, vol. 39, pp. 1589-1592, 2010.

- [10] J. Y. Kim, M. H. Kwon, Y. K. Min, S. Kwon, and D. W. Ihm, "Self-Assembly and Crystalline Growth of Poly (3, 4-ethylenedioxythiophene) Nanofilms," *Advanced Materials*, vol. 19, pp. 3501-3506, 2007.
- [11] Y. Xia, K. Sun, and J. Ouyang, "Solution-processed metallic conducting polymer films as transparent electrode of optoelectronic devices," *Advanced Materials*, vol. 24, pp. 2436-2440, 2012.
- [12] N. Kim, S. Kee, S. H. Lee, B. H. Lee, Y. H. Kahng, Y. R. Jo, *et al.*, "Highly conductive PEDOT: PSS nanofibrils induced by solution-processed crystallization," *Advanced materials*, vol. 26, pp. 2268-2272, 2014.
- [13] B. Cho, K. S. Park, J. Baek, H. S. Oh, Y.-E. Koo Lee, and M. M. Sung, "Single-crystal poly (3, 4-ethylenedioxythiophene) nanowires with ultrahigh conductivity," *Nano letters*, vol. 14, pp. 3321-3327, 2014.
- [14] M. Culebras, C. Gómez, and A. Cantarero, "Enhanced thermoelectric performance of PEDOT with different counter-ions optimized by chemical reduction," *Journal of Materials Chemistry A*, vol. 2, pp. 10109-10115, 2014.
- [15] O. Bubnova, Z. U. Khan, A. Malti, S. Braun, M. Fahlman, M. Berggren, *et al.*, "Optimization of the thermoelectric figure of merit in the conducting polymer poly (3, 4-ethylenedioxythiophene)," *Nature materials*, vol. 10, pp. 429-433, 2011.
- [16] G. H. Kim, L. Shao, K. Zhang, and K. P. Pipe, "Engineered doping of organic semiconductors for enhanced thermoelectric efficiency," *Nature materials*, vol. 12, p. 719, 2013.
- [17] Q. Wei, M. Mukaida, K. Kirihara, Y. Naitoh, and T. Ishida, "Recent progress on PEDOT-based thermoelectric materials," *Materials*, vol. 8, pp. 732-750, 2015.
- [18] E. Yang, J. Kim, B. J. Jung, and J. Kwak, "Enhanced thermoelectric properties of sorbitol-mixed PEDOT: PSS thin films by chemical reduction," *Journal of Materials Science: Materials in Electronics*, vol. 26, pp. 2838-2843, 2015.
- [19] Z. Zhu, C. Liu, H. Shi, Q. Jiang, J. Xu, F. Jiang, *et al.*, "An effective approach to enhanced thermoelectric properties of PEDOT: PSS films by a DES post-

- treatment," *Journal of Polymer Science Part B: Polymer Physics,* vol. 53, pp. 885-892, 2015.
- [20] D. A. Mengistie, C.-H. Chen, K. M. Boopathi, F. W. Pranoto, L.-J. Li, and C.-W. Chu, "Enhanced thermoelectric performance of PEDOT: PSS flexible bulky papers by treatment with secondary dopants," *ACS applied materials & interfaces*, vol. 7, pp. 94-100, 2014.
- [21] J. Wang, K. Cai, and S. Shen, "A facile chemical reduction approach for effectively tuning thermoelectric properties of PEDOT films," *Organic Electronics*, vol. 17, pp. 151-158, 2015.
- [22] D. Kim, Y. Kim, K. Choi, J. C. Grunlan, and C. Yu, "Improved Thermoelectric Behavior of Nanotube-Filled Polymer Composites with Poly(3,4-ethylenedioxythiophene) Poly(styrenesulfonate)," *ACS Nano*, vol. 4, pp. 513-523, 2010/01/26 2010.
- [23] R. Kroon, D. A. Mengistie, D. Kiefer, J. Hynynen, J. D. Ryan, L. Yu, *et al.*, "Thermoelectric plastics: from design to synthesis, processing and structure–property relationships," *Chemical Society Reviews*, vol. 45, pp. 6147-6164, 2016.
- [24] F. Li, K. Cai, S. Shen, and S. Chen, "Preparation and thermoelectric properties of reduced graphene oxide/PEDOT: PSS composite films," *Synthetic Metals*, vol. 197, pp. 58-61, 2014.
- [25] K. Zhang, Y. Zhang, and S. Wang, "Enhancing thermoelectric properties of organic composites through hierarchical nanostructures," *Scientific reports*, vol. 3, p. 3448, 2013.
- [26] Q. Jiang, C. Liu, J. Xu, B. Lu, H. Song, H. Shi, et al., "An effective substrate for the enhancement of thermoelectric properties in PEDOT: PSS," *Journal of Polymer Science Part B: Polymer Physics*, vol. 52, pp. 737-742, 2014.
- [27] H. Jin, J. Li, J. Iocozzia, X. Zeng, P. C. Wei, C. Yang, *et al.*, "Hybrid Organic–Inorganic Thermoelectric Materials and Devices," *Angewandte Chemie International Edition*, vol. 58, pp. 15206-15226, 2019.

- [28] C. J. An, Y. H. Kang, A.-Y. Lee, K.-S. Jang, Y. Jeong, and S. Y. Cho, "Foldable thermoelectric materials: improvement of the thermoelectric performance of directly spun CNT webs by individual control of electrical and thermal conductivity," *ACS applied materials & interfaces*, vol. 8, pp. 22142-22150, 2016.
- [29] C. Li, F. Jiang, C. Liu, W. Wang, X. Li, T. Wang, *et al.*, "A simple thermoelectric device based on inorganic/organic composite thin film for energy harvesting," *Chemical Engineering Journal*, vol. 320, pp. 201-210, 2017.
- [30] Q. Meng, K. Cai, Y. Du, and L. Chen, "Preparation and thermoelectric properties of SWCNT/PEDOT: PSS coated tellurium nanorod composite films," *Journal of Alloys and Compounds*, vol. 778, pp. 163-169, 2019.
- [31] E. J. Bae, Y. H. Kang, K.-S. Jang, C. Lee, and S. Y. Cho, "Solution synthesis of telluride-based nano-barbell structures coated with PEDOT: PSS for spray-printed thermoelectric generators," *Nanoscale*, vol. 8, pp. 10885-10890, 2016.
- [32] X. Hu, K. Zhang, J. Zhang, S. Wang, and Y. Qiu, "Thermoelectric properties of conducting polymer nanowire–tellurium nanowire composites," *ACS Applied Energy Materials*, vol. 1, pp. 4883-4890, 2018.
- [33] Y. Wang, C. Yu, M. Sheng, S. Song, and Y. Deng, "Individual Adjustment of Electrical Conductivity and Thermopower Enabled by Multiple Interfaces in Polyaniline-Based Ternary Hybrid Nanomaterials for High Thermoelectric Performances," *Advanced Materials Interfaces*, vol. 5, p. 1701168, 2018.
- [34] Y. Du, X. Liu, J. Xu, and S. Z. Shen, "Flexible Bi–Te-based alloy nanosheet/PEDOT: PSS thermoelectric power generators," *Materials Chemistry Frontiers*, 2019.
- [35] H. Ju and J. Kim, "Chemically exfoliated SnSe nanosheets and their SnSe/poly (3, 4-ethylenedioxythiophene): poly (styrenesulfonate) composite films for polymer based thermoelectric applications," *ACS nano*, vol. 10, pp. 5730-5739, 2016.

- [36] H. Ju and J. Kim, "Fabrication of conductive polymer/inorganic nanoparticles composite films: PEDOT: PSS with exfoliated tin selenide nanosheets for polymer-based thermoelectric devices," *Chemical Engineering Journal*, vol. 297, pp. 66-73, 2016.
- [37] X. Li, C. Liu, T. Wang, W. Wang, X. Wang, Q. Jiang, et al., "Preparation of 2D MoSe2/PEDOT: PSS composite and its thermoelectric properties," *Materials Research Express*, vol. 4, p. 116410, 2017.
- [38] X. Wang, F. Meng, Q. Jiang, W. Zhou, F. Jiang, T. Wang, *et al.*, "Simple layer-by-layer assembly method for simultaneously enhanced electrical conductivity and thermopower of PEDOT: PSS/ce-MoS2 heterostructure films," *ACS Applied Energy Materials*, vol. 1, pp. 3123-3133, 2018.
- [39] Y. Nonoguchi, M. Nakano, T. Murayama, H. Hagino, S. Hama, K. Miyazaki, *et al.*, "Simple Salt-Coordinated n-Type Nanocarbon Materials Stable in Air," *Advanced Functional Materials*, vol. 26, pp. 3021-3028, 2016.
- [40] E. W. Zaia, M. P. Gordon, V. Niemann, J. Choi, R. Chatterjee, C. H. Hsu, *et al.*, "Molecular Level Insight into Enhanced n-Type Transport in Solution-Printed Hybrid Thermoelectrics," *Advanced Energy Materials*, vol. 9, p. 1803469, 2019.
- [41] Y. Chen, M. He, B. Liu, G. C. Bazan, J. Zhou, and Z. Liang, "Bendable n-Type Metallic Nanocomposites with Large Thermoelectric Power Factor," *Advanced Materials*, vol. 29, p. 1604752, 2017.
- [42] G. Wu, Z.-G. Zhang, Y. Li, C. Gao, X. Wang, and G. Chen, "Exploring high-performance n-type thermoelectric composites using amino-substituted rylene dimides and carbon nanotubes," *ACS nano*, vol. 11, pp. 5746-5752, 2017.
- [43] C. Gao, Y. Liu, Y. Gao, Y. Zhou, X. Zhou, X. Yin, *et al.*, "High-performance ntype thermoelectric composites of acridones with tethered tertiary amines and carbon nanotubes," *Journal of Materials Chemistry A*, vol. 6, pp. 20161-20169, 2018.

- [44] C. Wan, R. Tian, M. Kondou, R. Yang, P. Zong, and K. Koumoto, "Ultrahigh thermoelectric power factor in flexible hybrid inorganic-organic superlattice," *Nature communications*, vol. 8, p. 1024, 2017.
- [45] G. S. Nolas, J. Sharp, and H. G. Thermoelectrics, "Basic principles and new materials developments," *Thermoelectrics. Berlin: Springer*, 2001.
- [46] D. Rowe, "CRC handbook of thermoelectrics: macro to nano," *Boca Ratcon: CRC Taylor & Francis,* 2006.
- [47] T. M. Tritt and M. Subramanian, "Thermoelectric materials, phenomena, and applications: a bird's eye view," *MRS bulletin,* vol. 31, pp. 188-198, 2006.
- [48] G. Chen, M. Dresselhaus, G. Dresselhaus, J.-P. Fleurial, and T. Caillat, "Recent developments in thermoelectric materials," *International Materials Reviews*, vol. 48, pp. 45-66, 2003.
- [49] M. S. Dresselhaus, G. Chen, M. Y. Tang, R. Yang, H. Lee, D. Wang, *et al.*, "New directions for low-dimensional thermoelectric materials," *Advanced materials*, vol. 19, pp. 1043-1053, 2007.
- [50] L. E. Bell, "Cooling, heating, generating power, and recovering waste heat with thermoelectric systems," *Science*, vol. 321, pp. 1457-1461, 2008.
- [51] H. J. Goldsmid, *Introduction to thermoelectricity* vol. 121: Springer, 2010.
- [52] R. Chasmar and R. Stratton, "The thermoelectric figure of merit and its relation to thermoelectric generators," *International journal of electronics*, vol. 7, pp. 52-72, 1959.
- [53] A. Bulusu and D. Walker, "Review oSf electronic transport models for thermoelectric materials," *Superlattices and Microstructures*, vol. 44, pp. 1-36, 2008.
- [54] A. F. Ioffe, *Physics of semiconductors*: Infosearch, 1960.
- [55] J. O. Sofo and G. Mahan, "Optimum band gap of a thermoelectric material," *Physical Review B*, vol. 49, p. 4565, 1994.

- [56] G. A. Slack and V. G. Tsoukala, "Some properties of semiconducting IrSb3," *Journal of Applied Physics*, vol. 76, pp. 1665-1671, 1994.
- [57] K. F. Hsu, S. Loo, F. Guo, W. Chen, J. S. Dyck, C. Uher, *et al.*, "Cubic AgPbmSbTe2+ m: bulk thermoelectric materials with high figure of merit," *Science*, vol. 303, pp. 818-821, 2004.
- [58] M. Zhou, J.-F. Li, and T. Kita, "Nanostructured AgPb m SbTe m+ 2 system bulk materials with enhanced thermoelectric performance," *Journal of the American Chemical Society*, vol. 130, pp. 4527-4532, 2008.
- [59] M. Zhou, J.-F. Li, H. Wang, T. Kita, L. Li, and Z. Chen, "Nanostructure and high thermoelectric performance in nonstoichiometric AgPbSbTe compounds: the role of Ag," *Journal of electronic materials*, vol. 40, pp. 862-866, 2011.
- [60] J. P. Heremans, V. Jovovic, E. S. Toberer, A. Saramat, K. Kurosaki, A. Charoenphakdee, et al., "Enhancement of thermoelectric efficiency in PbTe by distortion of the electronic density of states," *Science*, vol. 321, pp. 554-557, 2008.
- [61] Y. Pei, A. D. LaLonde, N. A. Heinz, X. Shi, S. Iwanaga, H. Wang, *et al.*, "Stabilizing the optimal carrier concentration for high thermoelectric efficiency," *Advanced materials*, vol. 23, pp. 5674-5678, 2011.
- [62] Y. Pei, X. Shi, A. LaLonde, H. Wang, L. Chen, and G. J. Snyder, "Convergence of electronic bands for high performance bulk thermoelectrics," *Nature*, vol. 473, p. 66, 2011.
- [63] Y. Pei, H. Wang, Z. M. Gibbs, A. D. LaLonde, and G. J. Snyder, "Thermopower enhancement in Pb 1– 1– x Mn x Te alloys and its effect on thermoelectric efficiency," *NPG Asia Materials*, vol. 4, p. e28, 2012.
- [64] B. Paul, P. Rawat, and P. Banerji, "Dramatic enhancement of thermoelectric power factor in PbTe: Cr co-doped with iodine," *Applied Physics Letters*, vol. 98, p. 262101, 2011.
- [65] M. G. Kanatzidis, "Nanostructured thermoelectrics: the new paradigm?," *Chemistry of materials*, vol. 22, pp. 648-659, 2009.

- [66] M. G. Kanatzidis and J. R. Sootsman, "Mechanical strength and thermoelectric performance in metal chalcogenide MQ (M= Ge, Sn, Pb and Q= S, Se, Te) based compositions," ed: Google Patents, 2012.
- [67] M. G. Kanatzidis, Q. Zhang, S. N. Girard, and K. Biswas, "Thermoelectrics compositions comprising nanoscale inclusions in a chalcogenide matrix," ed: Google Patents, 2014.
- [68] D. X. Crispin, "Retracted article: towards polymer-based organic thermoelectric generators," *Energy & Environmental Science*, 2012.
- [69] G. J. Snyder and E. S. Toberer, "Complex thermoelectric materials," in materials for sustainable energy: a collection of peer-reviewed research and review articles from Nature Publishing Group, ed: World Scientific, 2011, pp. 101-110.
- [70] B. Russ, A. Glaudell, J. J. Urban, M. L. Chabinyc, and R. A. Segalman, "Organic thermoelectric materials for energy harvesting and temperature control," *Nature Reviews Materials*, vol. 1, p. 16050, 2016.
- [71] S. Iwanaga, E. S. Toberer, A. LaLonde, and G. J. Snyder, "A high temperature apparatus for measurement of the Seebeck coefficient," *Review of Scientific Instruments*, vol. 82, p. 063905, 2011.
- [72] Z. Zhou and C. Uher, "Apparatus for Seebeck coefficient and electrical resistivity measurements of bulk thermoelectric materials at high temperature," *Review of scientific instruments*, vol. 76, p. 023901, 2005.
- [73] R. E. Hummel, "Semiconductors," in *Electronic Properties of Materials*, ed: Springer, 2001, pp. 104-165.
- [74] J. L. Bredas and G. B. Street, "Polarons, bipolarons, and solitons in conducting polymers," *Accounts of Chemical Research*, vol. 18, pp. 309-315, 1985.
- [75] J.-P. Fleurial, "Thermoelectric power generation materials: Technology and application opportunities," *Jom*, vol. 61, pp. 79-85, 2009.

- [76] F. Rosi, "Thermoelectricity and thermoelectric power generation," *Solid-State Electronics*, vol. 11, pp. 833-868, 1968.
- [77] D. Rowe and G. Min, "Evaluation of thermoelectric modules for power generation," *Journal of power sources*, vol. 73, pp. 193-198, 1998.
- [78] H. Scherrer, L. Vikhor, B. Lenoir, A. Dauscher, and P. Poinas, "Solar thermolectric generator based on skutterudites," *Journal of Power Sources*, vol. 115, pp. 141-148, 2003.
- [79] H. Xi, L. Luo, and G. Fraisse, "Development and applications of solar-based thermoelectric technologies," *Renewable and Sustainable Energy Reviews*, vol. 11, pp. 923-936, 2007.
- [80] S. Maneewan, J. Khedari, B. Zeghmati, J. Hirunlabh, and J. Eakburanawat, "Investigation on generated power of thermoelectric roof solar collector," *Renewable Energy*, vol. 29, pp. 743-752, 2004.
- [81] S. Maneewan, J. Hirunlabh, J. Khedari, B. Zeghmati, and S. Teekasap, "Heat gain reduction by means of thermoelectric roof solar collector," *Solar Energy*, vol. 78, pp. 495-503, 2005.
- [82] H. Shirakawa, E. J. Louis, A. G. MacDiarmid, C. K. Chiang, and A. J. Heeger, "Synthesis of electrically conducting organic polymers: halogen derivatives of polyacetylene,(CH) x," *Journal of the Chemical Society, Chemical Communications,* pp. 578-580, 1977.
- [83] H. Akamatu, H. Inokuchi, and Y. Matsunaga, "Electrical conductivity of the perylene–bromine complex," *Nature*, vol. 173, pp. 168-169, 1954.
- [84] Y. Sun, P. Sheng, C. Di, F. Jiao, W. Xu, D. Qiu, *et al.*, "Organic Thermoelectric Materials and Devices Based on p-and n-Type Poly (metal 1, 1, 2, 2-ethenetetrathiolate) s," *Advanced Materials*, vol. 24, pp. 932-937, 2012.
- [85] Y. Nakai, K. Honda, K. Yanagi, H. Kataura, T. Kato, T. Yamamoto, *et al.*, "Giant Seebeck coefficient in semiconducting single-wall carbon nanotube film," *Applied Physics Express*, vol. 7, p. 025103, 2014.

- [86] W. Zhao, S. Fan, N. Xiao, D. Liu, Y. Y. Tay, C. Yu, *et al.*, "Flexible carbon nanotube papers with improved thermoelectric properties," *Energy & Environmental Science*, vol. 5, pp. 5364-5369, 2012.
- [87] H. Yan, N. Sada, and N. Toshima, "Thermal transporting properties of electrically conductive polyaniline films as organic thermoelectric materials," *Journal of Thermal Analysis and Calorimetry*, vol. 69, pp. 881-887, 2002.
- [88] G. T. Craven and A. Nitzan, "Wiedemann-Franz Law for Molecular Hopping Transport," *arXiv preprint arXiv:1909.06220*, 2019.
- [89] N. Toshima, "Making an advance of organic thermoelectric materials: acceleration of energy recovery from waste heat with hybridization," *Gendai Kagaku*, vol. 532, pp. 42-46, 2015.
- [90] N. Basescu, Z.-X. Liu, D. Moses, A. Heeger, H. Naarmann, and N. Theophilou, "High electrical conductivity in doped polyacetylene," *Nature*, vol. 327, p. 403, 1987.
- [91] Y. Park, C. Yoon, B. Na, H. Shirakawa, and K. Akagi, "METALLIC PROPERTIES OF TRANSITION METAL HALIDES DOPED POLY-ACETYLENE; THE SOLITON LIQUID STATE," *Korea,* vol. 379, p. 50, 1991.
- [92] H. Kaneko, T. Ishiguro, A. Takahashi, and J. Tsukamoto, "Magnetoresistance and thermoelectric power studies of metal-nonmetal transition in iodine-doped polyacetylene," *Synthetic metals*, vol. 57, pp. 4900-4905, 1993.
- [93] O. T. Ikkala, L. O. Pietilä, L. Ahjopalo, H. Österholm, and P. J. Passiniemi, "On the molecular recognition and associations between electrically conducting polyaniline and solvents," *The Journal of chemical physics,* vol. 103, pp. 9855-9863, 1995.
- [94] L. Jun, Z. Lian-meng, H. Li, and T. Xin-feng, "Synthesis and thermoelectric properties of polyaniline," *Journal of Wuhan University of Technology-Mater. Sci. Ed.*, vol. 18, pp. 53-55, 2003.

- [95] R. Menon, C. Yoon, D. Moses, A. Heeger, and Y. Cao, "Transport in polyaniline near the critical regime of the metal-insulator transition," *Physical Review B*, vol. 48, p. 17685, 1993.
- [96] Y. Sun, Z. Wei, W. Xu, and D. Zhu, "A three-in-one improvement in thermoelectric properties of polyaniline brought by nanostructures," *Synthetic Metals*, vol. 160, pp. 2371-2376, 2010.
- [97] R. B. Aïch, N. Blouin, A. Bouchard, and M. Leclerc, "Electrical and thermoelectric properties of poly (2, 7-carbazole) derivatives," *Chemistry of Materials*, vol. 21, pp. 751-757, 2009.
- [98] M. He, J. Ge, Z. Lin, X. Feng, X. Wang, H. Lu, *et al.*, "Thermopower enhancement in conducting polymer nanocomposites via carrier energy scattering at the organic–inorganic semiconductor interface," *Energy & Environmental Science*, vol. 5, pp. 8351-8358, 2012.
- [99] B. Endrődi, J. Mellar, Z. Gingl, C. Visy, and C. Janáky, "Reasons behind the improved thermoelectric properties of poly (3-hexylthiophene) nanofiber networks," *RSC Advances*, vol. 4, pp. 55328-55333, 2014.
- [100] Y. Xuan, X. Liu, S. Desbief, P. Leclère, M. Fahlman, R. Lazzaroni, *et al.*, "Thermoelectric properties of conducting polymers: The case of poly (3-hexylthiophene)," *Physical Review B*, vol. 82, p. 115454, 2010.
- [101] Q. Zhang, Y. Sun, W. Xu, and D. Zhu, "Thermoelectric energy from flexible P3HT films doped with a ferric salt of triflimide anions," *Energy & Environmental Science*, vol. 5, pp. 9639-9644, 2012.
- [102] C. Bounioux, P. Díaz-Chao, M. Campoy-Quiles, M. S. Martín-González, A. R. Goni, R. Yerushalmi-Rozen, *et al.*, "Thermoelectric composites of poly (3-hexylthiophene) and carbon nanotubes with a large power factor," *Energy & Environmental Science*, vol. 6, pp. 918-925, 2013.
- [103] W. Lee, C. T. Hong, O. H. Kwon, Y. Yoo, Y. H. Kang, J. Y. Lee, *et al.*, "Enhanced thermoelectric performance of bar-coated SWCNT/P3HT thin films," *ACS applied materials & interfaces*, vol. 7, pp. 6550-6556, 2015.

- [104] L. Xu, Y. Liu, B. Chen, C. Zhao, and K. Lu, "Enhancement in thermoelectric properties using a P-type and N-type thin-film device structure," *Polymer Composites*, vol. 34, pp. 1728-1734, 2013.
- [105] A. Shakouri and S. Li, "Thermoelectric power factor for electrically conductive polymers," in *Eighteenth International Conference on Thermoelectrics. Proceedings, ICT'99 (Cat. No. 99TH8407)*, 1999, pp. 402-406.
- [106] Q. Zhang, H. Wang, Q. Zhang, W. Liu, B. Yu, H. Wang, *et al.*, "Effect of silicon and sodium on thermoelectric properties of thallium-doped lead telluride-based materials," *Nano letters*, vol. 12, pp. 2324-2330, 2012.
- [107] L. Fang, K. Zhou, F. Wu, Q. Huang, X. Yang, and C. Kong, "Effect of doping concentration on the thermolectric properties of nano Ga-doped ZnO films," in 2010 3rd International Nanoelectronics Conference (INEC), 2010, pp. 1175-1176.
- [108] S. N. Patel, A. M. Glaudell, D. Kiefer, and M. L. Chabinyc, "Increasing the thermoelectric power factor of a semiconducting polymer by doping from the vapor phase," *ACS Macro Letters*, vol. 5, pp. 268-272, 2016.
- [109] C. Han and R. Elsenbaumer, "Protonic acids: Generally applicable dopants for conducting polymers," *Synthetic metals*, vol. 30, pp. 123-131, 1989.
- [110] K. H. Yim, G. L. Whiting, C. E. Murphy, J. J. Halls, J. H. Burroughes, R. H. Friend, *et al.*, "Controlling Electrical Properties of Conjugated Polymers via a Solution-Based p-Type Doping," *Advanced Materials*, vol. 20, pp. 3319-3324, 2008.
- [111] Y. Nonoguchi, K. Ohashi, R. Kanazawa, K. Ashiba, K. Hata, T. Nakagawa, *et al.*, "Systematic conversion of single walled carbon nanotubes into n-type thermoelectric materials by molecular dopants," *Scientific reports,* vol. 3, p. 3344, 2013.
- [112] R. A. Schlitz, F. G. Brunetti, A. M. Glaudell, P. L. Miller, M. A. Brady, C. J. Takacs, *et al.*, "Solubility-limited extrinsic n-type doping of a high electron

- mobility polymer for thermoelectric applications," *Advanced materials*, vol. 26, pp. 2825-2830, 2014.
- [113] J. C. Grunlan, L. Liu, and O. Regev, "Weak polyelectrolyte control of carbon nanotube dispersion in water," *Journal of colloid and interface science,* vol. 317, pp. 346-349, 2008.
- [114] H. Bark, J.-S. Kim, H. Kim, J.-H. Yim, and H. Lee, "Effect of multiwalled carbon nanotubes on the thermoelectric properties of a bismuth telluride matrix," *Current Applied Physics*, vol. 13, pp. S111-S114, 2013.
- [115] C. Yu, Y. S. Kim, D. Kim, and J. C. Grunlan, "Thermoelectric behavior of segregated-network polymer nanocomposites," *Nano letters,* vol. 8, pp. 4428-4432, 2008.
- [116] K. C. See, J. P. Feser, C. E. Chen, A. Majumdar, J. J. Urban, and R. A. Segalman, "Water-processable polymer– nanocrystal hybrids for thermoelectrics," *Nano letters*, vol. 10, pp. 4664-4667, 2010.
- [117] B. Zhang, J. Sun, H. Katz, F. Fang, and R. Opila, "Promising thermoelectric properties of commercial PEDOT: PSS materials and their Bi2Te3 powder composites," *ACS applied materials & interfaces*, vol. 2, pp. 3170-3178, 2010.
- [118] C. Liu, F. Jiang, M. Huang, B. Lu, R. Yue, and J. Xu, "Free-standing PEDOT-PSS/Ca<sub>3</sub>Co<sub>4</sub>O<sub>9</sub> composite films as novel thermoelectric materials," *Journal of electronic materials*, vol. 40, pp. 948-952, 2011.
- [119] L. Vaisman, H. D. Wagner, and G. Marom, "The role of surfactants in dispersion of carbon nanotubes," *Advances in colloid and interface science*, vol. 128, pp. 37-46, 2006.
- [120] R. Bandyopadhyaya, E. Nativ-Roth, O. Regev, and R. Yerushalmi-Rozen, "Stabilization of individual carbon nanotubes in aqueous solutions," *Nano letters*, vol. 2, pp. 25-28, 2002.
- [121] N. R. Tummala, "SDS surfactants on carbon nanotubes: aggregate morphology," *ACS nano*, vol. 3, pp. 595-602, 2009.

- [122] N. Grossiord, J. Loos, O. Regev, and C. E. Koning, "Toolbox for dispersing carbon nanotubes into polymers to get conductive nanocomposites," *Chemistry of materials*, vol. 18, pp. 1089-1099, 2006.
- [123] Y. Dror, W. Pyckhout-Hintzen, and Y. Cohen, "Conformation of polymers dispersing single-walled carbon nanotubes in water: a small-angle neutron scattering study," *Macromolecules*, vol. 38, pp. 7828-7836, 2005.
- [124] G. P. Moriarty, J. N. Wheeler, C. Yu, and J. C. Grunlan, "Increasing the thermoelectric power factor of polymer composites using a semiconducting stabilizer for carbon nanotubes," *Carbon*, vol. 50, pp. 885-895, 2012.
- [125] L. Liu and J. C. Grunlan, "Clay assisted dispersion of carbon nanotubes in conductive epoxy nanocomposites," *Advanced Functional Materials*, vol. 17, pp. 2343-2348, 2007.
- [126] B. Yang, H. Ahuja, and T. N. Tran, "Thermoelectric technology assessment: application to air conditioning and refrigeration," *HVAc&R Research*, vol. 14, pp. 635-653, 2008.
- [127] M. Dresselhaus, Y. Lin, S. Cronin, M. Black, O. Rabin, and G. Dresselhaus, "Investigation of low-dimensional thermoelectrics," in *Proceedings of the Nonlithographic and Lithographic Methods for Nanofabrication Symposium*, 2001.
- [128] J.Tervo, A. Manninen, R. Ilola, and H. Hänninen, "State-of-the-art of thermoelectric materials processing," *VTT Technical Research Center of Finland, Vuorimiehentie,* 2009.
- [129] Y. Shinohara, K. Ohara, Y. Imai, Y. Isoda, and H. Nakanishi, "Problems of conductive polymers as thermoelectric materials," in *Proceedings ICT'03.* 22nd International Conference on Thermoelectrics (IEEE Cat. No. 03TH8726), 2003, pp. 298-300.
- [130] D. K. Taggart, Y. Yang, S.-C. Kung, T. M. McIntire, and R. M. Penner, "Enhanced thermoelectric metrics in ultra-long electrodeposited PEDOT nanowires," *Nano letters*, vol. 11, pp. 125-131, 2010.

- [131] M. Khalid, M. A. Tumelero, I. Brandt, V. C. Zoldan, J. J. Acuña, and A. A. Pasa, "Electrical conductivity studies of polyaniline nanotubes doped with different sulfonic acids," *Indian Journal of Materials Science*, vol. 2013, 2013.
- [132] G.-H. Kim, L. Shao, K. Zhang, and K. P. Pipe, "Engineered doping of organic semiconductors for enhanced thermoelectric efficiency," *Nature materials*, vol. 12, pp. 719-723, 2013.
- [133] J.-H. Hsu, W. Choi, G. Yang, and C. Yu, "Origin of unusual thermoelectric transport behaviors in carbon nanotube filled polymer composites after solvent/acid treatments," *Organic Electronics*, vol. 45, pp. 182-189, 2017.
- [134] S. Xu, C. Liu, Z. Xiao, W. Zhong, Y. Luo, H. Ou, *et al.*, "Cooperative effect of carbon black and dimethyl sulfoxide on PEDOT: PSS hole transport layer for inverted planar perovskite solar cells," *Solar Energy*, vol. 157, pp. 125-132, 2017.
- [135] W. Zheng, P. Bi, H. Kang, W. Wei, F. Liu, J. Shi, *et al.*, "Low thermal conductivity and high thermoelectric figure of merit in p-type Sb<sub>2</sub>Te<sub>3</sub>/poly (3, 4-ethylenedioxythiophene) thermoelectric composites," *Applied Physics Letters*, vol. 105, p. 023901, 2014.
- [136] E. J. Bae, Y. H. Kang, K.-S. Jang, and S. Y. Cho, "Enhancement of thermoelectric properties of PEDOT: PSS and tellurium-PEDOT: PSS hybrid composites by simple chemical treatment," *Scientific reports*, vol. 6, p. 18805, 2016.
- [137] H. Song and K. Cai, "Preparation and properties of PEDOT: PSS/Te nanorod composite films for flexible thermoelectric power generator," *Energy,* vol. 125, pp. 519-525, 2017.
- [138] E. W. Zaia, A. Sahu, P. Zhou, M. P. Gordon, J. D. Forster, S. Aloni, *et al.*, "Carrier scattering at alloy nanointerfaces enhances power factor in PEDOT: PSS hybrid thermoelectrics," *Nano letters*, vol. 16, pp. 3352-3359, 2016.

- [139] A. T. Reda, D. Zhang, and X. Lu, "Intercalation of glycine into hydroxy double salt and its adsorption performance towards Uranium (VI)," *Environmental Technology & Innovation*, vol. 16, p. 100474, 2019.
- [140] A. Österholm, T. Lindfors, J. Kauppila, P. Damlin, and C. Kvarnström, "Electrochemical incorporation of graphene oxide into conducting polymer films," *Electrochimica Acta*, vol. 83, pp. 463-470, 2012.
- [141] Y. He, T. Day, T. Zhang, H. Liu, X. Shi, L. Chen, *et al.*, "High thermoelectric performance in non-toxic earth-abundant copper sulfide," *Advanced Materials*, vol. 26, pp. 3974-3978, 2014.
- [142] Z.-H. Ge, B.-P. Zhang, Y.-X. Chen, Z.-X. Yu, Y. Liu, and J.-F. Li, "Synthesis and transport property of Cu<sub>1.8</sub>S as a promising thermoelectric compound," *Chemical Communications*, vol. 47, pp. 12697-12699, 2011.
- [143] Y. Zhao, H. Pan, Y. Lou, X. Qiu, J. Zhu, and C. Burda, "Plasmonic Cu2- x S nanocrystals: optical and structural properties of copper-deficient copper (I) sulfides," *Journal of the American Chemical Society*, vol. 131, pp. 4253-4261, 2009.
- [144] P. Qiu, Y. Zhu, Y. Qin, X. Shi, and L. Chen, "Electrical and thermal transports of binary copper sulfides Cu x S with x from 1.8 to 1.96," *APL Materials,* vol. 4, p. 104805, 2016.
- [145] M. Bharti, A. Singh, S. Samanta, and D. Aswal, "Conductive polymers for thermoelectric power generation," *Progress in Materials Science*, vol. 93, pp. 270-310, 2018.
- [146] Y. Sun, C. A. Di, W. Xu, and D. Zhu, "Advances in n-Type Organic Thermoelectric Materials and Devices," *Advanced Electronic Materials*, vol. 5, p. 1800825, 2019.
- [147] Z. H. Khan, "Synthesis of TiS<sub>2</sub> Nanodiscs for Supercapacitor Application," in *AIP Conference Proceedings*, 1953.
- [148] M. Barawi, E. Flores, M. Ponthieu, J. R. Ares, F. Cuevas, F. Leardini, *et al.*, "Hydrogen storage by titanium based sulfides: nanoribbons (TiS<sub>3</sub>) and nanoplates (TiS<sub>2</sub>)," *J. Electr. Eng.*, vol. 3, pp. 24-29, 2015.

- [149] Q. Zhao, R. Jamal, L. Zhang, M. Wang, and T. Abdiryim, "The structure and properties of PEDOT synthesized by template-free solution method," *Nanoscale research letters*, vol. 9, pp. 1-9, 2014.
- [150] S. Xiong, L. Zhang, and X. Lu, "Conductivities enhancement of poly (3, 4-ethylenedioxythiophene)/poly (styrene sulfonate) transparent electrodes with diol additives," *Polymer bulletin*, vol. 70, pp. 237-247, 2013.
- [151] L. Zhang, L. Ji, P.-A. Glans, Y. Zhang, J. Zhu, and J. Guo, "Electronic structure and chemical bonding of a graphene oxide–sulfur nanocomposite for use in superior performance lithium–sulfur cells," *Physical Chemistry Chemical Physics*, vol. 14, pp. 13670-13675, 2012.
- [152] A. Titov, E. Shkvarina, A. Merentsov, A. Doroshek, A. Shkvarin, Y. M. Zhukov, *et al.*, "Synthesis, structure and properties of the layered CuxTiS<sub>2</sub> compounds," *Journal of Alloys and Compounds*, vol. 750, pp. 42-54, 2018.
- [153] R. Bayón, R. Musembi, A. Belaidi, M. Bär, T. Guminskaya, C. H. Fischer, *et al.*, "Highly structured TiO<sub>2</sub>/In (OH) xSy/PbS/PEDOT: PSS to be used in photovoltaic applications," *Comptes Rendus Chimie*, vol. 9, pp. 730-734, 2006.

## **PUBLICATIONS from THESIS**

Contact Information: nasersubhy@gmail.com

nasersubhy@yahoo.com

## **Papers**

- 1. Ahmed, N. S., & Karaman, F. (2018). Poly (3, 4-ethylene dioxythiophene)/copper sulfide hybrid thermoelectric materials with large Seebeck coefficient around room temperature. Journal of Optoelectronics and Advanced Materials, 20(November-December 2018), 695-700.
- 2. Ahmed, N. S., & Karaman, F. (2019). A novel n-type hybrid composite with a large Seebeck coefficient around room temperature based on poly (3, 4-ethylene dioxydiophene) and titanium disulfide. Journal Of The Indian Chemical Society, 96(9), 1199-1204.

## **Conference Papers**

- N. S. Ahmed And F. KARAMAN, "A Simple Green Preparation Method for Zinc Sulfide Nanoparticles," 1ST International Conference On Innovations In Natural Science And Engineering (Icinse 2018), Famagusta, Cyprus (Kktc), pp.151, 201.
- Ahmed, Ns, & Karaman, F., (2018). Investigation Of Thermoelectric Properties Of Poly (Ethylene Dioxythiophene) -Poly (Styrene Sulfonic Acid) / Copper Sulfide Nanocomposites . 1st International Conferenceon Innovations In Natural Scienceand Engineering.
- Karaman, F., & Ahmed, NS, (2019). A novel n-type hybrid composite with a large Seebeck coefficient around room temperature based on poly (3,4-ethylene dioxydiophene) and titanium disulfide. Journal Of The Indian Chemical Society, vol. 96, 1199-1204.
- 4. Ahmed, Ns, & Karaman, F., (2017). Thermoelectric properties of the poly (3,4-ethylene dioxythiophene) zinc sulfide composites. The International Joint Science Congress of Materials Polymers, Ohrid, Macedonia.

5. Karaman, F., & Ahmed, Ns, (2019). Bioinspired Crystallization of Copper Sulfide In The Presence of Some Simple Sugars . 20th Frühjahrssymposium (JCF), Konstanz, Germany.